RESEARCH

UDOT CONNECTING COMMUNITIES

Utah Department of Transportation - Research Division
4501 South 2700 West, Box 148410 - Salt Lake City, Utah 84114-8410

Report No. UT-11.01

DESIGN, ANALYSIS, AND SEISMIC PERFORMANCE OF A HYPOTHETICAL SEISMICALLY ISOLATED BRIDGE ON LEGACY HIGHWAY

Prepared For:

Utah Department of Transportation
Research Division

Submitted by:

Utah State University
Department of Civil and Environmental Engineering

Authored by:

Keri L. Ryan
Brian Richins

January 2011

Report No. UT- 11.01

DESIGN, ANALYSIS, AND SEISMIC PERFORMANCE OF A HYPOTHETICAL SEISMICALLY ISOLATED BRIDGE ON LEGACY HIGHWAY

Prepared For:

Utah Department of Transportation Research Division

Submitted By:

Utah State University

Department of Civil & Environmental Engineering

Authored By:

Keri L. Ryan, Ph.D.

Brian Richins

January 2011

DISCLAIMER

The authors alone are responsible for the preparation and accuracy of the information, data, analysis, discussions, recommendations, and conclusions presented herein. The contents do not necessarily reflect the views, opinions, endorsements, or policies of the Utah Department of Transportation and the US Department of Transportation. The Utah Department of Transportation makes no representation or warranty of any kind, and assumes no liability therefore.

THIS PAGE INTENTIONALLY LEFT BLANK

Technical Report Documentation Page

1. Report No.	2. Government Accession No.	3. Recipient's Catalog No.
UT-11-01		

4. Title and Subtitle	5. Report Date
DESIGN, ANALYSIS, AND SEISMIC PERFORMANCE OF A HYPOTHETICAL SEISMICALLY ISOLATED BRIDGE ON LEGACY HIGHWAY	January, 2011
	6. Performing Organization Code

7. Author	8. Performing Organization Report No.
Keri L. Ryan, Brian Richins	N/A

9. Performing Organization Name and Address	10. Work Unit No.
Utah State University Department of Civil and Environmental Engineering 4110 Old Main Hill Logan, UT 84322-4110	11. Contract or Grant No. 08-9182

12. Sponsoring Agency Name and Address	13.Type of Report & Period Covered
Utah Department of Transportation 4501 South 2700 West Salt Lake City, Utah 84114-8410	Final 11/2007-01/2011
	14. Sponsoring Agency Code

15. Supplementary Notes

Prepared in cooperation with the Utah Department of Transportation and Federal Highway Administration

16. Abstract

The need to maintain the functionality of critical transportation lifelines after a large seismic event motivates the strategy to design certain bridges for performance standards beyond the minimum required by bridge design codes. To design a bridge to remain operational, one may stiffen and strengthen the load carrying members to increase the capacity, or alternatively use response modification devices such as seismic isolators to shift the dynamic characteristics of the bridge, henceforth reducing the seismic demands. Seismic isolation systems are attractive because they are directly conducive to accelerated bridge construction techniques. The two strategies are compared for a typical Utah highway bridge, using a three-span, pre-stressed concrete girder bridge that crosses Legacy Highway as a case study example. The existing Legacy Bridge, which was designed as a Standard bridge for a 2500-year return period earthquake, is evaluated as an Essential bridge for a 1000-year return period earthquake. Subsequently, this bridge is redesigned and evaluated as a seismically isolated bridge. Configuration changes needed to accommodate a seismic isolation system are discussed, and reductions to column and foundation elements are proposed. Example seismic isolator designs are provided for several different types of isolation systems commonly used in the United States. Inspection and maintenance practices for seismically isolated bridges are discussed.

17. Key Words	18. Distribution Statement	23. Registrant's Seal
Seismic Isolation, Essential Bridge, Performance Evaluation, Pushover Analysis, Response Spectrum Analysis, Inspection and Maintenance, Friction Pendulum Bearings, Lead-Rubber Bearings	UDOT Research Division 4501 South 2700 West-Box 148410 Salt Lake City, Utah 84114	

19. Security Classification	20. Security Classification	21. No. of Pages	22. Price
Unclassified	Unclassified	178	

THIS PAGE INTENTIONALLY LEFT BLANK

ACKNOWLEDGMENTS

The authors wish to thank Utah Department of Transportation for funding this project, and Daniel Hsiao for his effective management of the project. Additionally, the authors recognize the following individuals for their contributions: Fred Doehring of UDOT for thoughtful suggestions to refine the scope, Hugh Boyle of Baker Corp. for suggesting a project to investigate the use of seismic isolation bearings for accelerated bridge construction, and USU professors Paul Barr and Joe Caliendo for technical assistance throughout the project.

THIS PAGE INTENTIONALLY LEFT BLANK

Table of Contents

List of Figures

List of Tables

THIS PAGE INTENTIONALLY LEFT BLANK

Executive Summary

In this project, we examine the use of seismic isolation as an alternative to conventional approaches to achieve high seismic performance in typical highway bridges. A highway bridge designed and built in 2006 by the Utah Department of Transportation (UDOT) was chosen as a case study. This three-span, pre-stressed concrete girder bridge is located on State Street in Farmington, Utah, and crosses Legacy Highway. In this report, we present 1) proposed configuration changes to incorporate seismic isolation into the Legacy Bridge; 2) proposed modified designs of the columns and foundation system that provide significant savings in materials and construction costs; and 3) example designs for three different types of isolation devices available in the United States.

An important objective of the project is to compare the overall seismic performance and construction cost of a representative conventional bridge and isolated bridge. The performance objective is that the bridge remain operational in the design event with a 1000-year return period. The Legacy Bridge was designed for a life safety performance objective but for a design ground motion based on a 2475-year return period. Thus, we first evaluate whether the as-built design of the Legacy Bridge meets the higher performance objective for a 1000-year return period ground motion based on current AASHTO specifications.

For the conventional bridge, seismic displacement demands were computed by linear response spectrum analysis of the bridge model subjected to unreduced forces calculated from the design spectrum. Although the bridge is not expected to remain elastic, the displacement demands computed by this procedure are assumed to reflect the actual displacement demands according to the well-known equal displacement rule. To determine the capacity of the bridge, nonlinear pushover analysis was applied to individual bridge bents subjected to an appropriate load distribution from the superstructure. The displacement capacity of the bents is defined as the displacement at which the first plastic hinge occurs, modified by an appropriate ductility factor. In the procedure, the displacement demand/capacity ratios are evaluated and the bridge design is considered acceptable for demand/capacity ratios less than 1. The displacement-based approach in the current seismic specifications does not define acceptance criteria for operational performance; therefore, we defined equivalent acceptance criteria to be consistent with those defined in a force-based procedure.

The non-linear finite element analysis program SAP 2000 was used to evaluate both demands and capacity of the bridge structure. In order to determine the demands on the existing structure, a linear spine model of the bridge was developed for demand analysis, while a nonlinear model of individual bents was developed for pushover analysis and capacity determination. To verify the accuracy of the computer model and the functionality of the program, properties of the support column cross-section were verified by hand calculations. The nonlinear behavior of the bents in pushover analysis was modeled by incorporating plastic hinges at the column ends; the hinge properties were based on moment-curvature analysis of the section and a calculated plastic hinge length. Equivalent linearized spring stiffness matrices were used to represent the contribution of the pier and abutment pile groups. The stiffness matrices were developed by analyzing the pile groups in FB-Multipier. The FB-Multipier model also incorporated soil springs with properties based on the p-y curves provided in the design drawings.

The results of the demand-capacity analysis are summarized as follows. The peak displacement demands of the bent considering bidirectional load combinations are 0.60 inches in the transverse direction and 0.26 in inches in the longitudinal direction. Comparing these demands to the allowable displacement capacities (0.817 and 1.106 inches) produces demand-capacity ratios of 0.74 in the transverse direction and 0.23 in the longitudinal direction. Since the demand-capacity ratios are less than one, the column design satisfies the performance objective according to our interpretation of the code requirements. However, the maximum lateral force capacity has been reached, implying formation of a complete plastic hinge mechanism in the columns. If multiple full plastic hinges have formed, we question whether the bridge would actually provide the performance that has been targeted. On the other hand, the analysis is based on nominal material properties, and material overstrength has not been included in the analysis, such that the response in the design event may be better than predicted.

After evaluating the Legacy Bridge in its as built configuration, we redesigned this bridge to incorporate an isolation system. We used a procedure comparable to that used for the original Legacy Bridge in the design and evaluation of the Isolated Bridge. A spine model was developed using members and assumptions identical to the Legacy Bridge where applicable, and modified as necessary to incorporate configuration changes, member sizes, etc., chosen for the Isolated Bridge. The design and analysis was based on the newest guide specification for seismic isolation, updated in 2010. A force reduction factor $R = 1.0$ was used in the design of

the substructure to ensure elastic response, which exceeds the code permitted value $R = 1.5$. A multi-mode elastic method of analysis was used for demand determination, and component force evaluation was used to demonstrate that columns and foundations remain essentially elastic. The analysis was based on a target isolation period of 2.5 seconds and 20% damping for the design ground motions, which results in a design displacement of about 9 inches for the isolators.

For seismic isolation applications, isolation devices are generally placed at the top of the columns or bent cap just below the girders. For the Legacy Bridge, we recommend alternatively placing the isolators at the tops of the columns below the bent caps, to reduce the total number of isolators at each pier location from a minimum of 11 down to 3. This strategy requires stiffening the connection by using a diaphragm or cross beam to connect the girders rigidly to the bent cap. The current diaphragms can be stiffened by eliminating the elastomeric bearing pads and extending the region of reinforcement from the bent cap to the diaphragm. The separation of the bent cap from the columns is conducive to an accelerated bridge construction approach. The use of rigid cross-beams at the bridge ends is also recommended to transfer the loads to the abutments over three isolators. We adopted the same configuration for the abutment diaphragm/cross beam as used for the integral diaphragm/bent cap for the bridge piers. The gap between the abutment diaphragm and the backwall or wing walls must be sufficient to accommodate the maximum displacement.

The reduced forces found during the initial analysis of the isolated bridge were used as a starting point to redesign the columns and footings. The columns were designed using SAP utilities that select and check concrete column reinforcement according to the AASHTO code. For foundation redesign, a trial configuration was identified by modifying the existing foundations in proportion to the reduction in demand, and the trial configuration was iterated by analysis in FB-Multipier to produce an economic foundation design.

To pick a new column size, we made use of the moment interaction diagram for the column, which indicates the relationship between axial load and moment capacity. Initial analysis of the isolated bridge indicated that the peak moment demand was a little less than one third of the capacity of the Legacy Bridge columns; accordingly, we propose to reduce the area of the column by about a factor of 2. This was achieved by reducing the diameter from 6 ft to 4.5 ft, and reducing the reinforcing steel from 27 #10 bars to 24 #9 bars.

Based on significant reductions in lateral force demand, we propose to eliminate the outer rows of piles in the pile group configuration for the pier columns, reducing the total number of piles in each pile group from 36 to 12. The pier foundation piles can be shortened by a factor of 2. Based on the new pile geometry, we also propose a reduction in pile cap thickness from 6 feet to 3 feet, and a reduction of longitudinal reinforcement from 47 #10 bars in each direction (top and bottom) to 24 #8 bars, which reduces the area of longitudinal steel reinforcement by 68%. The configuration of the abutment foundations is affected by external considerations beyond the total force capacity, which limit potential configuration changes to the abutments. Assuming the pile spacing is preserved and the total width of the pile span is preserved, the number of piles cannot be reduced for the abutments. To confirm that the capacity is sufficient, we created new FB-Multipier models with the updated geometry for both pier and abutment pile groups, and conducted pushover analyses to obtain both the lateral and vertical capacities of each configuration.

To summarize the performance evaluation, the peak moment demand in the columns was reduced from ≈9800 k-ft for the Legacy Bridge to ≈2100 k-ft for the isolated bridge, which is a reduction by more than a factor of 4. The reduction in shear force demand is similar. Besides the significant reduction in force demands, the columns of the isolated bridge are expected to remain elastic while the Legacy Bridge columns are expected to form plastic hinges. In both bridges, the foundation response was predicted to remain linear. However, the foundation demands for the isolated bridge are reduced by considerable factors, which has allowed for a considerable reduction in foundation size to achieve the same performance. Therefore, not only can the isolated bridge design more reliably achieve the operational performance objective, but the significant cost savings in column and foundation elements may be sufficient to offset the cost increase due to the isolation devices and associated configuration changes.

Several different types of isolation devices could be designed to provide the required stiffness and energy dissipation capacity of the isolation system. Design examples are provided for lead-rubber bearings, single friction pendulum isolators, and triple friction pendulum isolators. Lead-rubber bearings would be an economical choice for small highway bridges; such devices are supplied by Dynamic Isolation Systems of Sparks, Nevada, and Seismic Energy Products of Athens, Texas. The dynamic properties of a lead-rubber bearing depend on the weight carried; therefore, different bearings are specified at the piers and the abutments since the pier bearings carry an average of about twice as much weight. The force-deformation relation of

the bearing is bilinear, where the yield strength is determined by the size of the lead core, and the post-yield stiffness is determined by the overall diameter of the bearing, thickness of rubber layers, and shear modulus of the rubber. Once the bearing properties have been selected, a series of other design checks are made including stability, strain capacity, property modification factors, vertical and torsional stiffness, etc.

For a friction pendulum bearing, the strength is controlled by the sliding coefficient of friction, and the post-yield stiffness is controlled by the radius of curvature. The dynamic properties of the bearing do not depend on weight carried; therefore, only one bearing design is needed. The triple pendulum bearing offers the capability to control the seismic performance of the bridge in low, medium, and high intensity earthquakes; and a multi-objective design strategy is presented.

Inspection and maintenance of bridges with seismic isolation systems should focus on two items: maintaining the isolation gap, and visual inspection of the bearings to check for obvious signs of wear that might suggest the need for premature replacement. The isolation gap should be kept free of debris, and structural modifications that affect the ability of the isolators to develop the design displacement should be avoided. Isolation bearings are generally built with a cover layer of rubber that protect the internal working parts of the bearings from exposure to environmental conditions. When inspecting a rubber bearing, one should look for discoloration, splitting, and cracking, and the observation of a powder residue when the bearing is touched. Bulging of rubber layers that can be observed through the cover rubber is an indication of internal delamination of the rubber from the steel shims, and means that the bearings should be replaced.

THIS PAGE INTENTIONALLY LEFT BLANK

1. Introduction

Seismic isolation is a method of improving a structure's performance during seismic events by changing the way it responds. By isolating a structure from the ground's motion, the forces transferred to the structure are reduced, with a corresponding reduction in the demand placed on members of the structure. This reduction in force is due to the nature of seismic response. Under random excitation, such as an earthquake, a structure tends to be excited at its natural frequencies, which depend on the mass and stiffness distribution of the structure. Displacement demands are a summation of the modal demands, which are associated with the structure's natural frequencies, or natural periods. Isolation changes the stiffness distribution of the structural system, lengthening the natural period and changing the dominant mode shape such that most of the displacement occurs in the isolators. A longer period accomplishes two objectives; first, the spectral acceleration is greatly reduced, which leads to lower total forces on the structure. Second, the earthquake excitation is nearly orthogonal to higher mode shapes, leading to suppression of higher mode response. Since the structural demands are contained mostly within the higher modes, forces and displacements are substantially reduced elsewhere in the structure. Isolation systems also include damping mechanisms, which dissipate energy during cyclic motion, and further reduce the force and displacement demands on the structure.

With these changes in the response, a structure can be economically designed for the elastic design spectrum, rather than using an inelastic spectrum, which represents a reduction of the elastic spectrum by a Response Modification Factor (R). This factor is "used to modify the element demands from an elastic analysis to account for ductile behavior and obtain design demands" (AASHTO, 2009a). The method of using reduced forces estimates the ductility capacity of the resisting elements, or the extent to which they can be damaged without catastrophic failures such as fracture, collapse, etc.

For bridges, isolation is expected to result in smaller seismic forces and a more efficient, less expensive design. However, isolation is still not widely used in the United States, especially in areas where seismic combinations do not control lateral design. This is due in part to inexperience with isolation devices and uncertainty about long-term performance and

maintenance. Cumbersome design procedures and extensive testing requirements for each project discourage inexperienced bridge engineers to propose isolated bridge solutions. Continuing research and education of seismic isolation will allow better standardization of the methods and materials used, and new codes will be able to incorporate the principles learned more effectively and uniformly. The cost and complexity of seismic isolation are likely to decrease as standardized practices become established.

An additional consideration for Utah Department of Transportation is whether columns and foundations should be designed for the reduced force demands observed as a result of the seismic isolation system, or for the equivalent force demands of the bridge as if it were not isolated. Although many states on both the western and eastern regions of the country have an inventory of seismically-isolated bridges, most states, including California, have not progressed in their use of seismic isolation to the point of adopting standard design strategy and policies for isolated bridges. In fact, many of the existing isolated bridges have been designed with significant assistance from consultants, including device vendors. Therefore, if Utah were to adopt such policies, they would be a model to other states who have so far approached seismic isolation design philosophy on a case-by-case basis.

In our opinion, sufficient conservatism has been introduced into the seismic isolation design approach. The isolation design that we present later in the report is based on a target value of $R = 1$, which means that the bridge will remain elastic in the design earthquake, and in even larger motions due to overstrength. Therefore, designing the columns and foundations as if the bridge was not isolated is unnecessary, and results in member capacities that greatly exceed code requirements. Isolation device vendors and expert consultants will advise likewise. The main concern is whether the lateral system can protect the safety of the bridge if the isolation devices should fail to respond. The most severe failure that could occur is that the devices "lock up" and subsequently do not lead to a reduction in demands. However, complete lock-up of devices has never been observed, and is such a remote possibility that it can be considered to have a statistical probability of zero. On the other hand, the period shift of the isolated bridge could be less than anticipated if the isolators stiffen or if the displacement is unknowingly limited. (Such issues are discussed further in Chapter 5 on inspection and maintenance practices.) Nevertheless, inadvertent nonconservative shifting of the dynamic properties is unlikely to be significant enough to cause complete failure of the bridge substructure. Furthermore, isolation devices are very reliable, and should be considered safer than other

elements along the load path that are routinely relied upon not to fail (e.g. superstructure, diaphragms, expansion joints, bent caps, columns, foundations.)

1.1 Project Overview

The purpose of this project is to examine the use of seismic isolation as an alternative to conventional approaches to achieve high seismic performance in typical highway bridges in the state of Utah. A highway bridge designed and built in 2006 by the Utah Department of Transportation (UDOT) was chosen as a typical case study (Figure 1-1). This three-span, pre-stressed concrete girder bridge is located on State Street in Farmington, Utah, and crosses Legacy Highway. The bridge in its as-built configuration is hereafter referred to as the Legacy Bridge.

In this report, we present 1) proposed configuration changes to incorporate seismic isolation into the Legacy Bridge; 2) proposed redesign of the columns and foundation system that provide significant savings in materials and construction costs while meeting the code requirements and performance objectives for the isolated bridge; and 3) example designs for three different types of isolation systems available in the United States. The design procedure for the isolation system follows the very recently released updated guide specification for seismic isolation design (AASHTO, 2010). The configuration of the bridge incorporating seismic isolation is referred to hereafter as the Isolated Bridge.

An important objective of the project is to compare the overall seismic performance and construction cost of a representative conventional bridge and isolated bridge. The performance objective is that the bridge remain operational in the design event with a 1000-year return period.

Figure 1-1: State Street Overpass, Farmington, UT

While the Legacy Bridge was designed under a former code, we first evaluate whether the as-built design of the Legacy Bridge meets the performance objective under the current AASHTO specifications (AASHTO, 2009a; 2009b). We then compare both the seismic performance and the construction costs of the Legacy Bridge and the Isolated Bridge.

1.2 Applicable Codes and Procedures

The Legacy Bridge was designed by the Structures Division of UDOT in 2006 using the AASHTO LRFD Bridge Design Specification (AASHTO, 2006), with seismic design based on the MCEER specification (ATC/MCEER, 2003). Since the design and construction of this bridge, the LRFD specification has been updated (AASHTO, 2009b), and a seismic design specification based on the MCEER specification has been adopted by AASHTO (AASHTO, 2009a). These latest AASHTO codes, which have been adopted by UDOT for bridge design, will be used for this project to evaluate the Legacy Bridge. The codes are hereafter referred to as the "LRFD Spec" (AASHTO, 2009b), and the "Seismic Spec" (AASHTO, 2009a).

One of the key differences between the former and current specifications is that the design ground motion was previously based on a 2475 year return period, or an event with a 3% chance of exceedance in 75 years (ATC/MCEER, 2003), and is now based on a 1000 year return period, or an event with a 7% chance of exceedance in 75 years (AASHTO, 2009a). Although the Legacy Bridge was designed for the larger event, the design did not consider a beyond code minimum performance objective. We will classify the bridge as "Essential" under the current LRFD and Seismic Specs, hence targeting operational performance under the 1000 year return period event (Sec. 3.10.5 of AASHTO, 2009b). Our evaluation of the Legacy Bridge will determine whether the design meets the current codes for an Essential Bridge.

Our re-design and evaluation of the Isolated Bridge relies on the newest guide specification for seismic isolation design (AASHTO, 2010), hereafter called the "Isolation Spec". The Isolation Spec is not a standalone document, but should be used with reference to the LRF Spec. The Seismic Spec uses a displacement-based evaluation procedure while the LRFD Spec uses a force-based procedure. The main difference between the two approaches is that pushover analysis is used to determine bridge capacity in a displacement based procedure, while bridge components are designed for the given reduced forces in a force-based procedure. Since we specify that the substructure components of the Isolated Bridge should remain completely

elastic when subjected to unreduced forces (R=1), a pushover analysis is not needed for the Isolated Bridge regardless of the evaluation approach, and thus the discrepancy in the evaluation procedures for the two bridges is minimal.

THIS PAGE INTENTIONALLY LEFT BLANK

2. Review of As Built Legacy Bridge Design

2.1 Methodology Overview

This chapter details the procedure used to evaluate the existing Legacy Bridge under the new code provisions, including remarks on items that specifically affect this project and assumptions used. We performed a design check of the Legacy Bridge under the current Seismic Spec, targeting operational performance in 1000 year earthquake. Recall that the bridge was designed using a previous code for life safety in a 2500 year earthquake. This design check emphasizes the components of the bridge that are controlled by seismic loading, namely the abutments, intermediate bents and foundation piers. The loading on the bridge was calculated according to the AASHTO load combinations defined in the LRFD Spec, with particular focus on the Extreme Event I combination, which considers seismic loading. The as-built Legacy Bridge design was assumed to be sufficient for load combinations dominated by vertical loading (dead load, live load, etc.), and these load combinations were generally not re-evaluated.

Section 5.4 of the Seismic Spec provides guidelines for the selection of appropriate analysis procedures depending on the bridge characteristics and design objectives. A time history analysis is recommended for Essential or Critical bridges; however, time history analysis is not required for the Isolated Bridge, and by our judgment is not necessary for this bridge. Aside from this, the bridge configuration is regular and a single mode method is sufficient. As a compromise, we have evaluated the bridge using a multi-mode procedure. As such, seismic displacement demands were computed by linear response spectrum analysis of the bridge model subjected to unreduced forces calculated from the design spectrum. Although the bridge is not expected to remain elastic, the displacement demands computed by this procedure are assumed to reflect the actual displacement demands according to the well known equal displacement rule. To determine the capacity of the bridge, nonlinear pushover analysis was applied to individual bridge bents subjected to an appropriate load distribution from the superstructure. We selected the displacement capacity of the bents as the displacement at which the first plastic hinge occurs, modified by an appropriate ductility factor. In the procedure, the displacement demand/capacity ratios are evaluated and the bridge design is considered acceptable for demand/capacity ratios

less than 1. The Seismic Spec does not define acceptance criteria for operational performance; therefore, we defined equivalent acceptance criteria to be consistent with those defined in a force-based procedure.

The non-linear finite element analysis program SAP 2000 was used to evaluate both demands and capacity of the bridge structure. In order to determine the demands on the existing structure, a linear spine model of the bridge was developed for demand analysis, while a nonlinear model of individual bents was developed for pushover analysis and capacity determination. To verify the accuracy of the computer model and the functionality of the program, properties of the support column cross-section have been verified by hand calculations. Basic hand analysis was also performed to verify other computer-generated results, such as bent stiffness and displacement, and the period of the structure; these calculations are described below in the related sections.

2.2 Design Loads and Site Spectrum

Loading for the structure was computed based on the AASHTO load combinations. Once the loading has been determined for each load type, they are combined according to the AASHTO Load Combinations defined in 3.4.1 of the LRFD Spec. SAP automatically calculates the effects of load combinations by superposing the analysis results for different load cases using combination factors specified by the user. Since many of the LRFD combinations involve loading that is insignificant or not present on this structure, only combinations involving dead, live, and earthquake loading were considered for this project. These combinations are Strength I, Strength IV, and Extreme Event I. The other Extreme Event combination was neglected, as it was not expected to control in the design region of this case study. The Strength I and Strength IV combinations, which use the maximum dead load factors indicated in Table 3.4.1-2 of the LRFD Spec (1.25 and 1.5, respectively), were expected to control axial force demands and hence considered for certain aspects of the substructure design. The minimum dead load factors (0.9 for each case) were not considered, as there is no uplift on the structure under any load combination, and these minimum factors would not control the design. Maximum resultant forces over all load combinations are presented in Section 2.6 as part of the design discussion.

Unfactored dead loads are determined automatically in the SAP model based on component weight, which is determined using the unit weight of the materials and the volume of

each member as computed by SAP. The total resulting dead load over each support corresponds to the seismic weight over that support, and the sum of these weights is equivalent to the seismic mass of the structure (Table 2-1).

Table 2-1: Foundation Dead Loads

Support	Dead Load (kips)
Abutment 1	1833
Bent 2	4223
Bent 3	3537
Abutment 4	1146

The live load factor γ_{EQ} for the Extreme Event I (seismic) load combination is determined on a project-specific basis under the Seismic Spec, and the Seismic Spec commentary states that a factor of 0 has traditionally been applied (Section C3.7 of AASHTO, 2009a), which means that live loads have been neglected entirely for this combination. Previous editions of the LRFD Spec explicitly specified a live load factor of 0 for earthquake load combination (Section C3.4.1 of AASHTO 2009b). Live loads have been neglected in part because of the improbability of critical live loads being present during the design earthquake event, as well as the ability of live loads to move independently of the structure. However, neglecting live loads in a seismic load combination is no longer widely accepted. The commentary for the LRFD Spec indicates that in lieu of a standard earthquake live load factor, 50% of the live load is a reasonable value for a wide variety of traffic conditions. Accordingly, we used a live load factor of 0.5 for the earthquake load combination. The live loads were not included in the seismic mass used for computation of the lateral forces, but have been included in the total vertical loading.

Live loads were determined using the Dr. Beam software utility, with a uniform lane load of 0.64 kips per linear foot, and the design truck specified in the LRFD code. The truck configuration and location producing the maximum shear at the girder ends over each pier and abutment was determined to maximize the vertical live load at a given support. Figure 2-1 has been taken directly from Dr. Beam, and illustrates the loading and deflection diagrams and envelopes at the critical truck position for Bent 2. The moments induced by live load were neglected, as the substructure connectivity will not transfer these moments to the supports.

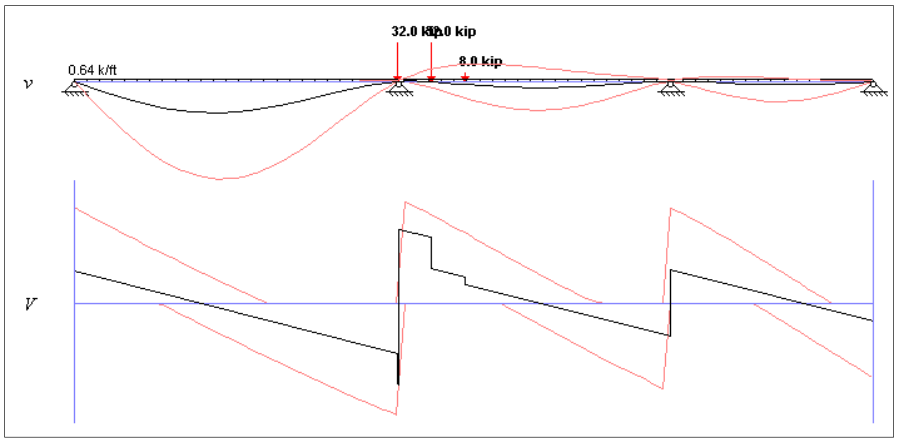

Figure 2-1: Simple Beam Model in Dr. Beam

These per-girder loads were multiplied by the shear distribution factor defined by Equation 4.6.2.2.3a-1 of the LRFD Spec, which gives a factor of 0.788. The equation for the shear distribution factor incorporates the Multiple Presence Factor, which accounts for the probable size and number of vehicles in adjacent lanes; therefore, the load resulting from a single truck on a single girder is modified by a distribution factor, and the resulting load is applied to all girders. Accordingly, the adjusted loads from Dr. Beam were multiplied by the number of girders (11) to produce the critical live loads shown in Table 2-2. The vertical live loads at each support do not occur simultaneously, but are independent. Thus, the maximum loads at each support were all applied to the same load case in SAP, which allows the critical loads for each support and each load combination to be generated from a single analysis trial. The total load from the girders is distributed evenly by the bent caps and the abutment pile caps; the loading was therefore applied as a uniform load across the bent, and as point loads on the abutment foundation springs to simplify the modeling process.

Table 2-2: Maximum Total Support Live Loads

Abutment 1	Bent 2	Bent 3	Abutment 4
854.6 kips	1005.4 kips	849.4 kips	667.4 kips

The lateral loading on the structure is dependent on the structure's seismic weight (which corresponds to the component dead loads) and the response spectrum. The response spectrum for the project was found using the AASHTO Seismic Design Parameters software application

(AASHTO, 2009c), which accompanies the LRFD Spec. This software application determines the site-specific spectrum parameters based on project latitude and longitude, including adjustments for site class. The blueprints for the structure indicate that the bridge location is Site Class D; the corresponding values for this site are shown below in Table 2-3. These values were used to define the spectrum in SAP, which is shown in Figure 2-2. In a response spectrum analysis, the spectrum is used to determine the lateral force demands in the bridge fundamental modes during the design earthquake (see Section 2.6).

Table 2-3: Site Parameters

F_{PGA}	1.15	A_s	0.415
F_a	1.17	S_{Ds}	0.977
F_v	1.77	S_{D1}	0.561

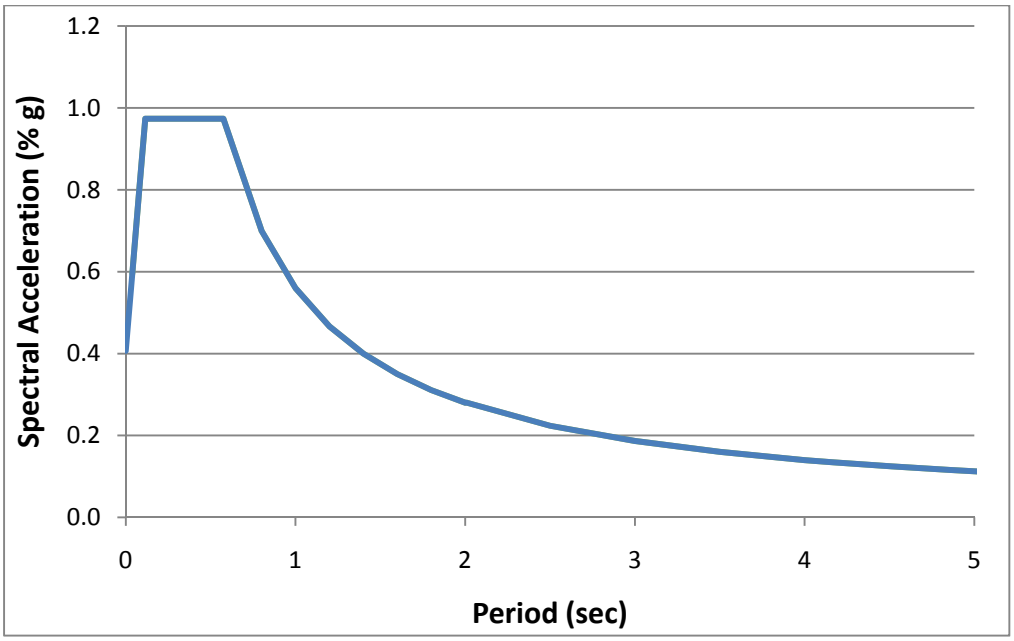

Figure 2-2: Site Acceleration Spectrum

2.3 Modeling Assumptions and Methods – Linear Bridge Model

Based on the geometry and connection detailing indicated in the design documents, several simplifying assumptions were made to ensure the proper model behavior during the analysis. The non-linear behavior of individual components was calculated and used to define

appropriate elastic properties for the linear analysis, in accordance with Section 5.6 of the Seismic Spec. Further non-linear investigation is discussed in Section 2.5. Throughout this document, only the completed bridge configuration has been considered. Prior to implementation of any design, analysis for each stage of construction should be performed to ensure constructability and structural stability. The assumptions specific to each section of the bridge are described below.

2.3.1 Superstructure

The contribution of nonstructural items, such as handrails and lighting components, has not been considered, although minor changes in detailing may be required for such components as part of the isolated redesign in order to accommodate the relative displacements between the substructure and the isolated superstructure. The design of the girders, deck, and other superstructure components was presumed to be adequate, as spanning members are typically not controlled by lateral considerations. Superstructure components have not been checked or redesigned. The slope and super elevation of the superstructure are small relative to the span and were considered to have negligible effect on the substructure design and performance. The superstructure was considered to be much stiffer than the supports, and was modeled as a single member using the properties of the entire deck cross section, including the girders, deck, and integral barriers. The superstructure was assumed to transfer seismic loads elastically within the design range.

Each deck span is a different length and therefore has different prestressing strand configurations and forces, which required that a separate cross section be created for each span. SAP includes a utility called Section Designer, which provides functionality to create custom sections using detailed non-linear material models. A typical section for a single girder was created, including the haunch and decking above the girder and longitudinal reinforcement in both the girder and the deck. The girder prestressing strands are represented by a single element in each girder, with a prestressing centroid height, area, and force equal to those indicated in the plans. This composite section was replicated to extend the same geometry and properties to the other girders in the section. The integral barriers were then added, and the procedure repeated for the two remaining spans, with appropriate adjustments to the prestressing elements.

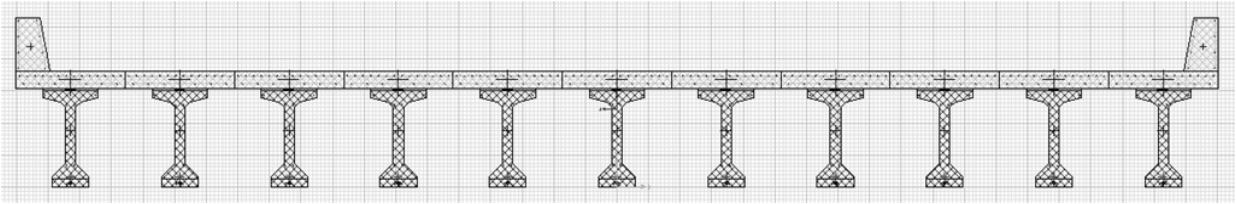

Figure 2-3: Typical Deck Cross-section

Based on the cross-section configuration and material properties, SAP automatically calculates section properties, including mass (weight) per unit length and inertia and stiffness about each axis; see Table 2-4 for these values. The frame geometry representing each span was divided into 4 frame segments to distribute the mass evenly throughout the span. To account for the weight of nonstructural items, the unit weight of the concrete was increased slightly from the SAP default of 144 lb/cu.ft. to 150 lb/cu.ft.

Table 2-4: SAP Section Properties

	Units	SPAN1	SPAN2	SPAN3
Gross Area	in^2	30,894	30,814	30,974
Torsional Constant, 11 Axis	in^4	2,898,047	2,851,642	2,948,688
Moment of Inertia, 33 Axis	in^4	29,313,569	29,165,283	29,461,126
Moment of Inertia, 22 Axis	in^4	2,364,145,134	2,349,087,994	2,379,110,007
Shear Area, 2 Axis	in^2	13,814	13,747	13,879
Shear Area, 3 Axis	in^2	15,329	15,308	15,348
Section Modulus, 33	in^3	427,185	424,350	430,014
Section Modulus, 22	in^3	5,178,850	5,145,866	5,211,632
Plastic Modulus, 33	in^3	582,842	580,767	584,913
Plastic Modulus, 22	in^3	6,410,813	6,376,106	6,445,413
Radius of Gyration, 33	in	30.803	30.765	30.841
Radius of Gyration, 22	in	276.628	276.104	277.144

2.3.2 Intermediate Bent Caps

The supports have a skew of 25 degrees relative to the longitudinal axis of the bridge. Therefore, in the SAP model, the local axes of all elements comprising the bents – column

frames, foundations springs, and all nodes - were rotated accordingly to simplify modeling and design procedures, and to accurately reflect connectivity assignments. Discussion specific to the bents or bent components refers to local bent axes throughout this document. Bent cap geometry, based on a typical section, was modeled in Section Designer so that its weight is computed accurately. However, several constraints were applied to the bent cap so that it is treated as a rigid member during analysis. In this way, the stiffness of the diaphragms that connect the superstructure to the bent is indirectly accounted for, even though the diaphragms above the bents have not been explicitly modeled. A rigid beam constraint and a torsional constrain were applied to each bent cap, to represent the distribution of superstructure load and transfer shear and moment evenly along the entire bent to the columns. The connection detailing (see Figure 2-4) of the diaphragms over the intermediate bents appears insufficient to develop moment resistance between the bent and the deck about the bent axis in the transverse direction, due to the materials placed under each girder and the lack of reinforcement at the exterior edges; therefore rotational freedom was assumed in this direction. Accordingly, the connection of the bent cap to the superstructure was fixed in the lateral direction and pinned longitudinally. The bent frame itself, consisting of the columns and the bent cap, is fixed-fixed in both directions.

The connection between the bent centerline and superstructure centroid was modeled by a rigid, massless link, with a joint located at the interface between the two components. A moment release is applied at this joint to reflect the rotational freedom described above. Figure 2-5 illustrates the assumptions and geometry used to model the bents; further clarification of other components in this figure and the corresponding assumptions can be found in the following sections.

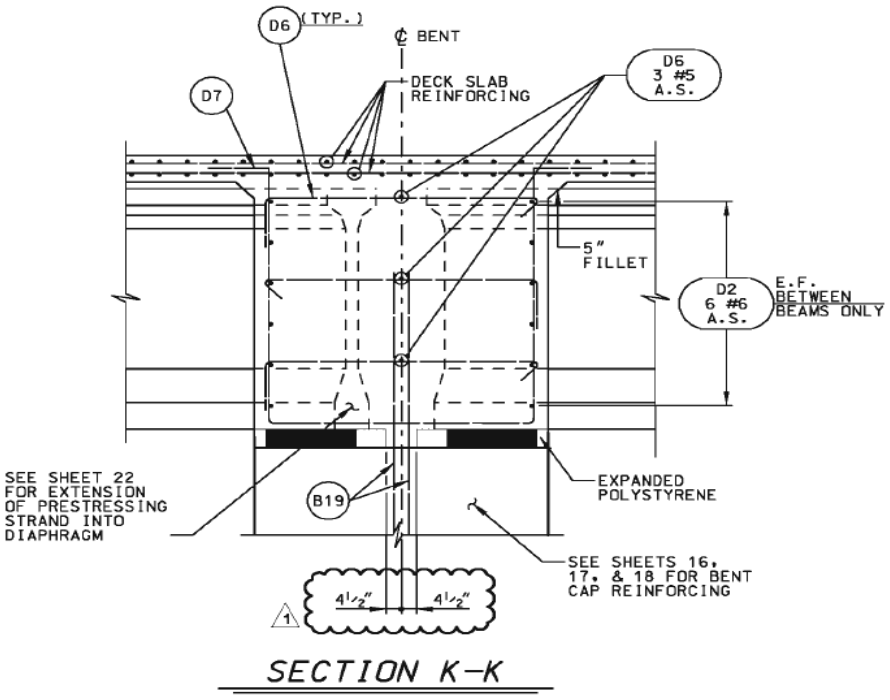

Figure 2-4: Bent Connection Detail

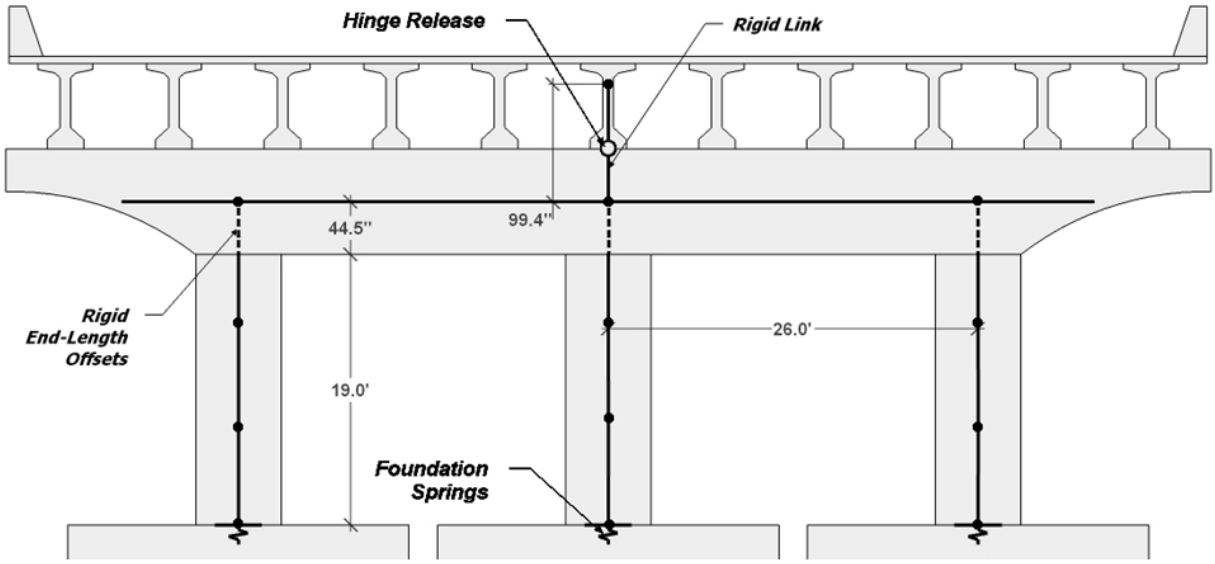

Figure 2-5: Bent Centerline Model

2.3.3 Intermediate Bent Columns

Due to the size and reinforcement of the columns and their connection detailing to the bent cap and the foundation, the columns were considered fixed-fixed in each direction. Rigid end-length offsets (Figure 2-5) were used at the top of each column to represent the difference between actual connectivity and the centerline connection of the model. The columns were divided into 3 elements to distribute the mass accurately to the foundations and bent caps. Because of the stiffness of the deck and the abutments, the bent columns constitute most of the flexibility in the structure, and therefore control the lateral response. As such, the properties and response of the cross section must critically be modeled accurately by the software during analysis. The SAP section analysis and corresponding hand calculations are presented below.

2.3.3.1 SAP Moment-Curvature Analysis

In addition to section creation, the SAP Section Designer contains a module for moment-curvature analysis of such sections. This utility includes templates for several commonly used sections as defined by the California Department of Transportation (CALTRANS), including an octagonal section with spiral hoop reinforcement, which is the section used for the columns. These templates allow the user to define a section by choosing section dimensions, materials, and reinforcement bar quantity, sizes, and spacing. The geometry and material strengths specified in the design documents were used to define the cross section, using the non-linear material models specified in Section 8.4 of the Seismic Spec.

The Mander unconfined concrete model was used for the outer concrete material, and the Mander confined concrete model was used for the core. Mild steel with strain hardening was used for the reinforcement. The figures below show the material definition dialogues from SAP; properties for each material correspond to the properties indicated in the design document. Detailed values for each material model are located in Appendix A1-A3.

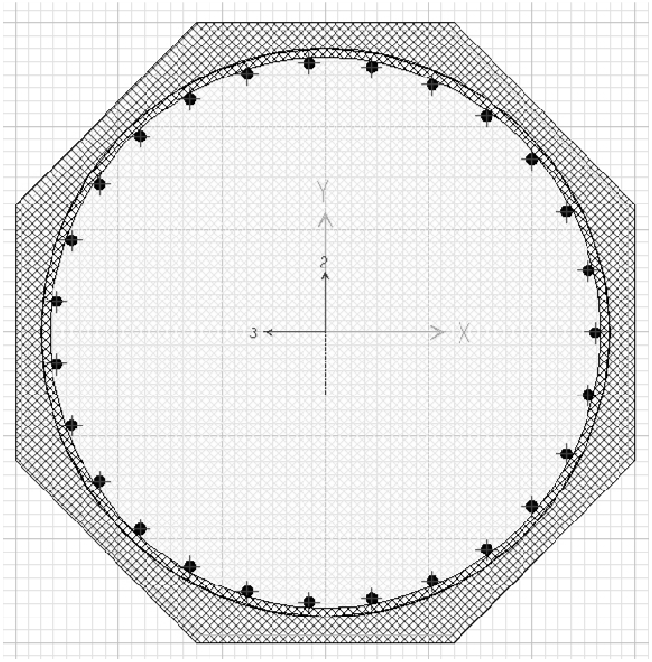

Figure 2-6: Column Cross Section

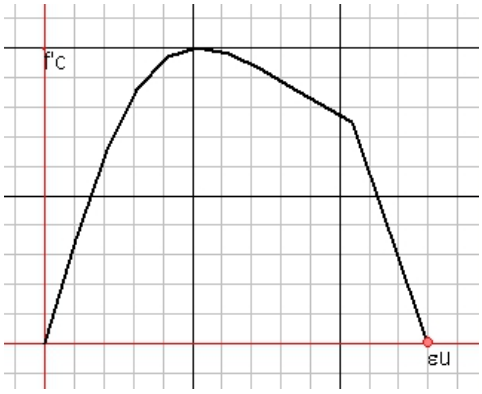

Figure 2-7: Mander Unconfined Concrete Model

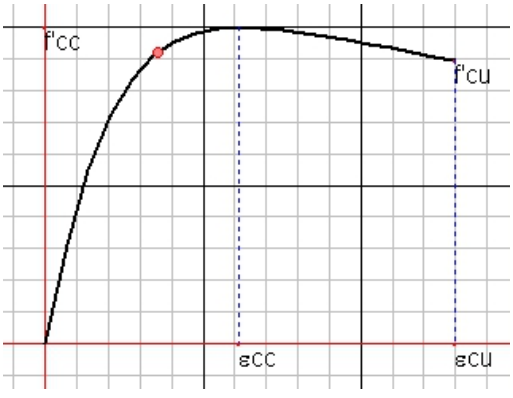

Figure 2-8: Mander Confined Concrete Model

Figure 2-9: Mild Steel (Park) Model

After ensuring that the section was properly defined, its moment-curvature properties were calculated using SAP's built-in features, described above. The moment-curvature plot for the column section (with no axial load) are shown in Figure 2-10, and the corresponding moment and curvature data values are found in Table 2-5. Further investigation of column moment-curvature under axial loading is discussed in Section 2.5.

Table 2-5: SAP Moment-Curvature Values for Bent Column

Curvature	Moment (k-in)
0	0
2.75E-05	29,678
6.88E-05	59,210
0.00012375	65,933
0.0001925	68,385
2.75E-04	70,700
3.71E-04	73,902
4.81E-04	74,584
6.05E-04	76,566
7.43E-04	78,762
8.92E-04	80,290
1.06E-03	80,578
1.24E-03	80,935
1.43E-03	80,462
1.63E-03	80,487
1.86E-03	51,659
2.09E-03	36,352
2.34E-03	27,100
0.0026	22,970
0.002875	19,245

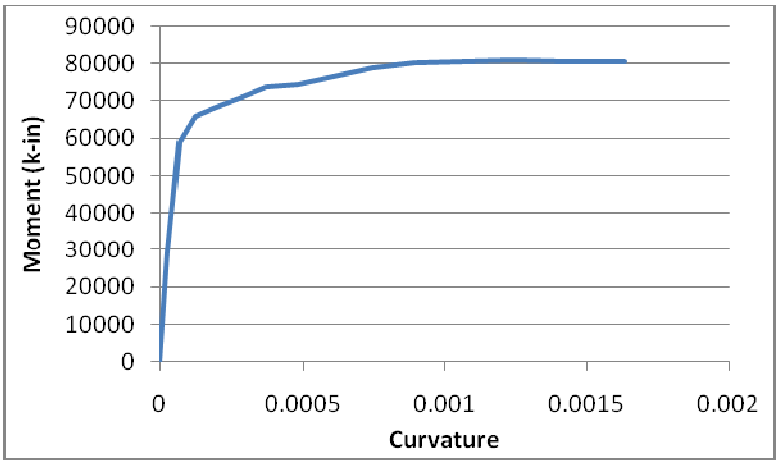

Figure 2-10: SAP Moment-Curvature Analysis of Bent Column

2.3.3.2 Manual Moment-Curvature Analysis

In order to verify the SAP moment-curvature output, the method of fiber sections was used to manually determine section response across a given range of curvature, with each fiber's stress contribution being computed separately and the total reaction across the section being

statically balanced. Simple bi-linear material models were used, with properties approximately equal to those of the models described above (Figure 2-11). The concrete model was assigned a compressive strength of 4 ksi, with a corresponding stiffness of 3605 ksi, and no tensile capacity. The steel was assigned a stiffness of 29,000 ksi, a yield strength of 60 ksi, and a post-yield stiffness ratio of 0.03. Because the material models used in the manual analysis did not match those for SAP analysis in the post-yield range, the analysis was used only to verify the initial stiffness and strength in the elastic region. The contribution of each material within a given fiber was computed separately, as it is difficult to otherwise account for differences in post-yield behavior and the modulus of each material.

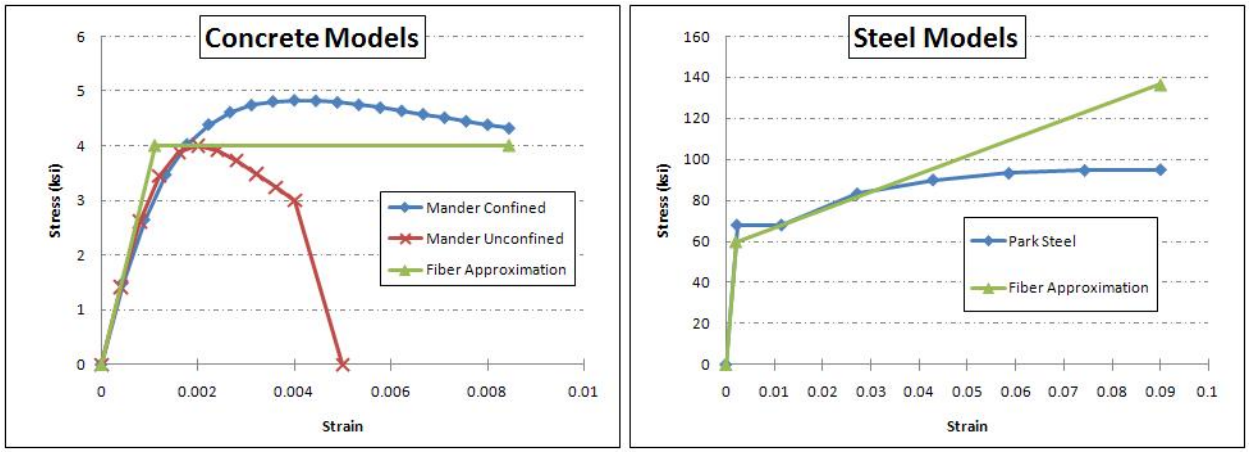

Figure 2-11: Comparison of Material Models for Moment-Curvature Analysis by SAP and Manual Analysis Approaches

As the static fiber analysis must be repeated at multiple points across a range of curvatures to develop moment-curvature relations, an Excel spreadsheet was developed to automate the process. Section geometry was defined and divided into discrete layers, or fibers. The area of the steel was not subtracted from the area of the concrete, as this was considered negligible. Material models were represented mathematically by defining initial modulus values, limiting strains, and post-yield stiffness coefficients consistent with the plan specifications for the materials. Values were chosen for the fiber thickness (0.5 in), starting and ending strains (±.005) in the extreme top fiber, and a strain increment value (.0001). A preliminary estimate was input for the location of the neutral axis. The strain and force in each fiber is calculated from these initial conditions, and used to find the net moment and axial forces on the section.

The manual moment-curvature analysis was automated through the use of a custom VBA macro (see Appendix A5). The macro uses the Solver add-in to find the location of the neutral axis required to satisfy static equilibrium across the section for the given stress in the top fiber. The angle of curvature is computed from the strain of the top fiber and the depth to the neutral axis, and the curvature and corresponding moment are recorded. The macro then increments the strain in the top fiber, the strain and force in all other fibers, and the required location of the neutral axis. This process is repeated until the ending value of the strain is reached. A second function within the code allows the results to be output on plots of the forces in each fiber for visual verification of the procedure. Figure 2-12 shows the state of the section at the end of analysis. The left image indicates the location of the neutral axis and the state of each longitudinal bar, while the right image shows the stress (ksi) in each fiber. The plot gridlines are spaced 12 inches apart, while the total section height is 72 inches.

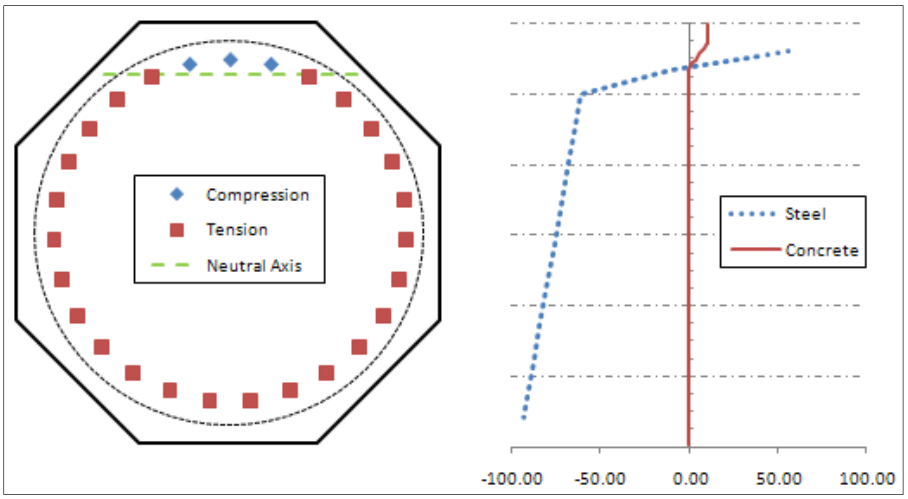

Figure 2-12: Neutral Axis Determination and Fiber Stresses Produced by Manual Section Analysis

The moment-curvature analysis computed by SAP and computed by the manual approach are compared in Figure 2-13. The results of the manual analysis for the initial stiffness of the section are practically identical to the SAP results – within 0.01% – and initial yield begins in approximately the same region. The initial stiffness (*EI*) of the section was found to be equal to 7,492,708 kip-ft^2. The results of the comparison are satisfactory for the elastic range, and the discrepancies in the post-yield region are easily accounted for by the differences in the material

models. Therefore, we have confirmed that our implementation of materials and sections of the SAP model is correct, and can rely on the SAP section analysis hereafter without further detailed verification outside the program.

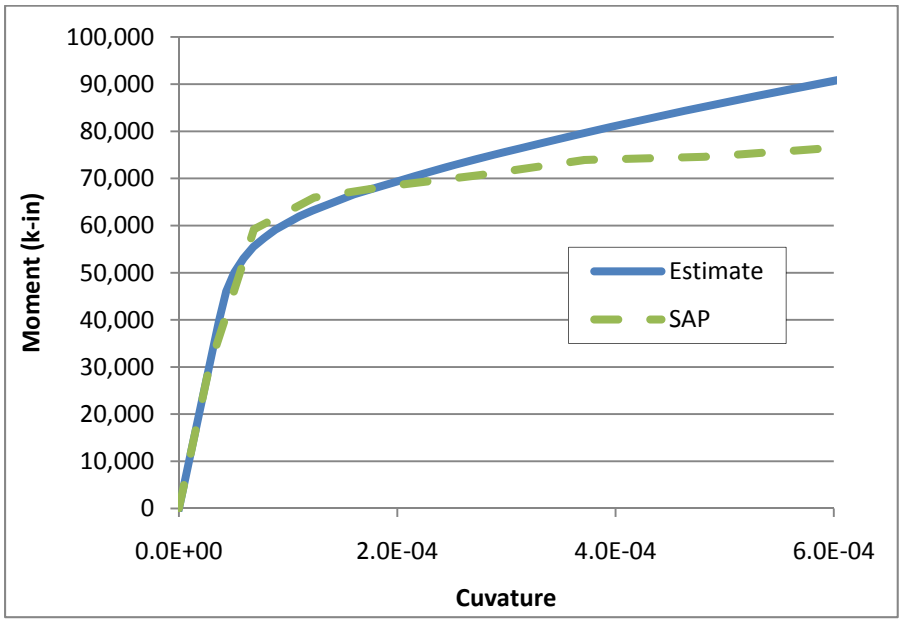

Figure 2-13: Comparison of Column Section Moment-Curvature Produced by SAP and by Manual Analysis

2.3.4 Pile Foundations and Abutments

The soil drill logs in the plans were used to determine soil properties, and the bent pile groups and integral abutment pile caps have been analyzed using FB-Multipier, a geotechnical software package developed by the University of Florida and the Florida Department of Transportation that includes nonlinear finite element analysis capability. The results of FB-Multipier analysis were used to define the stiffness properties of foundation springs in the SAP model.

The in-situ strength and stiffness of the foundation piles are critical considerations of the substructure response. Pile behavior is a complex phenomenon that depends on non-linear soil properties, pile cross section and length, and connectivity and loading conditions. The full reaction of a pile group also depends on the pile spacing and the pile cap geometry. The standard geotechnical approach is to determine the strength and reaction of a single pile, and then estimate the pile group strength by combining the strength of individual piles with appropriate factors to

account for reductions in strength due to the pile group geometry. FB-Multipier requires the user to define only basic parameters such as soil profile, pile cross section, and pile group geometry (Figure 2-14), and then performs all the adjustments and calculations automatically using standard geotechnical assumptions and procedures. Though FB-Multipier has the capability to model and analyze a spine element bridge connected to individual foundation elements, and perform finite element analysis of the entire model, SAP 2000 was preferred for this purpose. Thus, FB-Multipier is used specifically to determine foundation stiffness matrices and detailed soil properties for input into SAP 2000.

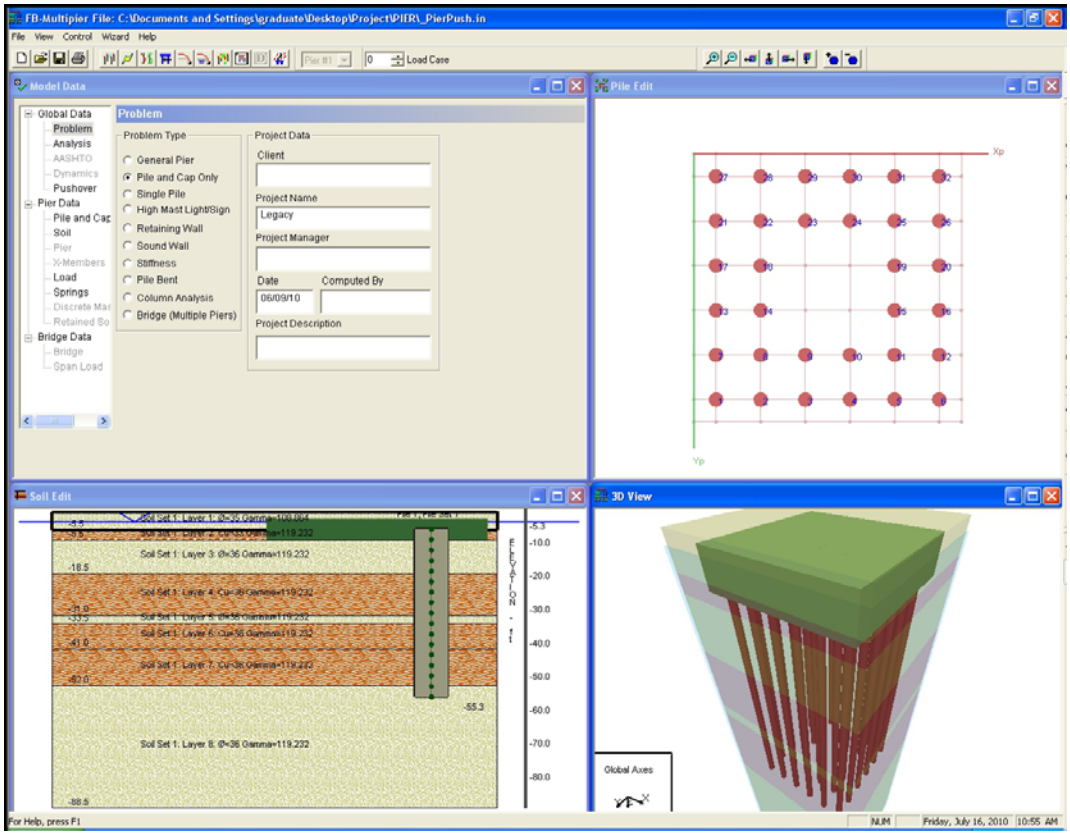

Figure 2-14: FB-Multipier Pier Model Definition

Two foundation models were created in FB-Multipier - one of a single pier foundation and one of an abutment foundation. The models include the cross section and materials of the piles, the stiffness and thickness of the pile cap, pile spacing and geometry, and the soil profile, including water table depth. For each model, initial loading conditions were based on the

assumption that this is a short-period bridge, with the full vertical load being applied. The lateral moment and shear loading for each model, described below, were applied bi-axially to engage the soil in both directions. Bi-axial loading accounts for the skew of the bridge and for the arbitrary direction of seismic loading. Soil springs were added to account for the lateral contribution of the passive resistance of the pile caps, which is not otherwise included in the analysis. These soil springs are based on the p-y curves of the appropriate layer of soil, which are generated by FB-Multipier based on soil properties as defined in the drill logs. For the bent foundations, a single spring in each direction represents positive and negative displacement for each axis. However, the behavior of the abutment (Figure 2-15) is more complicated, as the stiffness is much different along each axis. Furthermore, the passive resistance of the backwall applies only when the structure pushes the backwall against the soil. This uni-directional behavior requires the use of gap elements in SAP, which have no resistance in the "open" direction, to represent the backwall contribution. The gap elements were assigned an equivalent linear stiffness based on the calibrated displacement of the FB-Multipier foundation springs. A soil spring is still used in FB-Multipier abutment model to represent the resistance of the soil in the transverse direction, which indirectly accounts for the effect of the wingwalls. Not modeling the wingwalls directly is a reasonable assumption since the relative stiffness of the wingwalls is small compared to the backwall.

To determine the stiffness for each type of soil spring, the p-y curves, which are based on a unit area, are multiplied by the area of the face of the corresponding element (the pier pile cap or backwall) to obtain the total stiffness of the spring. To summarize, the SAP models includes one spring for each bent pier foundation - a foundation spring, representing the stiffness of the pile group and lateral passive resistance of the pile cap - and two springs for each abutment foundation - a similar foundation spring and a uni-directional spring representing the one-way passive resistance of the backwall.

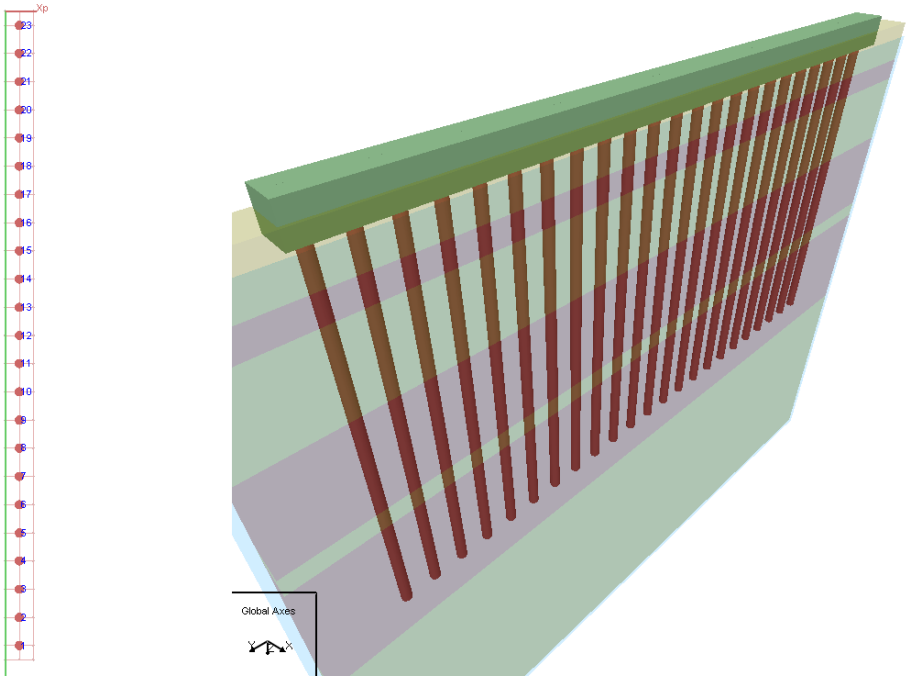

Figure 2-15: FB-Multipier Abutment Model Definition

The analysis procedure used to determine the pushover curve and foundation spring properties is as follows. The pushover analysis involves a series of incremental analyses of the foundation model, with a constant load increment defined as a percentage of the total expected lateral loads. The lateral load and average lateral displacement of the pile heads at each load step are recorded. The loading applied for the pushover analysis begins at a fraction of the expected lateral load and is incremented until the pier fails. Note that overturning moments were also applied and increased proportional to the lateral loads during the pushover analysis, since the load application point of the lateral seismic force is well above the foundations. The response was verified to be continuous under the design loads; that is, that neither the pile group nor any of the soil layers failed until several times the design load was applied, resulting in a smooth pushover curve. The abutment foundation consists of a single line of piles, and therefore the strength and associated lateral stiffness is expected to be directionally dependent. Therefore, pushover analysis for the abutment foundation was performed separately along each axis of displacement.

Following the pushover analysis, a stiffness analysis was performed, which generates the stiffness matrix. For a stiffness analysis, the analysis type is changed from "Pushover" to "Stiffness", and the appropriate loading is applied to an automatically generated central node in

the cap, in accordance with program documentation. The foundation response is nonlinear, and an appropriate estimate of the equivalent linear properties at the design displacement is required to define linear elastic springs for the elastic SAP analysis. Since FB-Multipier gives a tangent stiffness instead of secant stiffness, the loading for the stiffness analysis must be computed at a point on the pushover curve where the tangent stiffness is equal to the secant stiffness at the expected peak load. Figure 2-16, which is based on simplified loading of the pier model, illustrates the process of finding the appropriate tangent point on the pier pushover curve. The pushover curve in Figure 2-16 was generated by incrementing the axial load, lateral load, and moment by 5% of the peak expected values at each step. These loads were applied at a 45-degree angle to engage the soil in both directions. After determining the loading point on the pushover curve used to define the secant stiffness, a point on the curve was identified where the tangent stiffness is approximately equal to the secant stiffness. The point where the tangent slope is parallel to the average slope out to the foundation load capacity determines the lateral loading to be input for the stiffness analysis.

The actual pushover curves for the foundations are based on loading from analysis of the calibrated SAP model. Using capacity design principles, the lateral seismic force transferred to the pier foundations are limited to the shear capacity of the column. Separate pushover curves were generated for vertical and lateral loading. A pre-load case was added to each directional analysis, wherein the entire load was applied initially in the orientation not under investigation, while the load in the direction under consideration was increased by 5% increments. This type of loading, which engages the soil in all directions, more accurately represent real-world conditions. As a result, the pushover plots reflect non-zero initial load and displacement. Use of a pre-load case is also required to calibrate the soil springs for the stiffness calculation; otherwise, the lateral resistance of the pile caps is not included in the resulting stiffness matrix.

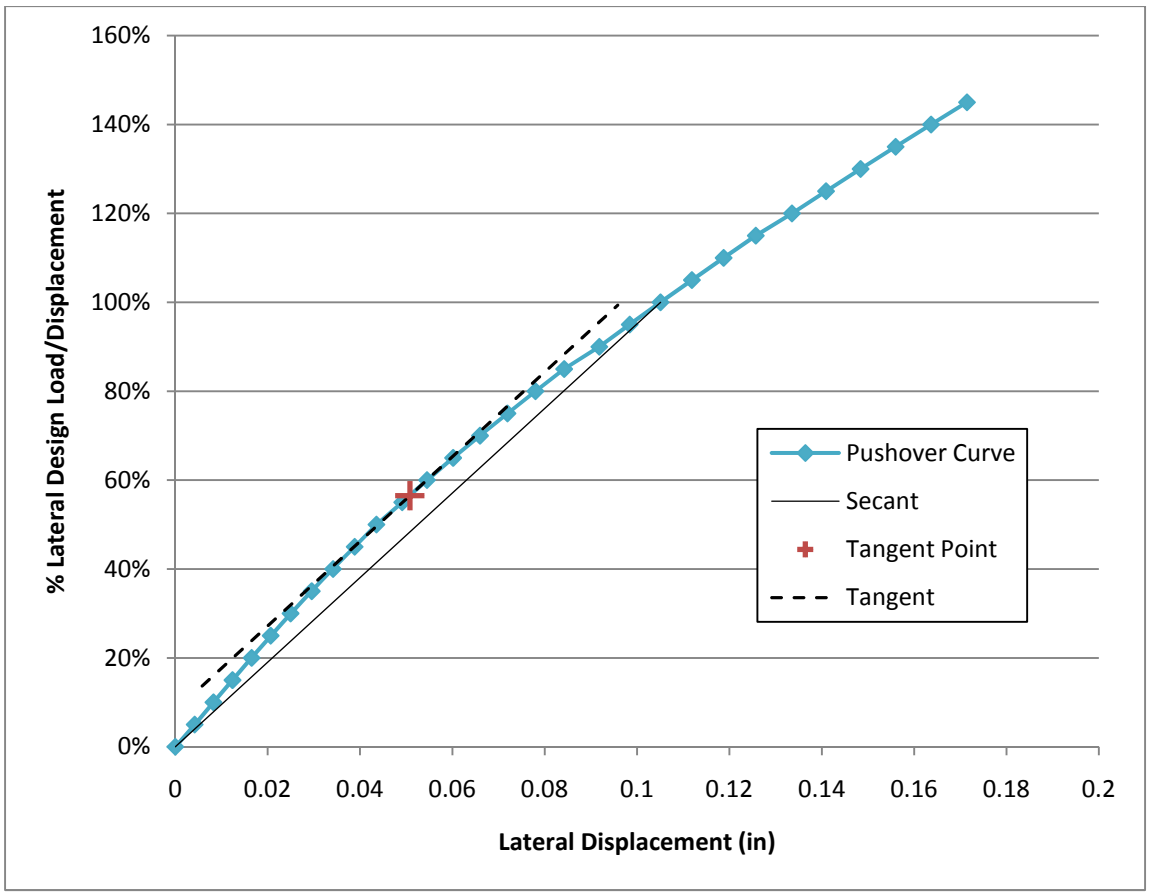

Figure 2-16: Pier Foundation Pushover Curve with Calibrated Secant and Tangent Stiffnesses

Figure 2-17 and Figure 2-18 show the lateral pushover curves for each model, with a separate curve shown for each direction of loading. The pier stiffness differs only slightly in each direction, because the loading is not equal in each direction, which is also reflected in the differing displacement values. The geometry of the abutment foundation (a single line of piles) and the backwall contribution account for the significant difference in slope of the abutment pushover curves.

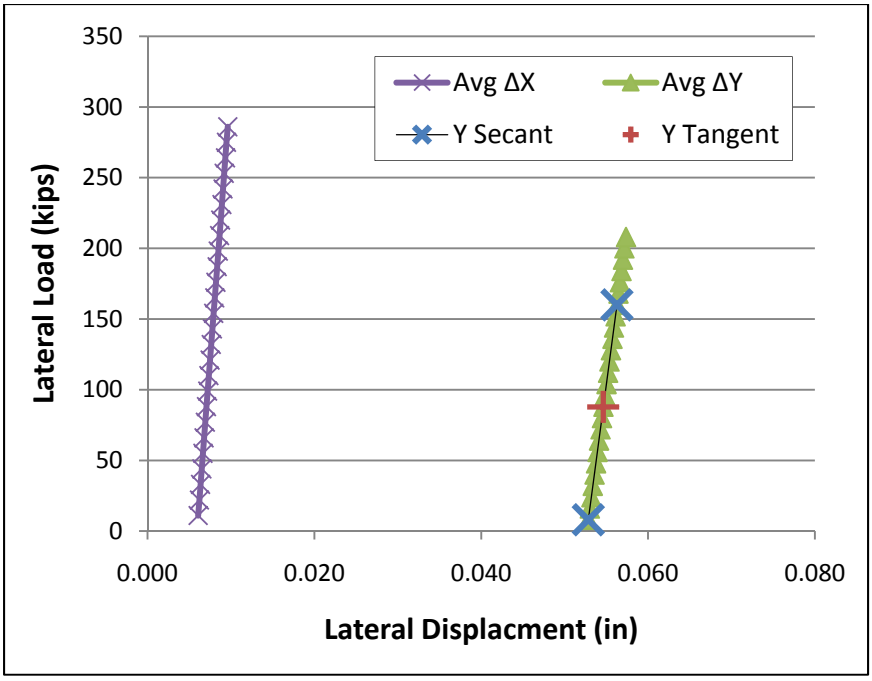

Figure 2-17: Lateral Pier Pushover Curves

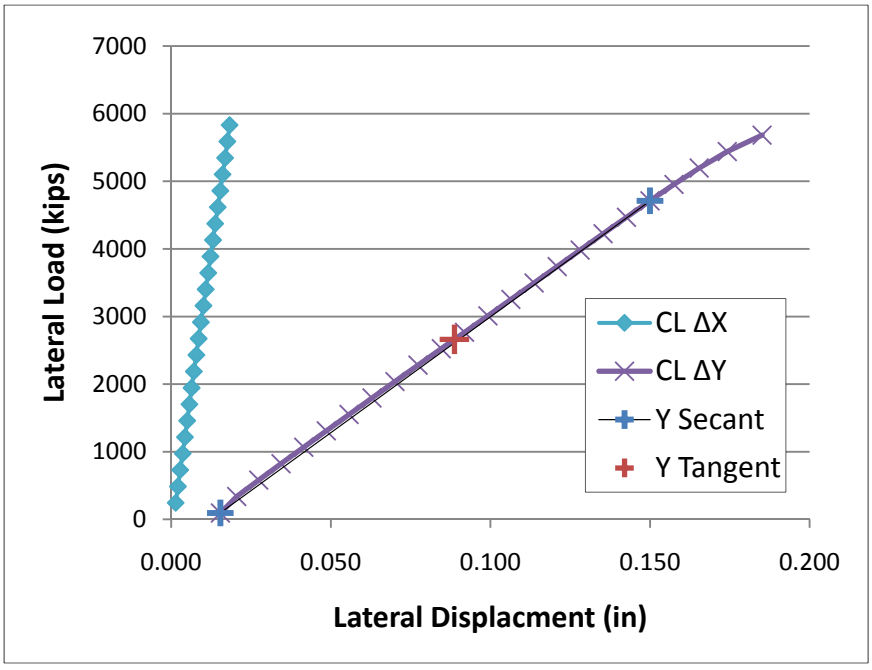

Figure 2-18: Lateral Abutment Pushover Curves

The longitudinal stiffnesses of both foundations remain nearly linear in the regions considered for tangent stiffness; the secants lie almost directly on each of the pushover curves,

with only a slight variance observable on the abutment Y curve. The tangent points are found mathematically using the procedure described above; the secant is taken from the initial loading point to the location corresponding to 100% of the design loads (shown only on the Y curves). The tangent point for each foundation is again taken at the point of loading where the tangent is parallel to this secant line, which was found to occur at 55% of the design load for the piers, and 58% for the abutments.

Based on the input lateral loading, an FB-Multipier stiffness analysis of the pile group generates a 6x6 stiffness matrix for an equivalent foundation spring. The final, calibrated stiffness matrices resulting from the iterative FB-Multipier analysis are presented below in Table 2-6 and Table 2-7 for the pier and abutment foundations, respectively.

Table 2-6: Pier Foundation Stiffness Matrix

	ΔZ	ΔX	ΔY	θZ	θX	θY
Fz	55,720	10	3	8	-82,260	-14,250
Fx	10	5,655	0	337	-4	264,400
Fy	3	0	4,879	-692	-237,600	-6
Mz	8	337	-692	81,000,000	-21,750	-33,090
Mx	-82,260	-4	-237,600	-21,750	439,800,000	-116,500
My	-14,250	264,400	-6	-33,090	-116,500	440,800,000

Translations: kips/in Rotations: kip-in/rad

Table 2-7: Abutment Foundation Stiffness Matrix

	ΔZ	ΔX	ΔY	θZ	θX	θY
Fz	35,290	-26	-13	-443	-104,900	9,559
Fx	-26	2,552	-8	-9,226	1,288	156,300
Fy	-13	-8	1,656	-4	-118,800	-778
Mz	-443	-9,226	-4	255,800,000	2,428,000	-306,900
Mx	-104,900	1,288	-118,800	2,428,000	3,567,000,000	-25,840
My	9,559	156,300	-778	-306,900	-25,840	16,270,000

Translations: kips/in Rotations: kip-in/rad

The stiffness matrix generated by FB-Multipier was used to define a foundation spring stiffness matrix in the SAP model. The terms were rearranged to convert from the local foundation coordinates in FB-Multipier to the local axes of the SAP spring elements. FB-

Multipier uses standard X-Y-Z axes, where the Z-axis is the vertical axis, while the SAP spring elements are defined with 1-2-3 axes, where the 1-axis corresponds to the vertical axis for a zero length spring. Accordingly, X-Y-Z components were converted to 2-3-1 components through standard matrix transformation approaches.

The iterative calibration procedure mentioned above is described here in more detail. After analysis of the initial model was performed using the estimated lateral loading, the foundation springs were adjusted iteratively to calibrate the stiffness to the actual foundation demands. In successive iterations, the forces for each spring element generated by SAP analysis replaced the estimated loads in the FB-Multipier stiffness models, and the effective stiffness of the soil springs was adjusted to match the calculated foundation displacements. The analyses were then repeated, and the soil springs and foundation stiffness matrices recalculated and corrected in SAP. Both the SAP and FB-Multipier models were adjusted iteratively until the results were within an acceptable tolerance. As the SAP generated loads were used for the initial load estimates, the terms in the stiffness matrices associated with lateral movement converged within a few iterations. Figure 2-17 and Figure 2-18 are the pushover curves and equivalent properties for the final calibrated foundation springs, while Table 2-6 and Table 2-7 indicate the final calibrated stiffnesses of the foundation springs that are used throughout the remainder of the analysis discussion.

2.4 Bridge Response Characteristics

After creating the SAP model using the elements described above, the SAP model was analyzed to find the characteristics of its response. The model was adjusted iteratively until all spring elements were assigned appropriate properties; only the calibrate model will be discussed. Modal analysis was performed to determine the natural modes and periods of the structure; a sufficient number of modes have been included to account for more than 90% of the modal mass in the horizontal plane (Table 2-8). The first few horizontal mode shapes were checked visually to ensure that the bridge response indicated is realistic. Aerial views of these mode shapes (against a wire shadow of initial position) are shown in Figure 2-19.

Table 2-8: Modal Analysis Results – Periods and Directional Mass Participation

Mode	Period (sec)	X	Y	RZ
1	0.400	76.0%	17.5%	27.8%
2	0.309	15.8%	67.6%	19.3%
3	0.259	1.8%	12.3%	48.1%
	Sum:	93.6%	97.4%	95.1%

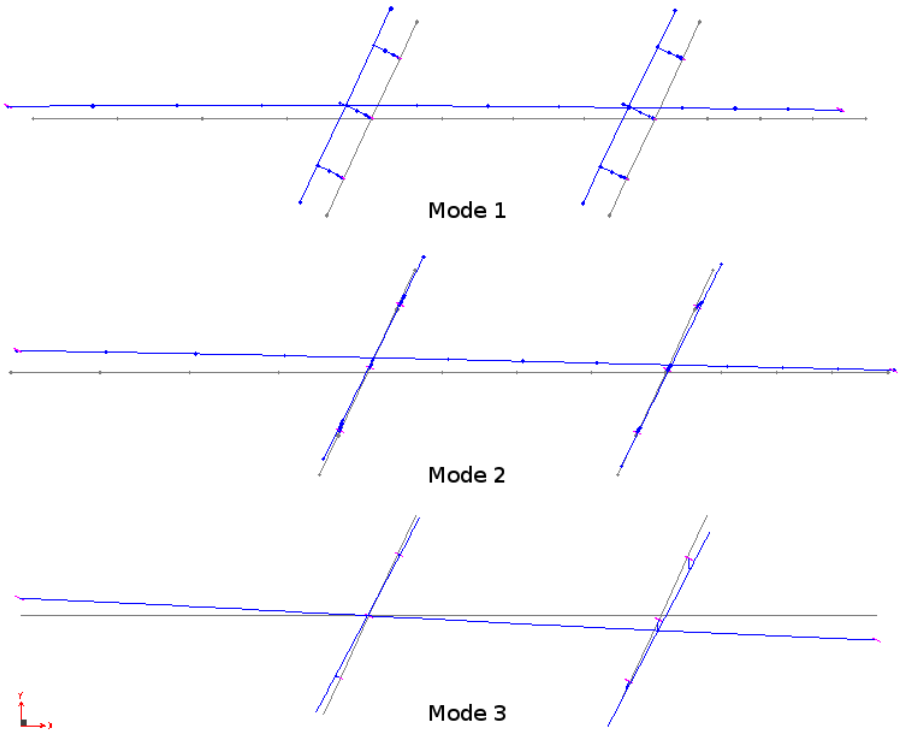

Figure 2-19: First 3 Mode Shapes of the Legacy Bridge

The first mode is primarily transverse, in the weak direction of the bents, while the second and third modes are rotational in the horizontal plane, and together these modes constitute nearly all of the lateral response. The rotation is due to the skew of the foundations; as the bridge moves longitudinally, the resisting abutments response is perpendicular to the skew angle, creating a twisting force on the bridge, while the trailing abutment, being weak in the transverse direction, provides little resistance to rotation about the other abutment. The periods associated with these modes are 0.400, 0.309, and 0.259 seconds, respectively. As expected, the fundamental periods are located in the constant acceleration region of the design spectrum,

which indicates that the existing structure will experience high lateral loading during an earthquake.

To verify that these results are reasonable, the structure's period was estimated based on its mass (m) and the stiffness (k) of the bents, since the majority of the bridge flexibility is contained within the bents. Since the bent caps and foundations are much stiffer than the columns, the bent stiffness in the transverse direction can be approximated as 3 times the stiffness of a single fixed-fixed column, which is given as $12EI/h^3$. For the longitudinal direction, the stiffness is estimated based on a fixed-free column, which is $3EI/h^3$. The clear height of the column, h = 19 feet, and EI for the columns, computed in Section 2.3.3, is about 7.5 million kip-ft^2, giving a lateral bent stiffness of about 39,320 k/ft in the transverse direction and 9830 k/ft in the longitudinal direction. The weight applied is taken from the maximum bent dead load determined by SAP, and is roughly 4400 kips. The period is estimated using the equation for a single degree of freedom system, $T = 2\pi\sqrt{m/k}$, where m is the weight from SAP divided by the acceleration of gravity. The resulting estimated period is 0.37 seconds for the transverse direction, and 0.74 seconds for the longitudinal direction. The transverse estimate is fairly close to the computed periods for transverse motion, while the longitudinal period is much longer. The discrepancy is justified since the approximation includes most of the seismic mass (all mass carried by the bridge piers) but entirely neglects the stiffness of the abutments, which is substantial and would significantly reduce the computed period if included. Furthermore, the first and mode period produced by the SAP model includes coupling in the longitudinal and transverse direction, which the approximate calculation does not account for.

2.5 Pushover Analysis and Capacity Determination

A pushover analysis was performed to determine the displacement capacity of the structure, which is controlled by the bents. The displacement capacity is determined based on appropriate acceptance criteria. The Seismic Spec does not suggest acceptance criteria for operational performance objectives. Therefore, we consulted the LRFD Spec, which requires a response modification factor R = 2 for operational performance. Using typical R-μ-T relations (Chopra, 2003), the expected ductility consistent with R = 2 and an estimated bridge period T = 0.4 sec, is:

$$\mu = \frac{(R^2 + 1)}{2} = \frac{(2^2 + 1)}{2} = 2.5$$

Based on this result, and incorporating engineering judgment, we adopt an allowable ductility capacity of $R = 2$ to meet the bridge performance objectives.

Since the displacement demand of the bents is beyond the elastic capacity of the columns, a non-linear analysis is required. A non-linear model of a single bent was created, using the same element definitions and bent cap constraints as for the complete bridge model. Plastic hinges were defined at the top and bottom of end of each column to accurately represent lateral deformation behavior, based on moment-curvature relation from the section analysis and a calculated plastic hinge length. The hinge length is defined by Equation 4.11.6-1 of the Seismic Spec; for this situation, the equation was controlled by the lower bound, $L_p \geq 0.3 f_{ye} d_N$, where f_{ye} is the expected yield strength of the steel (60 ksi) and d_N is the nominal diameter of the longitudinal reinforcing bars in the column (1.27 inches for #10 bars), giving a plastic hinge length of 23 inches. Because plastic hinge behavior depends on the axial force on the cross section, a separate hinge model was defined for each column to account for different axial loads from overturning moment in the transverse direction. The maximum factored axial loads were extracted from the SAP analysis data, which include both the maximum and minimum axial column loads (due to overturning effects). Moment-curvature analysis was then executed in SAP for each column in order to account for varying section behavior under different axial loads, and the resulting curve data compiled in a spreadsheet for further analysis. Figure 2-20 plots the moment-curvature curves for each column load with the curve for zero axial load shown for reference, which illustrates that the column axial capacity increases with axial load up to the maximum axial load applied in the analysis.

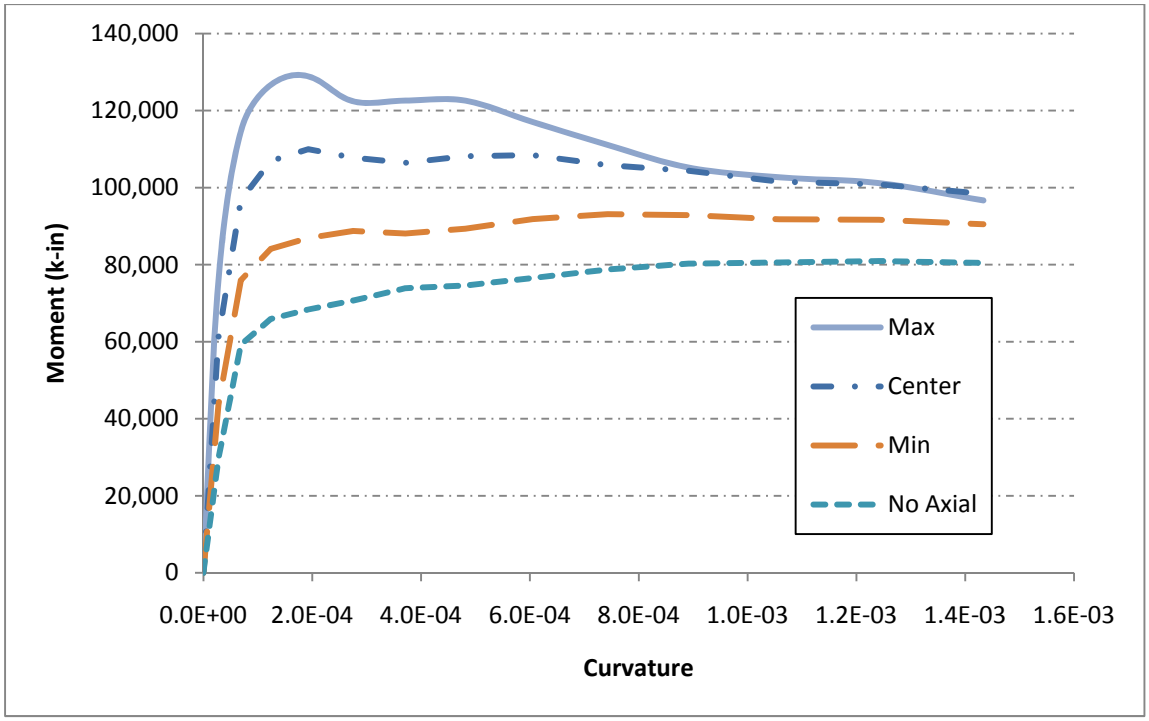

Figure 2-20: Moment-Curvature Analysis of the Bridge Column for Varying Axial Loads

Section 8.5 of the Seismic Spec provides guidance for modeling the moment-curvature response of a RC member for pushover analysis. In accordance with this section, an idealized elastic-perfectly plastic moment-curvature response for a section was created by defining an equivalent plastic moment that balances the areas of energy dissipation between the idealized and actual moment-curvature curves (Figure 2-21). This process was automated through spreadsheet formulas that automatically compute the areas between the plastic moment approximation and the actual curve data points, based on an initial guess for plastic moment, and use the built-in Solver functionality to find the plastic moment that results in equal areas above and below the M_P approximation.

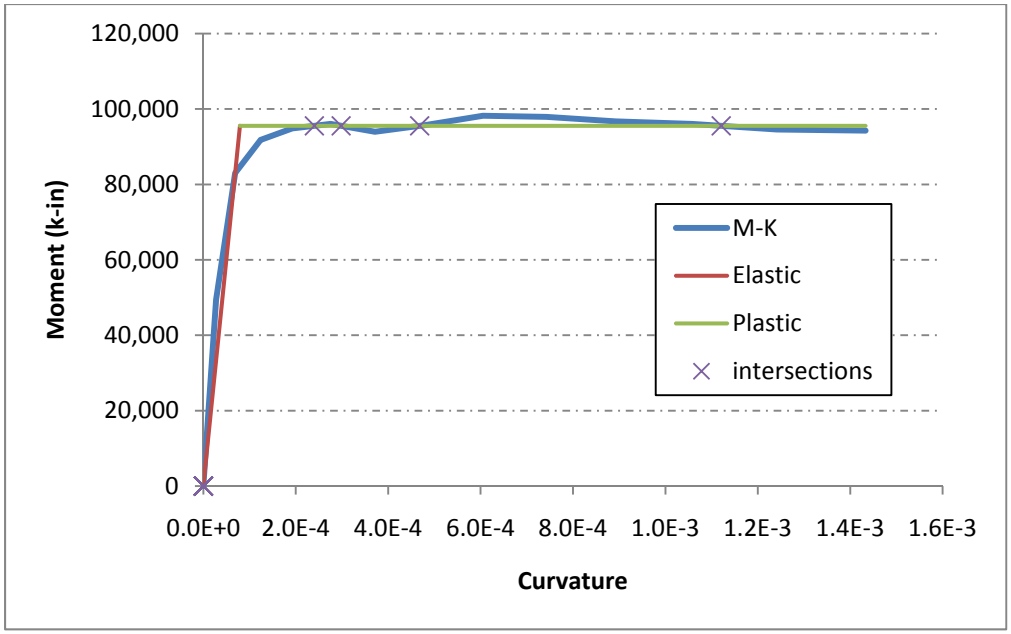

Figure 2-21: Sample Idealized versus Actual Moment-Curvature Relation

The axial loads and corresponding plastic moments and associated yield curvatures are listed below in Table 2-9. These properties were used to define the elastic, perfectly plastic hinges for the corresponding column in the SAP pushover model. The hinges all have the same length, as determined above.

Table 2-9: Plastic Hinge Parameters

	Axial Load (k)	M_p (k-in)	Curvature □
Low	746	90,414	8.183E-05
Mid	1799	104,648	7.437E-05
High	2851	114,012	6.845E-05

After defining the hinges, a non-linear pushover analysis was executed in the longitudinal and transverse directions to determine yield force and ultimate capacity of the bent, and the pushover curves are shown in Figure 2-22. The axial column forces given by this analysis did not change significantly from the initial estimates. As expected, the bent frame is much stiffer in the transverse direction. The yield displacement of the bent was defined as the displacement at which the first plastic hinge forms, which is 0.408 inches in the transverse direction and a displacement of 0.553 inches in the longitudinal direction. The column displacements are

calculated using the entire bent model, including foundation springs; therefore, the displacements indicated include the contribution of the foundation springs. The displacement demands will also presented as total displacement at the top of the bent, including bent columns and foundation elements. Using the allowable ductility capacity $\mu = 2$ determined above, the displacement capacity according to the Seismic code is 0.817 inches in the transverse direction and 1.106 inches in the longitudinal direction. The displacement capacities are compared to the displacement demands from response spectrum analysis determined in the next section.

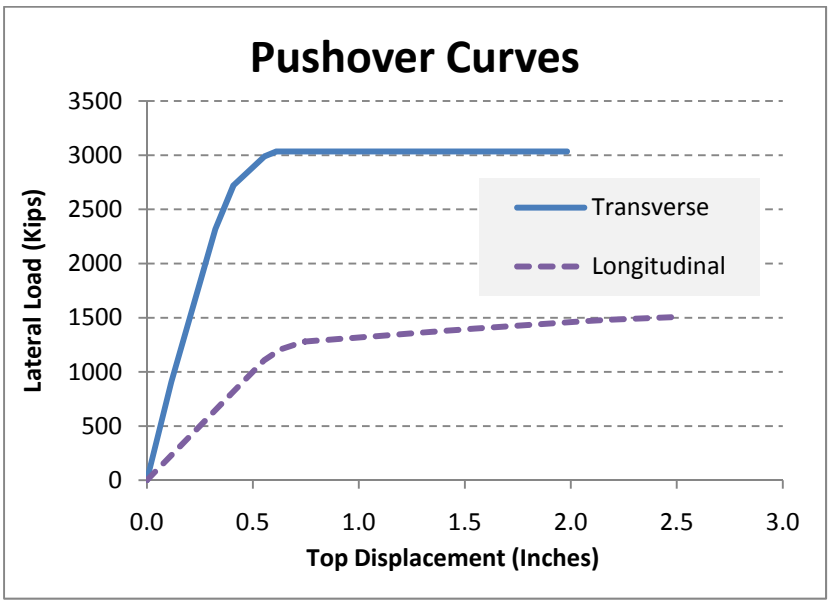

Figure 2-22: Bent Pushover Curves

2.6 Response Spectrum Analysis and Demand/Capacity Check

Following the pushover analysis to determine the capacity, response spectrum analysis was completed to determine the demands. If yielding occurs in the bridge, the force demands will not be accurate, but displacements predicted by the analysis represent the actual displacement demands according to the equal displacement rule. Several iterations of response spectrum analysis were performed, integrated with the calibration process for the foundation springs as described in Section 2.4. The results reported here represent the final converged values.

Recall that the three periods associated with the lateral response of the bridge, determined after iterative analysis and calibration of the foundation springs, are 0.400, 0.309, and 0.259 seconds, which are all in the constant acceleration region of the spectrum. These modes account for over 90% of the total participating modal mass for horizontal motion; the seismic response is almost entirely defined by these modes. A CQC modal combination rule was used to combine the peak responses in different modes. For bidirectional effects, two load cases were considered: 1) 100% of the displacement in the longitudinal direction combined with 30% of the displacement in the transverse direction, and 2) 100% of the displacement in the transverse direction combined with 30% of the displacement in the longitudinal direction (Sec. 4.4 of the Seismic Spec).

The final results over all load combinations were analyzed to find the maximum demands on the structure. The peak displacement demands of the bent considering both bidirectional load combinations are 0.60 inches in the transverse direction and 0.26 in inches in the longitudinal direction. Comparing these demands to the allowable displacement capacities found in the previous section (0.817 and 1.106 inches) produces demand-capacity ratios of 0.74 in the transverse direction and 0.23 in the longitudinal direction. For the transverse direction, the peak displacement demand is shown on a plot of the bent pushover curve (Figure 2-23). Since the demand-capacity ratios are less than one, the column design satisfies the performance objective according to our interpretation of the code requirements. (Interpretation was required since specific acceptance criteria was not given by the Seismic Spec for higher performance objectives.) However, the maximum lateral force capacity has been reached, implying that several of the columns form plastic hinges. If multiple full plastic hinges have formed, we question whether the bridge would actually provide the performance that has been targeted. For instance, plastic hinge formation in a column would be accompanied by significant spalling of the outer shell of concrete, and the substructure of the bridge would likely require extensive inspection and major repair after the design event. On the other hand, the analysis is based on nominal material properties, and material overstrength has not been included in the analysis, such that the response in the design event may be better than predicted. This performance provides a basis for comparing the alternative approach using seismic isolation.

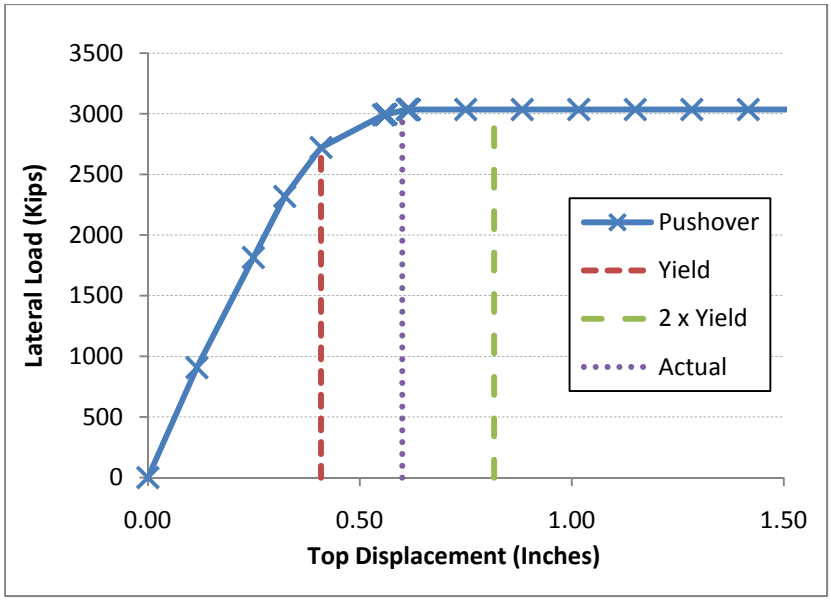

Figure 2-23: Pushover Yield Displacement Comparison in Transverse Direction

The foundation response is not required to be evaluated under the global demand/capacity procedure used by the Seismic Spec; however, the foundations would normally be designed to remain elastic when subjected to the maximum forces that could be transferred from the piers, which are determined by the column lateral capacity. In essence, the pile group evaluation was already completed in Section 2.3.4, which described the development of equivalent spring models to represent the foundation properties. Figure 2-17 illustrated that when the pier foundation is subjected to lateral forces that equal or slightly exceed the column capacity, the force-deformation curve is nearly linear. The nonlinearity of the foundation pushover curves is due to the non-linear response of the soil; however, no yielding occurs in the piles or pile caps under the design loads. For completeness in investigating the Legacy Bridge, the foundation capacities will be formally verified, including pile group capacity and pile cap strength. The strength of individual piles was already accounted for in the analysis of the pile group.

To check lateral capacity, the lateral forces and corresponding moments were increased in FB-Multipier pushover analysis until failure of the pile system. The vertical (dead and live) loads were applied and held constant, and the lateral (seismic) forces incremented until failure, which was found to occur at 5.5 times the design load for the piers, and 1.3 times the design load for abutments. Since the pushover analysis does not include manual safety factors for the soil, these values are considered to be equivalent to a design safety factor. The inclusion of the

wingwalls in the stiffness analysis might increase the estimated transverse strength of the abutments, however, based on the plans, we concluded that the wingwalls were not sufficiently strong to act integrally with the rest of the abutment.

The pushover process was repeated to find vertical capacity, this time applying full lateral loads and incrementing the vertical loads. For this procedure, the actual pushover curves were not generated, but the point of failure was found, which occurs when the program can no longer find a solution. The failure point is reported as a scalar multiple of the incremental loads, added to the initial loading. The total vertical failure load was found to be 9 times the maximum vertical design loads for the abutments, and nearly 80 times the maximum vertical load for the piers. Clearly, the design was laterally controlled.

The capacity of the pier pile caps to resist one-way shear, punching shear, and bending moment was verified using the parameters given in Section 5.13.3 of the LRFD Spec. The maximum factored loads from the SAP analysis were used to determine the demands on the pier cap. The capacity of the abutment cap was not evaluated, as it is integral with the diaphragms at the ends of the deck, and moment and shear loads are distributed more evenly over the entire abutment foundation, transferring the load almost directly to the piles.

One-way shear in the pier cap was evaluated at a vertical plane located d_v away from the column face, where d_v is the distance between the centroid of the concrete stress block and the centroid of the reinforcing steel. The self-weight of the cap and the soil above it are subtracted from the vertical capacity of the piles under the cantilevered section to determine a maximum possible shear demand on the section (2,265 kips). The demand was compared to the total factored shear capacity of the longitudinal bars and the confined concrete, which was found to be 17,560 kips, much larger than the possible demand. Therefore, the cap is sufficient for one-way shear.

Punching shear is based on the surface area of the hole that would result from the column pushing through the pier cap, which would start at the face of the column at the top of the cap, and widen in all directions at a 45-degree angle, which is the typical orientation of a shear failure. To simplify the calculation of the area, the hole is instead assumed to be square and to have vertical sides. The equivalent width of the square is computed as:

$$d_{sq} = d_{eq} + 2\frac{d_y}{2}$$

where d_{eq} is the width of a square having the same area as the actual column, and d_y is the depth of the shear face, accounting for half the depth on each side. The sides of the equivalent (square) hole are centered over the faces of the theoretical (pyramid-shaped) hole. The total area of the shear face is equal to the perimeter of this square multiplied by the shear depth of the cap, d_v. The shear capacity of the concrete and steel intersecting this hole, found to be 8,100 kips, was compared to the maximum shear that could be generated by the piles outside of the hole, neglecting the contribution of the soil and the cap's self weight, equal to 2,197 kips. Based on this, the pile cap is concluded to be sufficient for punching shear.

Finally, the moment capacity of the cap was evaluated under the assumption that the cap acts as a cantilever, fixed at the face of an equivalent column (as defined above) and free at the ends of the cap. The potential moment acting on this plane is computed by taking the maximum factored vertical capacity of each pile (given as 400 kips in the plans) resisting the movement of this cantilever multiplied by its lever arm, and subtracting from this moment the moment induced by the self-weight of the cap and the soil above it. The resulting moment was found to be 23,780 k-ft. (Although the pile cap is capacity-protected by the column capacity, the maximum possible moment of the pile group is used for pile cap design.) This moment is resisted by the concrete in compression and reinforcing steel in tension, just as in a typical concrete beam. Whitney's stress block approximation is used to evaluate the moments on the beam section, assuming that the thickness of the cap is sufficient and the location of the reinforcing steel is appropriate. The height a of the stress block and the area of tensile reinforcing steel A_s required to resist this moment are linked by two equations:

$$a = \frac{A_s f_y}{0.85 f_c' b} \qquad A_s = \frac{M_u}{\phi f_y (d - a/2)}$$

where b is the width of the cap, f_y is the strength of steel, M_u is the factored moment found above, and d is the distance from the top of the cap to the centroid of the reinforcing steel. Solving for the two unknowns gives a stress block height a = 5.1 inches and an area of steel A_s = 83.3 in^2. The calculated area of steel would require 66 #10 bars in each direction, whereas only 47 #10 bars are provided in each direction, indicating that the cap reinforcement is insufficient. Alternatively, the cap could be thickened, increasing the area of the concrete stress block and the length of the moment arm between the resisting elements. However, as the cap is more than

sufficient in shear, additional steel is the preferred approach, unless spacing requirements or material and construction costs dictate otherwise.

This evaluation indicates that the design of the pier foundations is adequate under the new requirements, except for the additional reinforcing steel required for the pier cap. However, the abutment design may be inadequate, as it failed laterally at only 1.3 times the design load. This is not considered a sufficient factor of safety to account for uncertainty in the geotechnical analysis; typical safety factor values are usually on the order of at least 2 or 4 to allow for the high variability of soil that is likely to be present, as well as the difficulty of accurately calculating soil properties from minimal testing information. As previously mentioned, this might be moderated by inclusion of the wingwall contribution, but due to uncertainty about the detailing of the wingwall connections, we chose not to include them. A more dependable approach would be to add a second row of piles, which is expected to roughly double the cost of the abutment foundations.

THIS PAGE INTENTIONALLY LEFT BLANK

3. Design of Isolated Bridge

After evaluating the Legacy Bridge in its as built configuration, we redesigned this bridge to incorporate an isolation system. We used a procedure comparable to that used for the original Legacy Bridge in the design and evaluation of the Isolated Bridge. A spine model was developed using members and assumptions identical to the Legacy Bridge where applicable, and modified as necessary to incorporate configuration changes, member sizes, etc., chosen for the Isolated Bridge. The reader is referred to the relevant portions of Chapter 2 for the detailed description of the modeling procedure and assumptions. This chapter describes the overall design and evaluation of the Isolated Bridge, including configuration changes, structural element modifications, and expected response. However, the procedure is not highly dependent on the isolation system design, as a number of different devices could provide the target response characteristics of the Isolated Bridge. Subsequently, Chapter 4 describes the theory and design process for the isolation devices, and present sample designs for several different isolation devices commonly used in the United States.

3.1 Methodology Overview

The historical design philosophy for bridges has been to design the bridge substructure, which is the primary lateral resisting system, for reduced forces relative to the forces required to provide elastic or damage free response. As described in Chapter 2, this conventional approach has been replaced by a displacement-based approach in the new Seismic Spec. However, the LRFD Spec still adopts a force-based approach for seismic design. Under the LRFD spec, the prescribed response modification factor is $R = 2$ for an Essential bridge, which was accounted for in the preceding displacement-based analysis of the existing Legacy Bridge. For comparison, a bridge classified as Standard would be designed for $R = 3$. The Isolation Spec also uses a force-based approach. The Isolation Spec prescribes that the force reduction factors should be half of the values prescribed in the LRFD spec, but need not be less than 1.5. However, in our judgment, a bridge classified as Essential should be damage free in the design (1000 year) earthquake, and providing the better performance does not greatly affect the cost for an isolated

bridge. Thus, a force reduction factor $R = 1.0$ was used in the design of the substructure. The substructure design forces for an Essential bridge both with and without isolation are compared in Section 3.3.

Section 7 of the Isolation Spec provides guidance on the selection of an analysis procedure and essentially defers to the LRFD Spec. For a bridge in Seismic Zone 4 classified as Regular in configuration and performance category of Essential, a multi-mode elastic method of analysis is recommended for demand determination. Time history analysis is required only if the effective period exceeds 3 seconds or the system is highly damped such that the effective damping ratio exceeds 30%, which as will be shown later, are beyond the target parameter ranges for this bridge. Because the bridge site is located within 6 miles of an active fault, a site specific procedure is recommended, but was not adopted here so that the comparison of the Isolated Bridge is consistent with the evaluation of the existing Legacy Bridge. For capacity determination, we used a component evaluation procedure to show that the substructure elements remain elastic.

The incorporation of an isolation system greatly reduces the seismic demands to the overall bridge, and allow for significant reductions to the stiffness and strength of the substructure even while providing elastic response. Initially, the response of the Isolated Bridge was evaluated assuming column and foundation elements are unaltered. Following this, reduced designs for the column and foundation elements have been proposed and substantiated by numerical analysis. Finally, the response of the Isolated Bridge was re-evaluated following the design change, and confirmed to meet the design objectives. If changes to the column size are undesirable, such as for aesthetic reasons, modifications to the column reinforcement size and spacing could be pursued as an alternative.

3.2 Bearing Locations and Configuration Changes

For seismic isolation applications, isolation devices are generally placed at the top of the columns or bent cap just below the girders. However, for certain types of bridges, such as lightweight bridges, the placement of an isolator under each girder is acknowledged to be problematic because the load carried per isolator is low (Buckle et. al., 2006).

The Legacy Bridge is representative of the class of lightweight bridges because it consists of relatively short spans and has 11 girders across each span. Placing an isolator under each

girder at both abutment ends and both bents would require a minimum of 44 bearings. If expansion joints were used at the bents, the number of bearings would increase to 66. Using this many bearings is cost prohibitive for a routine 2 or 3 span highway bridge. The majority of isolated bridge applications to date have been larger, higher profile bridges, but seismic isolation of smaller bridges is still beneficial and the design approach should therefore be cost effective. The general approach to reduce the number of bearings and increase the weight per bearing is to use a cross beam or diaphragm at the abutments and piers to connect the girders, supported on 2 or 3 isolators at each abutment seat and pier cap (Buckle et. al., 2006). The flexibility of the cross beam can introduce other problems, but these problems can be mitigated if the cross beams are very stiff.

Based on these considerations, we propose that at the bridge piers, isolators be placed at the top of each column, just below the bent cap. This configuration requires almost no changes to the geometry of the bents (Figure 3-1). The column tops would no longer be integral with the bent cap and would be more flexible in the lateral direction due to their modified connectivity; however, the isolators greatly reduce the lateral forces transferred from the superstructure, and the increase in flexibility is not a concern, as will be shown. Furthermore, locating the isolators below the bent caps allows the substantial weight of the bent cap to participate in the isolated mass of the superstructure, increasing the overall isolation effect.

The separation of the bent cap from the columns is conducive to an accelerated bridge construction approach. The reinforcement detailing of the bent caps is greatly simplified. The bent caps could be precast at ground level, and lifted into place after the isolators have been installed on top of the columns. This process should be faster and safer than forming and pouring the bent caps in place, and eliminate the time associated with waiting for the cast-in-place concrete to reach a suitable strength before continuing construction. This procedure would also be compatible with other rapid construction approaches, such as lifting prebuilt decks into place.

The Legacy Bridge has already been designed with relatively stiff diaphragms, and slight changes would allow the diaphragms to act essentially integrally with the bent caps. To achieve this, the reinforcement connecting the bent cap and the diaphragm could be modified by adding reinforcement along the outside edges. The elastomeric pads could be eliminated if thermal expansion could be accommodated by another mechanism. Integrating the bent cap with the diaphragm might even allow for a reduction in the size of the bent cap, which is primarily

determined by shear requirements, but this design detail has not been calculated here. The superstructure design, which is controlled by vertical loads, is still considered sufficient and therefore unaltered for the Isolated Bridge design.

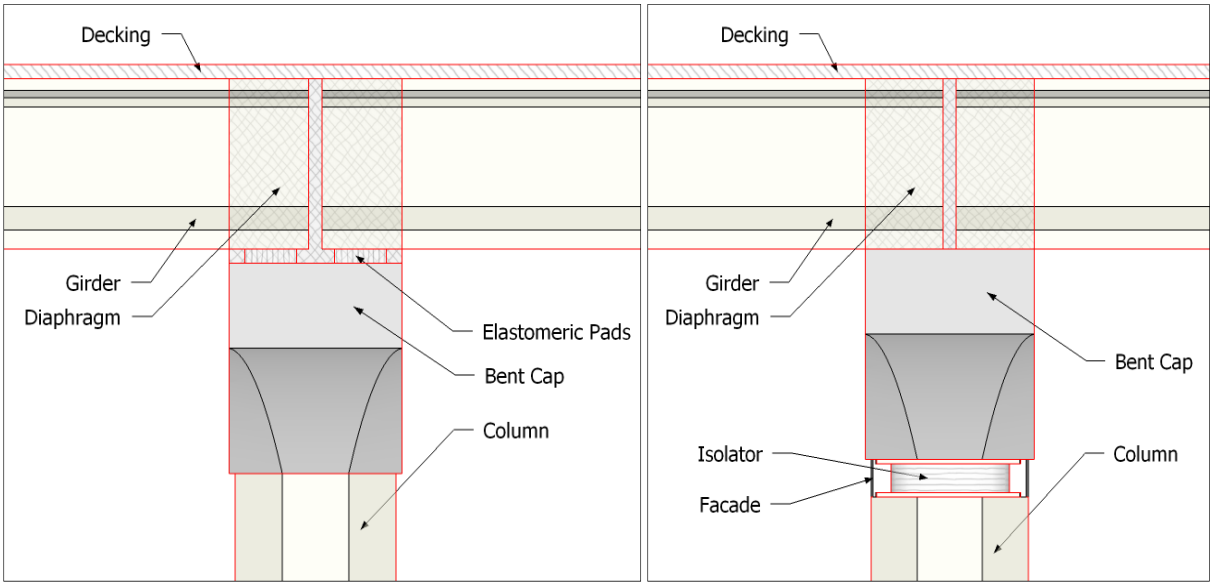

Figure 3-1 : Legacy Bridge and Isolated Bridge Bent Cross Sections

Placing isolators at the abutments requires an additional crossbeam to tie the ends of the girders together, and to transfer the load from the girders to the three supporting isolators. The crossbeam would be integral with a diaphragm connecting the girder ends. To simplify the design process, we adopt the same configuration for the abutment diaphragm/cross beam as used for the integral diaphragm/bent cap for the bridge piers (Figure 3-2). The geometry and reinforcement of these elements can be found in the bridge blueprints. This approach is conservative, as the vertical forces at the abutments are less than half of those at the intermediate bents. A more detailed design of these beams would minimize the added cost associated with these additional members, but the detailed design of the cross beams is not required for the bridge analysis.

The abutment piles and cap are lowered to accommodate the additional height of the superstructure added by the spreader beam, and the backwall is set back to provide the clear space required to accommodate the isolator design displacement (Figure 3-2). Maintaining a connection between the pile cap and backwall suggested as part of the redesign, to prevent

possible cracking due to relative displacements. The gap to the backwall must be sufficient to accommodate code-specified displacements of approximately 20 inches in the MCE event (See Section 4.2.3.2). This gap is usually bridged by extending the decking or using steel plates. Non-continuous sacrificial blocks are sometimes added to the backwall to reduce the spanning distance of the roadway (Figure 3-2); these would still accommodate the displacements of the design event, but would likely be damaged and require repair or replacement after a major event.

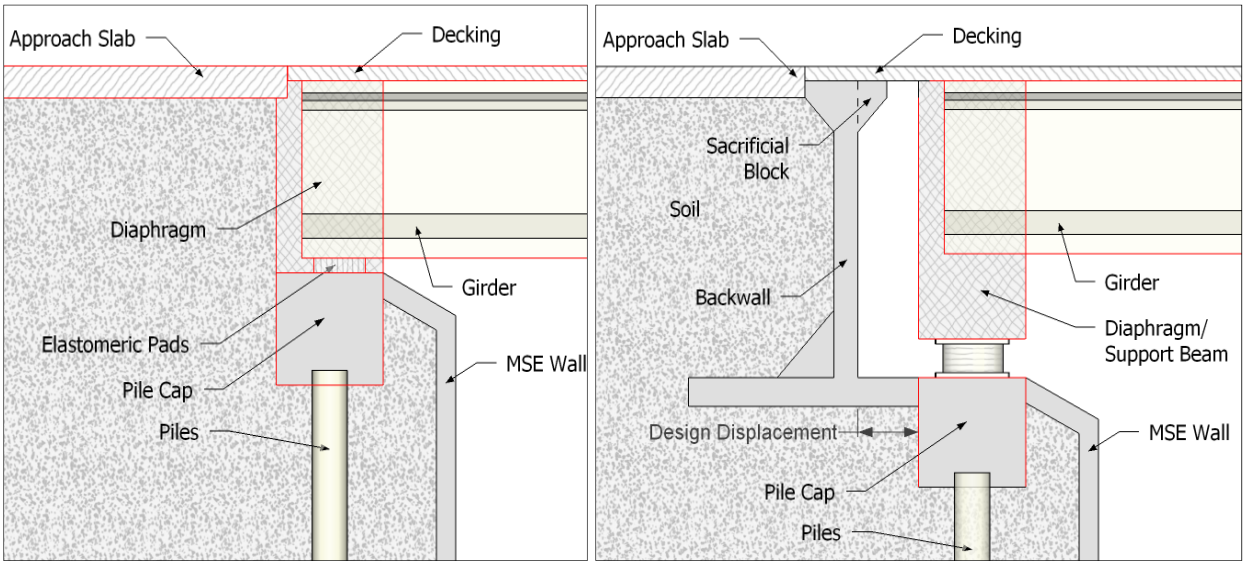

Figure 3-2: Legacy Bridge and Isolated Bridge Abutment Cross Sections

As aesthetic considerations appear to be part of the Legacy Bridge design, it may be desirable to conceal the isolators. This could be accomplished by use of a façade attached to the top of each column bent (**Error! Reference source not found.**) and a similar façade at each abutment, either with a small gap at the top to accommodate displacement or fully connected to the bent cap. A connected façade element would be sacrificial and would need to be repaired or replaced after a seismic event, but would provide more protection from the elements. Either way, these components would not affect the performance of the structure.

3.3 Initial Analysis Procedure and Results Prior to Substructure Redesign

As described previously, analysis was first performed using the columns and foundations for the existing Legacy Bridge, to generate a realistic starting point for designing the new columns and foundations. The final analysis of the Isolated Bridge, following incorporation of a redesigned substructure, is found in Section 0.

A new SAP model was created by copying the Legacy Bridge model, and incorporating several modeling changes that represent the configuration changes described above. The bent columns were shortened slightly to make room for the isolators, and the end-length offsets removed, with rigid links now representing the distance between the top of the isolator and the centerline of the bent cap. The moment release was removed from the links connecting the bent caps to the deck, as the cap is now expected to act integrally with the superstructure. The abutment foundations were lowered slightly to accommodate the isolation changes, and a beam with rigid constraints added to the end of the deck to represent the new crossbeam, which accounts for the increased weight and distributes the superstructure loads to the isolators. The rigid beam constraints were assigned to these crossbeams for reasons similar to those relating to the bent caps (Section 2.3.2); since the crossbeams are rigid, detailed design of the spreader beams was unnecessary, which is another reason the bent cap/diaphragm section was used in lieu of developing a detailed cross-section. However, the additional weight contributed by these members (19 k/ft or 1573 kips at each abutment) affects the isolator design (see Chapter **Error! Reference source not found.** for further discussion).

A rigid, massless link was attached to the bottom of the abutment isolators to connect them with the single abutment foundation spring developed in FB-Multipier. Although the lateral foundation demands for the isolated structure are expected to be much lower, the foundation springs were not changed, since the purpose of the initial model is only to determine a starting point for redesign. The calibrated model of the final isolated design includes re-calibrated foundation springs for both the abutment and the piers.

The isolator design is developed in detail in Chapter **Error! Reference source not found.**; for the SAP model, it is sufficient to define links with equivalent properties. The isolators were modeled as two joint links, with vertical, lateral, and torsional stiffnesses equal to the secant stiffnesses at the design displacement on the actual bi-linear curve. The connection of the isolators to the superstructure and to the columns/foundations is assumed to be fixed.

The dead, live and seismic loads for the Isolated Bridge were found analytically using essentially the same approach as was used for the existing Legacy Bridge. As already mentioned, the additional crossbeams at the abutments increased the unfactored dead loads at those locations; these loads were incorporated automatically to the computer model since dead loads are calculated from material properties and geometry. The live load at the abutments was applied as a distributed load to the crossbeams instead of as a point load to the foundation spring.

Similar to the Legacy Bridge, the lateral loading for the Isolated Bridge is based on the design spectrum. A standard design spectrum is based on 5% damping, which is the usual assumption for most structures. However, an isolation system incorporates additional energy dissipation to further reduce the seismic demands to the bridge, which must be accounted for when calculating the design forces. For this purpose, we recognize the target parameters of the isolation system, which have been selected as effective isolation period $T_{eff} = 2.5$ sec and effective damping ratio $\beta_{eff} = 20\%$. (Further rationale behind these selections is provided in Chapter 4). To account for the increased damping, the Isolation Spec provides that the design spectrum be scaled for the increased damping ratio over a period range corresponding to the isolation modes, or the modes at which the isolation system is engaged (as shown in Figure 3-3). The transition to reduced damping is specified to occur at a period equal to 80% of the effective isolation period. The standard 5% damped spectrum is used for the remaining modes, below the transition period, which include more structural participation.

To implement this approach correctly in SAP, the user must carefully modify the standard spectrum generated by the program by redefining individual points. While this approach correctly calculates the spectral acceleration in each mode, it is not possible to account for the modified damping ratios in the application of modal combination rules such as SRSS and CQC in a program like SAP. That is, SAP does not allow the user to directly specify damping ratios in individual modes or over specified period ranges, unless they are the same for the entire structure. The inability to replicate this effect is expected to have negligible influence on the overall response of this bridge, which is regular in configuration and dominated by a few modes. Figure 3-3 shows the modified spectrum used for the Isolated Bridge analysis.

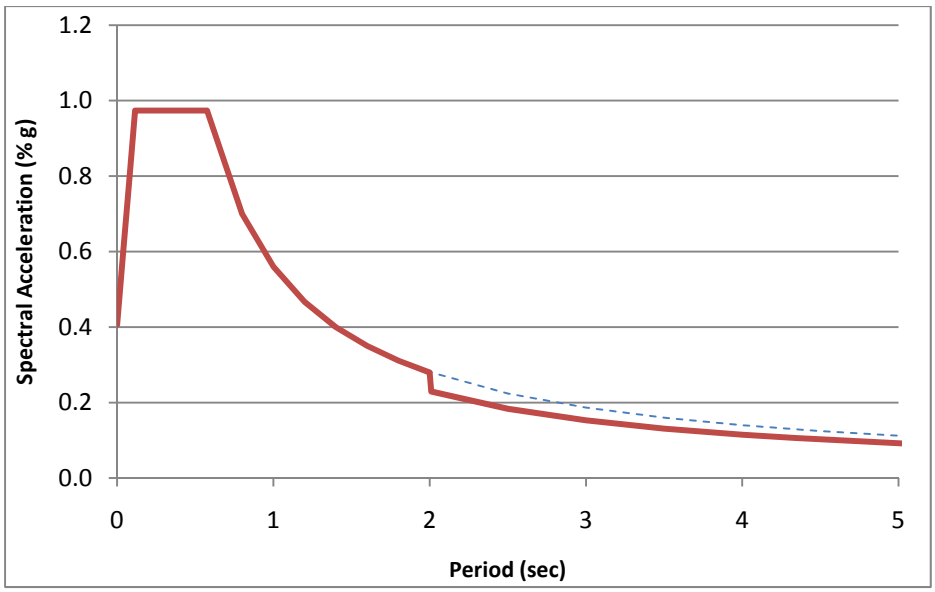

Figure 3-3: Damping Modified Design Spectrum at the Bridge Site

Based on the target period of 2.5 seconds and target damping ratio of 20%, the spectral acceleration is reduced from 0.974 for the Legacy Bridge to 0.1477 for the isolated bridge, which is only 15% of the original demand. The displacement demand under these design parameters is 9.03 inches (see Section **Error! Reference source not found.**); this is the magnitude of superstructure displacement expected during a design event. The gap included in the abutment configuration should be at least equal to the design displacement of the MCE, which is approximately 17.8 inches (see Section **Error! Reference source not found.**).

Because the weights supported by each abutment and pier are widely varying, two standard isolators have been designed, one for abutment isolators and the other for bent isolators. The response of the isolation system is characterized by a bilinear force-deformation hysteresis loop. The parameters of the loop have been chosen such that at the design displacement, the secant stiffness corresponds to the target period and the energy dissipated (area of the loop) corresponds to the energy dissipated in the target damping ratio (see Section **Error! Reference source not found.**). For linear response spectrum analysis, however, the stiffness assigned to the link elements in SAP is simply the effective stiffness or secant stiffness at the target displacement. The effective stiffness has been computed as 12.11 kips/in for the abutment isolators and 21.27 kips/in for the bent isolators at a design displacement of 9.03 inches.

An analysis of the complete bridge model was performed in SAP to determine the first several frequencies and mode shapes of the structure, as well as force and displacement demands on the isolators and other elements. The calculated isolator displacements for the initial analysis average 8.43 inches for both the abutment and bent isolators; this is a difference of about 7% from the target displacement, which is considered sufficiently close for a coarse preliminary analysis prior to substructure redesign. The natural periods for the first two modes of the isolated bridge are 2.62 and 2.47 seconds, and nearly 95% of the mass participates in these two modes of lateral response. The observed fundamental period exceeds the target period of 2.5 seconds because of the superstructure flexibility and 3-dimensional effects; however, as expected, the increase in period is relatively small. The mode shapes are depicted in Figure 3-4; the demands on the substructure are listed in the following sections as part of the redesign discussion. These modes are orthogonal and are no longer parallel to the skew of the foundations. In these modes, the superstructure moves rigidly above the isolators, while deflection in the columns is negligible and nearly all of the displacement occurs in the isolators.

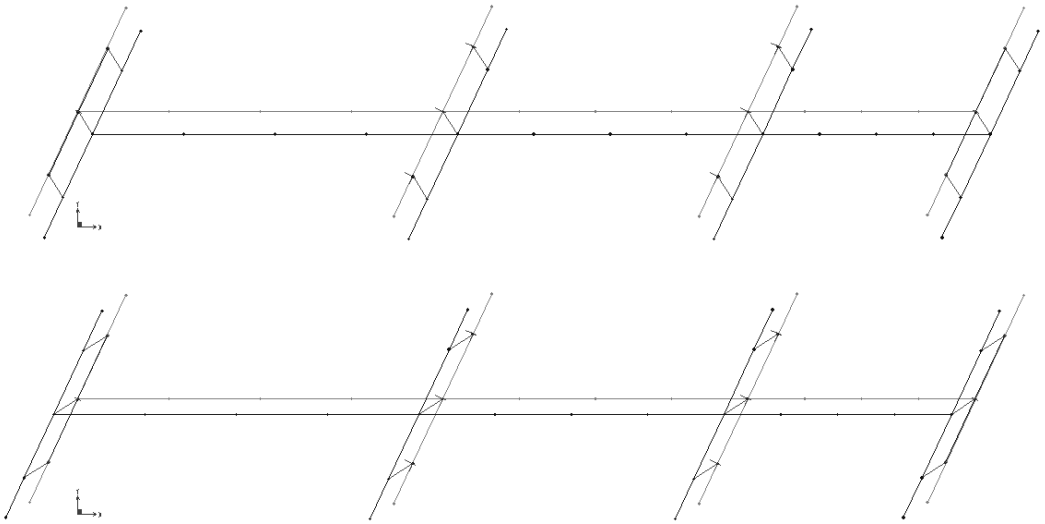

Figure 3-4: Fundamental Mode Shapes of Isolated Bridge

Because the assumed effective stiffness and damping in the isolation system may not match the values at the deformation demand observed in the analysis, an iterative procedure is required during which the effective properties are adjusted to correspond to those of the isolation system at the actual isolator deformations. However, the preliminary analysis performed here is

only for the purpose of finding approximate demands to the columns and foundation as a basis for redesign. Therefore, the results presented, both above and in Section 3.4, are for the first iteration. The force demands to the columns and foundations have been substantially reduced, and it is possible to use much smaller column and foundation elements while still meeting the objective of linear elastic response for a design event. The procedure used to redesign these elements is presented next.

3.4 Isolated Substructure Redesign

The reduced forces found during the initial analysis of the isolated bridge were used as a starting point to redesign the columns and footings. The columns were designed using SAP utilities that select and check concrete column reinforcement according to the AASHTO code. For foundation redesign, a trial configuration was identified by modifying the existing foundations in proportion to the reduction in demand, and the trial configuration was iterated by analysis in FB-Multipier to produce an economic foundation design.

3.4.1 Column Design

A trial size for the new columns was chosen based on the reduction in column forces. The maximum forces and moments over all load combinations are shown below in Table 3-1, for both the Legacy Bridge and the Isolated Bridge; the latter expressed both in force units and as a percentage of the Legacy Bridge values. These force and moment demands represent maximum values in any direction, and may not occur at the same time. The shear and moment demands are significantly reduced; even the axial force demand is noticeably lower, since much of the overturning effect is eliminated by the isolation system.

Table 3-1: Peak Column Demands for Legacy Bridge and Isolated Bridge (Prior to Redesign)

	P (k)	V2 (k)	V3 (k)	T (k-ft)	M2 (k-ft)	M3 (k-ft)
Legacy Bridge	2850.7	369.9	918.8	315.1	9831.7	6303.6
Isolated Bridge	2319.7	214.5	217.1	0.0	1970.7	3076.9
Ratio Iso/Legacy	81%	58%	24%	0%	20%	49%

To pick a new column size, we made use of the moment interaction diagram for the column, which shows the relationship between axial load and moment capacity. The interaction surface represents the critical combinations of axial force and bi-axial moment that would result in column failure, and defines the capacity of the columns for combined loading in any arbitrary direction. This 3D surface is easily generated by SAP within the Section Analysis module, and is typically simplified to a single 2D envelope curve for design. The interaction surface for a column of the Legacy Bridge is shown in Figure 3-5. Since the column cross section is radially symmetric, all sections of this surface are the same, and we will only make use of the 2D diagram. Also shown in Figure 3-5 are the code-specified corrections to this surface, such as adjustments to material strengths, phi factor, and limits on the pure compression failure region, which are automatically generated by SAP. Both the theoretical curve and the phi-modified design curve are shown in the left side of Figure 3-5 for comparison.

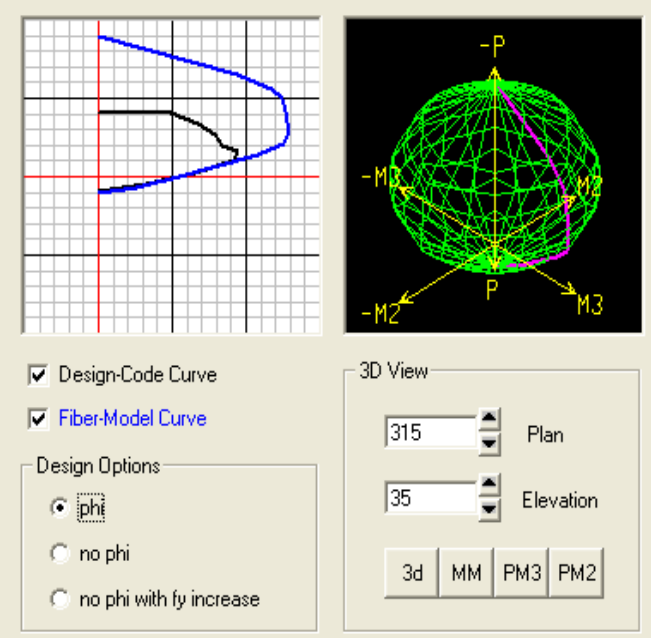

Figure 3-5: Representative Theoretical and Phi-Modified Interaction Diagram Generated by SAP

Figure 3-6 illustrates the phi-modified moment-interaction diagrams for the columns of the Legacy Bridge and the proposed columns for the Isolated Bridge. The process used to determine the Isolated Bridge columns will be described. Also shown in Figure 3-6 are the critical demand points for the controlling load combinations for both Legacy Bridge and Isolated Bridge. The demand to capacity ratio was calculated as the ratio of lengths of lines drawn from

the origin to the critical demand point and from the origin to the intersection of the design interaction surface in the same direction. Comparing these lengths indicates the percentage of the allowable capacity being used for a given relationship between axial load and moment. For example, the demand-capacity ratio for the Legacy Bridge using the critical demand point with the largest moment is 1.27, indicating that demand has exceeded column capacity. The observation that demand exceeds capacity for the Legacy Bridge, based on the interaction surface, is corroborated by the findings of the pushover analysis, which indicated that the columns formed plastic hinges at the demand displacement.

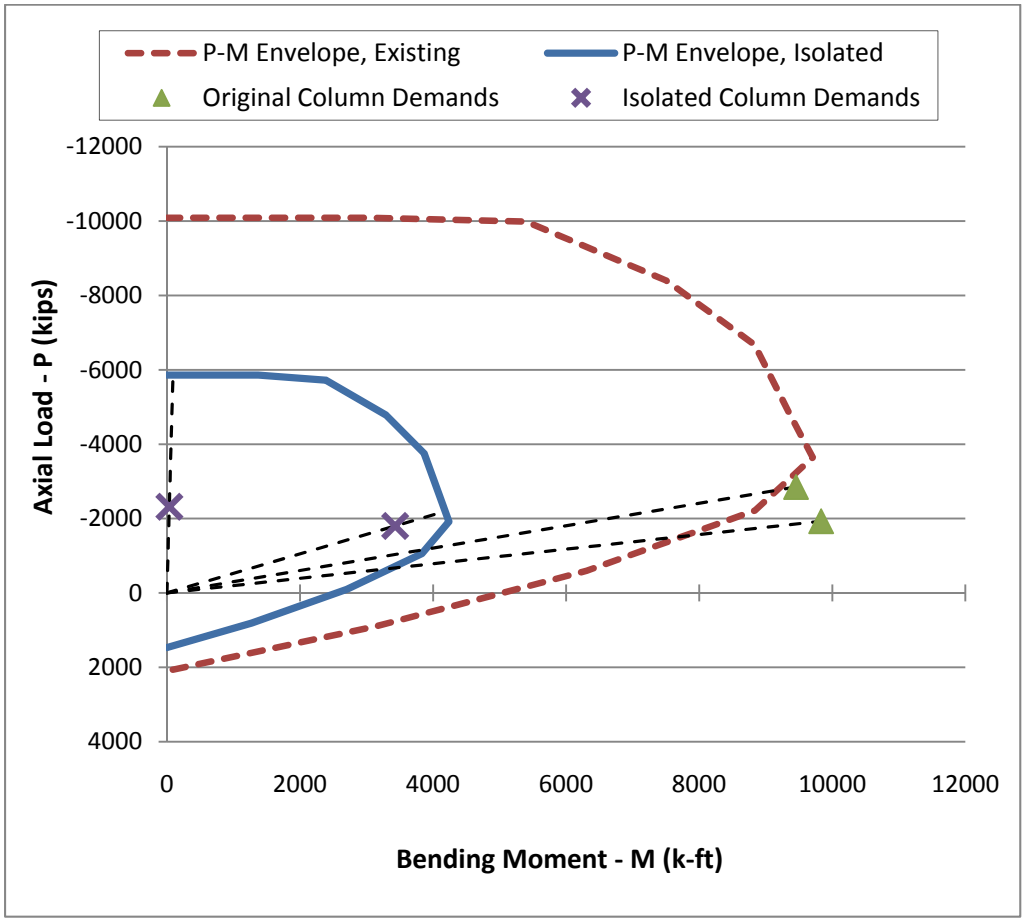

Figure 3-6: Moment Interaction Diagrams for Legacy Bridge and Isolated Bridge, with Critical Demand Points

To estimate the allowable reduction in column size, we plotted the critical demand points for the Isolated Bridge relative to the Legacy Bridge column interaction surface. The peak moment demand is at a little less than one third of the capacity of the Legacy Bridge columns; accordingly, the area of the column can be reduced by about a factor of two. Since the column is

approximately circular, the area varies with the square of the radius, and a target column diameter for the Isolated Bridge was calculated as the existing diameter: 6’ /√ 2 = 4.25 feet. We rounded this to 4.5 feet to be conservative, and to allow for reduction of the reinforcing steel, which we reduced from 27 #10 bars to 24 #9 bars. The proposed column cross section for the Isolated Bridge is illustrated in Figure 3-7.

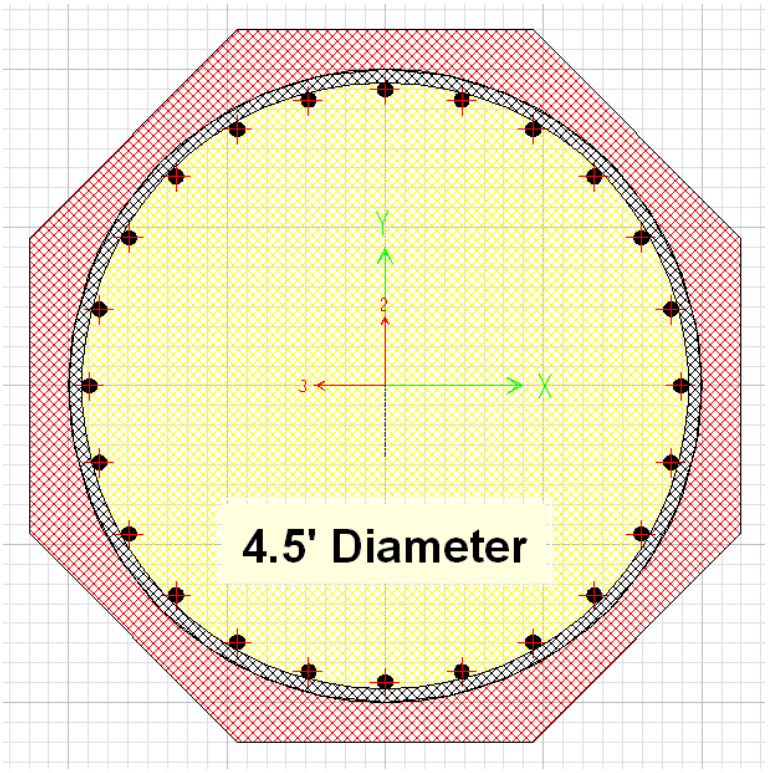

Figure 3-7: New Column Cross Section

The column interaction surface for the proposed cross section for the Isolated Bridge is also shown in Figure 3-6, and the demand-capacity ratio based on the Extreme load critical demand point was found to be 0.82. The new cross section is reasonably efficient, and has sufficient reserve capacity to allow for the increased demands that may result from the reduced stiffness. Although the critical axial loading now comes from the Strength I combination, Figure 3-6 shows that the moment demand still controls the column design. The design can be accepted as long as the critical demand point from the final bridge analysis is inside the phi-modified column interaction surface, which is to be verified in Section 3.5.

3.4.2 Pier and Abutment Foundation Design

The foundation springs calibrated for the Legacy Bridge were used in the initial analysis of the Isolated Bridge, as described in Section 3.3. The maximum force and moment demands over all combinations are presented in Table 3-2 for each axis of force, as well as the ratio of the Isolated Bridge to the Legacy Bridge demands. These peak demands are independent and do not necessarily occur at the same time or from the same load combination.

Table 3-2: Peak Foundation Demands for Legacy Bridge and Isolated Bridge (Prior to Redesign)

		P (k)	V2 (k)	V3 (k)	T (k-ft)	M2 (k-ft)	M3 (k-ft)
Pier	Legacy Bridge	2851	377	926	315	9832	6304
	Isolated Bridge	2320	125	94	0	1944	802
	Ratio Iso/Legacy	81%	33%	10%	0%	20%	13%
Abutment	Legacy Bridge	3787	4866	2685	8468	5335	11440
	Isolated Bridge	5094	375	365	219	3099	6674
	Ratio Iso/Legacy	135%	8%	14%	3%	58%	58%

Most of the peak force/moment demands decreased significantly for the Isolated Bridge, with the exception of a moderate increase of the maximum vertical load on the abutment due to the additional beam required for the isolated configuration. Since lateral forces control the foundation design, we assume that the foundation element capacity can be reduced in proportion to the reduction in demand, preserving the safety factor that was found for the original Legacy Bridge design.

For a target estimate of the required capacities of the new foundations, we assumed a design safety factor of 4 for both the lateral and vertical capacity. The ultimate capacity of the original foundation was computed by multiplying the original loads by the factors computed and the new target foundation capacities computed as 4 times the peak analytical demand in each direction. The ratio of these capacities is considered roughly equal to the required ratio of the new to the existing foundation geometry which summarizes the values used in this calculation.

Table 3-3: Target Capacities for Foundation Elements for the Isolated Bridge Redesign

		P (k)	V2 (k)	V3 (k)
Pier	Original Load	2851	377	926
	Original Overstrength Factor	78	5.5	5.5
	Original Ultimate Capacity	222,378	2073.5	5093
	New Load	2320	125	94
	New Target Factor	4	4	4
	New Target Capacity	9280	500	376
	% Original Strength	4%	24%	7%

		P (k)	V2 (k)	V3 (k)
Abutment	Original Load	3787	4866	2685
	Original Overstrength Factor	9	1.3	1.3
	Original Ultimate Capacity	34,083	6325.8	3490.5
	New Load	5094	375	365
	New Target Factor	4	4	4
	New Target Capacity	20,376	1500	1460
	% Original Strength	60%	24%	42%

Due to the complex nonlinear soil-structure interaction of pile elements that varies depending on configuration, spacing, depth, and so on, foundation design can be an iterative trial and confirmation process. Our strategy is to preserve the existing pile section and pile spacing of 3 times the pile diameter, and instead reduce the length (depth) and number of piles where possible. The lateral response of a pile group is more closely related to the number of piles along the leading edge than the total number of piles, since the capacity of piles in the trailing rows is reduced due to the movement of the soil in front of the piles. We assumed that moments do not control the foundation design for the Isolated Bridge, and that the vertical capacity of the pile system depends primarily on the total axial capacity of individual piles.

Since the lateral loading is expected to control the design, we propose to reduce the number of piles in each direction proportional to the reduction in lateral demand. The piers are estimated to require a capacity of only 24% of their original load, which suggests that only 2 rows of piles are needed in each direction. We propose to eliminate the outer row of piles in each direction, maintaining the hollow square in the center of the pile group. Removing the

outermost rows of piles reduces the total number of piles in each pier from 36 to 12. Figure 3-8 is taken from FB-Multipier, and shows a plan view of the new pile group geometry of the pier.

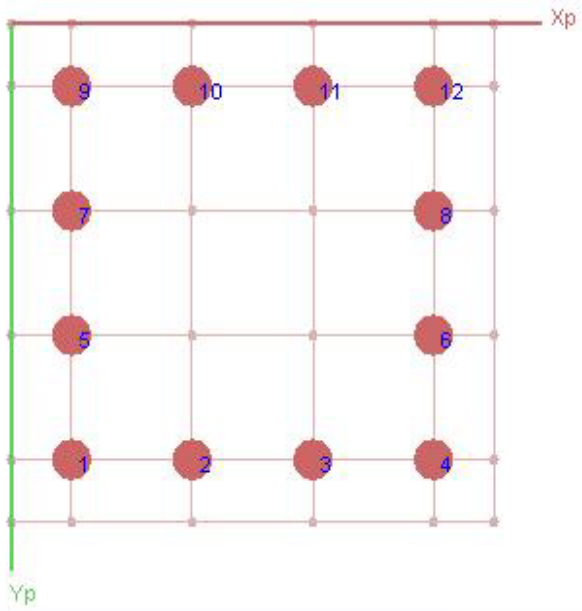

Figure 3-8: Plan View of New Pier Foundation

Pile length (or depth) is the next consideration; embedment length plays a significant part in both the vertical and lateral capacity of individual piles. The vertical resistance of an individual pile is dominated by skin friction, which is proportional to the pile length, and the pile cap also contributes to vertical resistance. The required vertical force capacity of the pier pile group for the Isolated Bridge is only 4% of the capacity provided by the Legacy Bridge design (Table 3-3); however, the number of piles has already been reduced from 32 to 12, such that the vertical force capacity has already been reduced by a factor of about 2/3. This suggests that the lengths could be reduced by a factor of about 8, assuming that the average skin friction in the upper soil layers is roughly equal to the average skin friction over all layers. However, to ensure that the piles are sufficiently long to approximate a fixity condition for lateral resistance, we propose to shorten the pier piles by only 50%. Furthermore, it is possible that the length of the piles in the Legacy Bridge design was controlled by other factors besides vertical pile capacity, in which case the pile embedment length cannot be reduced.

The pile cap was evaluated using the same procedure as in Section **Error! Reference source not found.**. Since the number of piles (and the effective moment arm in relation to the column

face) has been reduced, the thickness and reinforcement required for the cap to withstand the maximum theoretical moment in the foundation is also reduced. Based on the new pile geometry, we also propose a reduction in pile cap thickness from 6 feet to 3 feet, and a reduction of longitudinal reinforcement from 47 #10 bars in each direction (top and bottom) to 24 #8 bars, which reduces the area of longitudinal steel reinforcement by 68%. The length of the longitudinal steel is also reduced in proportion to reduction in the number of pile rows, or a 1/3 reduction, and the length of the vertical steel by the reduction in cap thickness (50%).

The configuration of the abutment foundations is affected by external considerations beyond the total force capacity, which limit potential configuration changes to the abutments. For instance, the weight of the bridge transferred to the abutments should be evenly distributed over the piles. Therefore, assuming the pile spacing is preserved and the total width of the pile span is preserved, the number of piles cannot be reduced for the abutments. Also, given that the vertical force demand at the abutments has increased, we do not recommend shortening the length of the abutment piles even though such measures would still appear to produce a design that satisfies code.

To confirm that the capacity is sufficient, we created new FB-Multipier models with the updated geometry for both pier and abutment pile groups.

Figure 3-9 illustrates the graphical interface for the pier pile group. We conducted pushover analyses to obtain both the lateral and vertical capacities of each configuration. The load capacities for the new pier pile group configuration, after calibration with the SAP analysis (see Section 2.3.4), were found to be 3.75 times the lateral demand (design lateral load) and 46.5 times the vertical demand force. The factors of safety are appropriate; the vertical force capacity could not be further reduced without adversely affecting the lateral capacity.

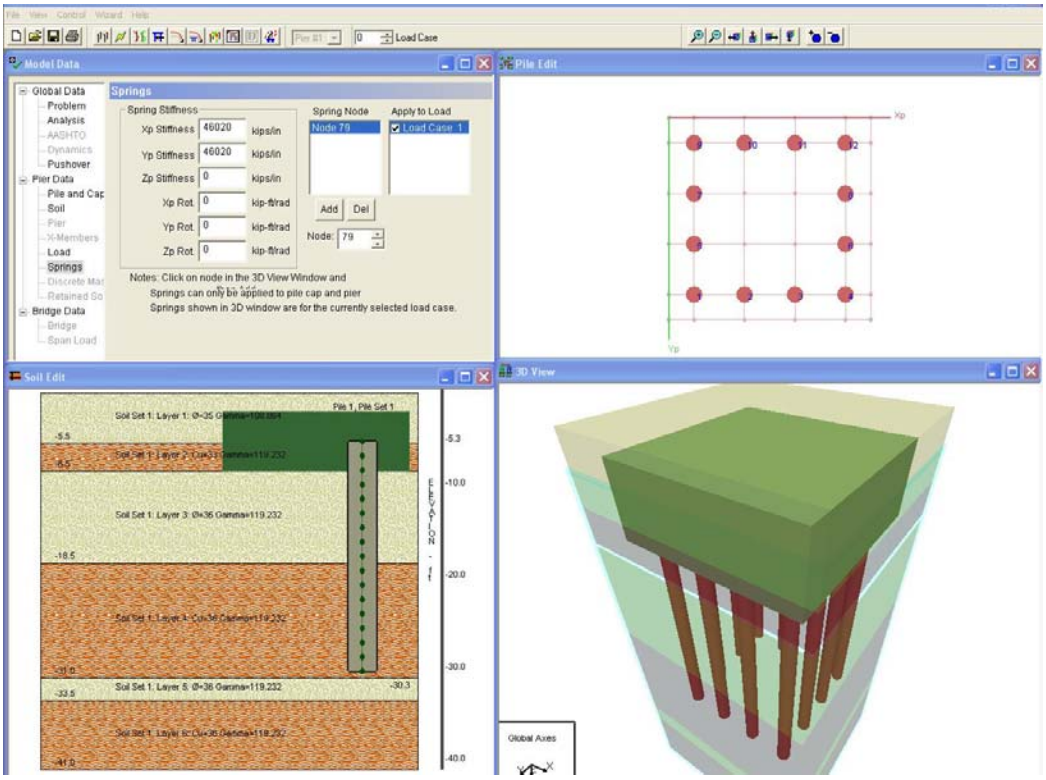

Figure 3-9: FB-Multipier Model - New Pier Foundation

The new capacity to demand ratios for the abutment pile group, based on pushover analysis, were found to be 6.5 for lateral loads and 16.5 for vertical loads, which represent a conservative and economical design. Due to the geometry changes of the abutment, the backwall is no longer considered to contribute to the horizontal stiffness, which is sufficient without the participation of the backwall. The assumed separation of the abutment and the backwall will reduce the material and detailing that would otherwise be necessary for a moment connection to the backwall.

The calibrated foundation springs used in the final isolated SAP model are presented below in Table 3-4 and Table 3-5.

It is important to recognize that these foundation designs are theoretical and may not be constructable due to field conditions, pile limitations, or other unknowns related to a given design or site. A drivability analysis should be performed by a licensed professional engineer as part of any complete design that is intended to be constructed.

Table 3-4: Isolated Pier Foundation Stiffness Matrix

	ΔZ	ΔX	ΔY	θZ	θX	θY
Fz	8,928	1	10	-26	-31,130	2,394
Fx	1	2,015	0	651	67	107,900
Fy	10	0	2,006	28	-104,500	-52
Mz	-26	651	28	15,990,000	-5,510	51,160
Mx	-31,130	67	-104,500	-5,510	40,410,000	-8,169
My	2,394	107,900	-52	51,160	-8,169	41,450,000

Translations: kips/in Rotations: kip-in/rad

Table 3-5: Isolated Abutment Foundation Stiffness Matrix

	ΔZ	ΔX	ΔY	θZ	θX	θY
Fz	17,040	0	0	0	-7,600	-75
Fx	0	3,398	0	3	0	179,600
Fy	0	0	1,887	0	-125,500	0
Mz	0	3	0	323,900,000	-725	-20
Mx	-7,600	0	-125,500	-725	1,725,000,000	61
My	-75	179,600	0	-20	61	16,920,000

Translations: kips/in Rotations: kip-in/rad

3.5 Final Verification of Isolated Bridge Response

As already discussed, isolating a structure changes the seismic response by shifting the period away from the high acceleration region of the spectrum, reducing the lateral force demands, and changing the fundamental mode shapes so that nearly all of the displacement demand occurs in the isolators. As shown in Section 3.4.1, the reduction in overall demands greatly reduces the forces on the bents, and the column section sizes can be significantly reduced. The reduction in column force demand also passes to the foundations, such that a substantially reduced pier pile group is possible. The reduction in column and foundation size should lead to a significant cost decrease in materials and labor, making up for the added cost due to the isolation system and special detailing.

The FB-Multipier and SAP analyses were repeated, and the foundation and isolator spring properties, along with the damping-modified spectrum, were adjusted iteratively until the

observed force and displacements did not change, within sufficient tolerance, from one iteration to the next. The final isolator displacements are 8.25 inches for the bent isolators, and 8.39 inches for the abutment isolators, and the final damping was found to be a little over 21%. The final isolated periods are 2.61 and 2.46 seconds, and over 96% of the modal mass is included for lateral motion (

Table 3-6). The third (rotational) mode is not expected to have significant participation in the lateral response (0.1% in the X and Y directions), and has been included in these results only to bring the rotational modal mass in the horizontal plane up to 90% for the sake of completeness. The final mode shapes are shown in Figure 3-10; these mode shapes have not changed substantially from the initial mode shapes computed before the redesign of the columns and foundation elements (Figure 3-4).

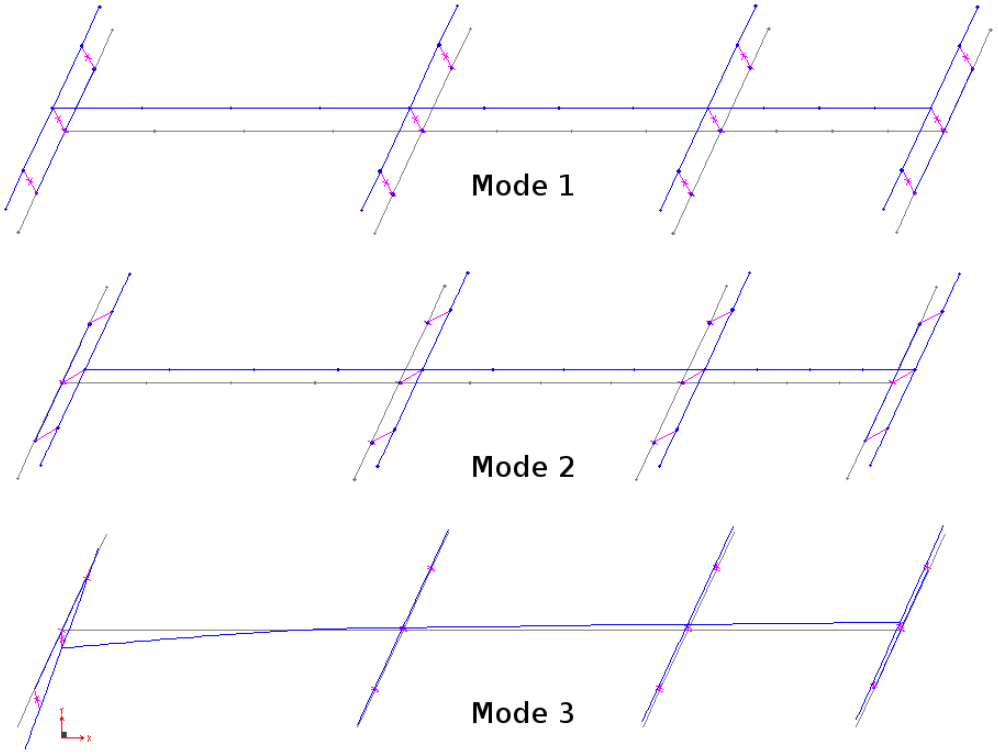

Figure 3-10: Isolated Mode Shapes

Table 3-6: Isolated Modal Analysis Results – Periods and Directional Mass Participation

Mode	Period (sec)	X	Y	RZ

1	2.607	21.2%	70.7%	63.4%
2	2.462	74.9%	25.7%	5.5%
3	0.187	0.1%	0.1%	23.0%
	Sum:	96.2%	96.5%	91.9%

3.6 Performance Comparison of Legacy Bridge and Isolated Bridge

The column and foundation force and moment demands determined by analysis of the final, calibrated SAP model of each bridge are compared in Table 3-7 and Table 3-8, respectively. Recall that the peak demands may not occur at the same time or in the same location, but provide a good overall illustration of the effects of isolation.

Table 3-7: Peak Column Demands for Legacy Bridge and Final Isolated Bridge

	P (k)	V2 (k)	V3 (k)	T (k-ft)	M2 (k-ft)	M3 (k-ft)
Legacy Bridge	2850.7	369.9	918.8	315.1	9831.7	6303.6
Initial Isolated Bridge	2319.7	214.5	217.1	0	1970.7	3076.9
Final Isolated Bridge	2275.7	179.4	178.9	0.0	1617.8	2118.2
Initial Percentage	81%	58%	24%	0%	20%	49%
Final Percentage	80%	48%	19%	0%	16%	34%

Comparison with the initial estimates of reduced force show that all substructure demands were significantly reduced in the final isolated configuration, many even further than originally estimated based on the initial isolated configuration, which used the columns and foundations of the existing Legacy Bridge. The discrepancy between the initial and final Isolated Bridge analyses is related to the reduction in column and foundation sizes and adjustments to the spectral damping and isolator properties.

The peak moment demand in the columns was reduced from 9832 k-ft to 2118 k-ft, which is more than a factor of 4. The reduction in shear force demand is similar. The reduction in moment demand from the initial to the final configuration of the Isolated Bridge is simply due to the fact that the redesigned column attracts less force for the same displacements. The performance of the Isolated Bridge columns is clearly more favorable, since the peak moment

and axial force demands are inside the interaction diagram, indicating that the column remains elastic and no plastic hinging occurs. In the Legacy Bridge, the peak moment and axial force demands are outside of the interaction surface, indicating that plastic hinges do form.

In both bridges, the foundation response was predicted to remain linear. However, the foundation demands for the isolated bridge are reduced by considerable factors which has allowed for a considerable reduction in foundation size to achieve the same performance.

Table 3-8: Peak Foundation Demands for Legacy Bridge and Final Isolated Bridge

		P (k)	V2 (k)	V3 (k)	T (k-ft)	M2 (k-ft)	M3 (k-ft)
Pier	Legacy Bridge	2851	377	926	315	9832	6304
	Initial Isolated Bridge	2320	125	94	0	1944	802
	Final Isolated Bridge	2320	214	217	0	1944	802
	Initial Percentage	81%	33%	10%	0%	20%	13%
	Final Percentage	81%	57%	23%	0%	20%	13%
Abutment	Legacy Bridge	3787	4866	2685	8468	5335	11440
	Initial Isolated Bridge	5094	375	365	219	3099	6674
	Final Isolated Bridge	2320	88	1	0	1937	802
	Initial Percentage	135%	8%	14%	3%	58%	58%
	Final Percentage	61%	2%	0%	0%	36%	7%

4. Design of Seismic Isolation Bearings

4.1 Overview of Isolation Devices

Four viable vendors in the U.S. manufacture devices suitable for seismic isolation applications in bridges. Dynamic Isolation Systems of Sparks, NV and Seismic Energy Products of Athens, TX manufacture elastomeric bearings. For seismic isolation applications, elastomeric bearings consist of layers of rubber separated by thin steel shims (Figure 4-1). The rubber layers provide the lateral flexibility, while the steel shims increase the vertical stiffness to support large axial loads and prevent bulging of the rubber. To provide the energy dissipation, a lead core is press fit into the center of the bearing. The lead is initially very stiff, but yields under modest forces and flows to provide hysteretic energy dissipation (Figure 4-1).

The lateral force-deformation of a lead-rubber bearing is generally idealized as a bilinear relation. The stiffness of rubber k_r determines the second slope or post-yield stiffness k_2, while the strength of the lead core Q_D determines the yield force (Figure 4-2). The initial stiffness of the bearing is generally assumed to be 10 times the post-yield stiffness (DIS, 2007).

Low damping natural rubber bearings are also available, but are generally used in combination with other devices to provide adequate damping. Additional product information from DIS and EPS is provided in Appendix B.

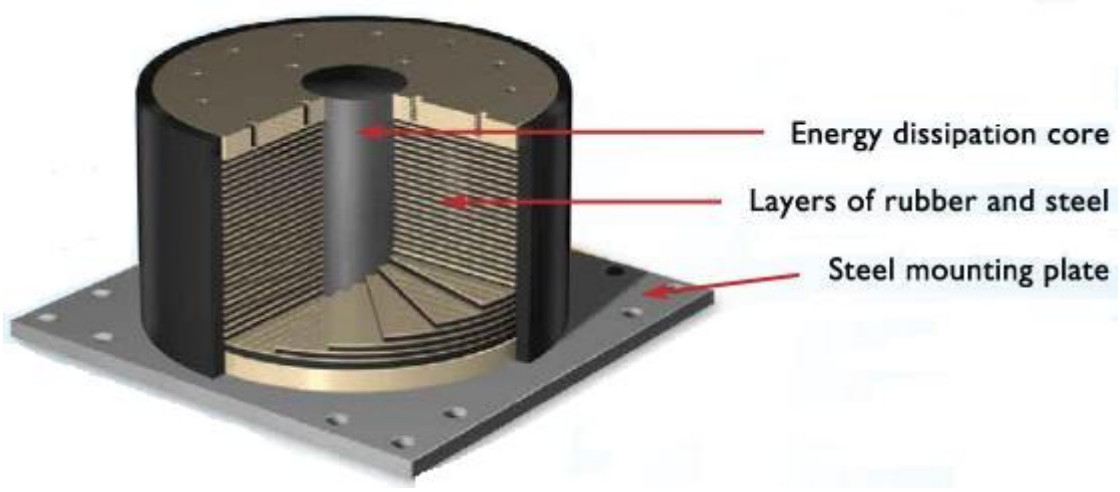

Figure 4-1: Cross-sectional view of lead-rubber bearing (Source: DIS, 2007)

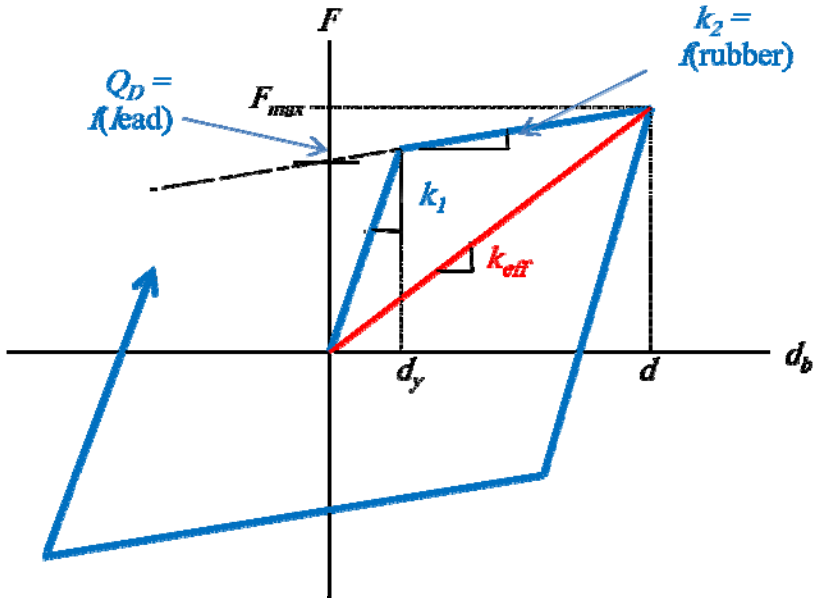

Figure 4-2: Bilateral force-deformation relation for a lead-rubber bearing

Earthquake Protection Systems of Vallejo, CA manufactures several different devices based on the friction pendulum system (FPS) concept. The original single pendulum bearing consists of a slider moving around in a curved dish (Figure 4-3). The friction coefficient of the sliding interfaces determines the strength of the system and hysteretic energy dissipation. A flat frictional sliding surface would produce a rigid-perfectly plastic force-deformation. However, the curvature of the dish provides a restoring force, and the physics of the motion in the dish is analogous to a pendulum. The post-yield stiffness k_2 and corresponding period T_2 of the single pendulum device are described by

$$k_2 = \frac{W}{R} \quad \text{and} \quad T_2 = 2\pi\sqrt{\frac{R}{g}}$$

The resultant force-deformation of the single pendulum device is also bilinear, as shown in Figure 4-4. The initial stiffness is generally assumed to be a large but finite value when used in dynamic analysis procedures.

EPS also manufactures a variety of devices with multiple sliding surfaces to provide more customizable force-deformation behavior. The double pendulum bearing is an extension of the single pendulum device, using a single slider sandwiched between curved sliding surfaces on top and bottom (Figure 4-5(a)). As an extension of this idea, EPS manufactures a double

concave rail device with tension resistance (Figure 4-5(b)). The triple pendulum bearing is essentially a small double pendulum bearing sandwiched inside a larger double pendulum bearing (Figure 4-6). The friction coefficients and radii of the multiple sliding surfaces can be selected independently to optimize the performance of the isolation system for multi-level seismic hazard. The triple pendulum bearing is now the most widely promoted device by EPS, but to our knowledge has not been used yet for a bridge in the United States.

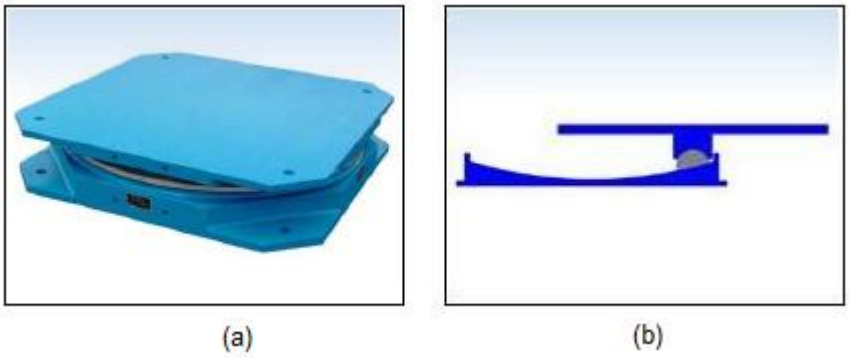

Figure 4-3: Single friction pendulum bearing: (a) manufactured device and (b) cross-sectional view of deformed configuration (Source: EPS, 2010).

An important distinction from elastomeric bearings, both the stiffness and strength of FPS devices are proportional to the supported weight, so that their effective period and strength ratio are independent of the supported weight. Thus, the size of the devices is relatively insensitive to the weight above. The maximum expected vertical load is used only to size the innermost slider. The desired displacement capacity is the most important factor in determining the size of the device. Additional product information from EPS is provided in Appendix B3-B4.

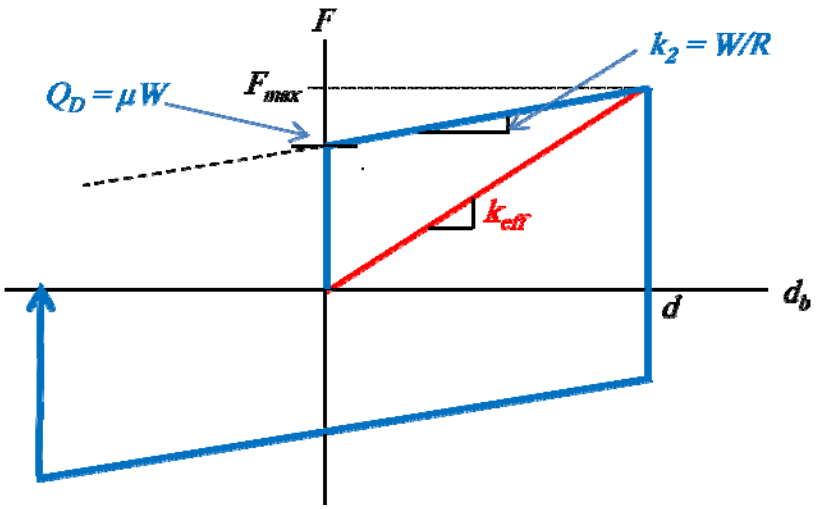

Figure 4-4: Bilinear rigid-plastic force deformation relation for a single friction pendulum relation

RJ Watson of Buffalo, NY manufactures the Eradiquake isolation system, which is another type of sliding isolation device. The Eradiquake bearing consists of a flat plate slider mounted on a disk bearing with urethane springs to provide a restoring force. The Eradiquake bearing has generally been used for seismic isolation applications in low to moderate seismic zones (Buckle et. al., 2006).

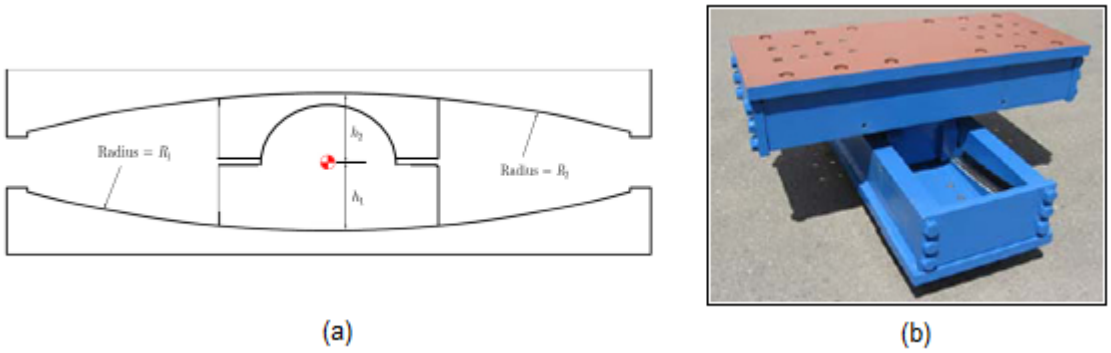

Figure 4-5: (a) Cross-sectional view of double pendulum bearing, and (b) EPS double concave tension capable bearing. (Source: EPS, 2010).

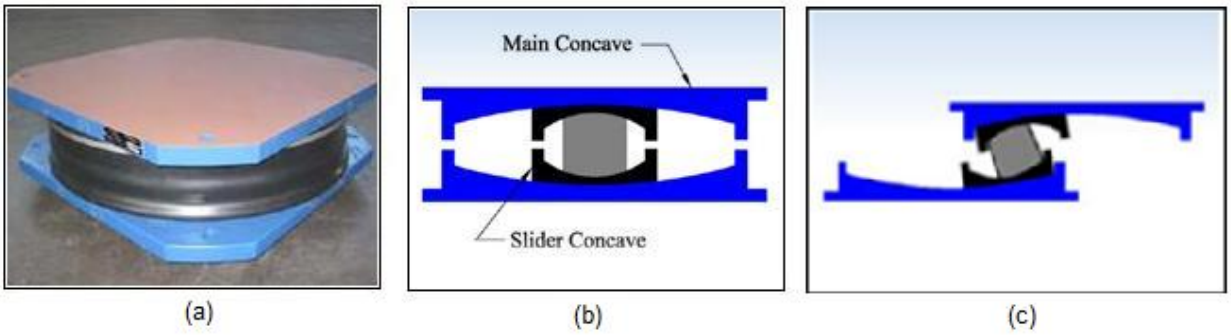

Figure 4-6: Triple friction pendulum bearing: (a) manufactured device; cross-sectional view of bearing in (b) undeformed configuration and (c) laterally deformed configuration. (Source: EPS, 2010).

For this study, example designs are developed for isolation systems consisting of lead-rubber bearings, single friction pendulum bearings, and triple friction pendulum bearings.

4.2 Design of Lead Rubber Bearings

4.2.1 Target Parameters

As discussed previously, the design of lead-rubber bearings depends on the supported weight. The total weight to be supported by the bearings at each abutment and pier, based on a computer generated SAP model and supported by hand calculations, is estimated in Table 4-1. Only the dead load, with a load factor of 1.0, is considered in the design of the bridge. Although live load is usually not included in the seismic load for bridge design, Section 2.2 of the Isolation Spec (AASHTO, 2010) advises that a percentage of the total live load should be included for isolated bridges, at the discretion of the engineer. The argument for considering live load is to ensure that the displacement demands of the isolation system can be accommodated if the period of the bridge is lengthened due to unanticipated weight. Based on the Average Daily Trips indicated on the plans, the Legacy Bridge is not a heavily trafficked bridge under normal conditions, and the isolation system will be designed with sufficient reserve displacement capacity. Therefore, live load is not considered in determining the seismic weight of this bridge.

Due to the unequal span lengths, the weight supported at each pier and abutment is substantially different. However, designing many different size bearings is not cost effective. For this bridge, we opt to design one bearing for use at the abutments and one bearing for use at the piers, where each bearing type supports the average weight indicated in Table 4-1. The actual load supported on each bearing will be higher or lower than the average values used in design.

As a final design step, the axial load capacity of each bearing type should be re-evaluated against the peak axial load demand determined from the seismic analysis including overturning effects, and the design modified as necessary. The design will be explained in detail for a pier bearing first, followed by a summary of the design calculations for both bearings.

Table 4-1: Estimated supported weight for design of lead-rubber bearings

	Supported Weight (kip)	Total Weight (kip)	Avg Weight per Bearing (kip)
Abutment 1	2540	4420	740
Abutment 4	1880		
Pier 2	4438	7800	1300
Pier 3	3368		

A logical approach for the design of lead-rubber bearings is to design the bearings for a target period and damping ratio in the design (1000 year) earthquake. Examples that target isolation periods around 1 second and high damping ratios have been illustrated (Buckle et. al., 2006). In our judgment, a longer isolation period is preferable to reduce the demands on the bridge, and can be accommodated without excessive or unsafe displacement demands on the bridge. Such measures will also ensure that the isolation system is activated even in a smaller event. Thus, we select a target period T_{eff} = 2.5 sec and a target damping ratio ξ = 20%. The target effective stiffness for the pier bearing is thus:

$$k_{eff} = \left(\frac{W}{g}\right)\left(\frac{2\pi}{T_{eff}}\right)^2 = \left(\frac{1300 \text{ kip}}{386 \text{ in/s}^2}\right)\left(\frac{2\pi}{2.5 \text{ sec}}\right)^2 = 21.27 \text{ kip/in}$$

Recalling that the 1 second spectral acceleration coefficient S_{D1} = 0.56, the design force coefficient, or elastic seismic response coefficient C_{smd}, is calculated according to (Eqs. 7.1-2 and 7.1-3 of the Isolation Spec):

$$C_{smd} = \frac{S_{D1}}{T_{eff} B_L} = \frac{0.56}{(2.5)(1.52)} = 0.148$$

where B_L, a spectrum modification factor for damping, is calculated as:

$$B_L = \left(\frac{\xi}{0.05}\right)^{0.3} = \left(\frac{0.20}{0.05}\right)^{0.3} = 1.52$$

The displacement demand d of the isolators is calculated (Eq. 7.1-4 of the Isolation Spec):

$$d = \left(\frac{g}{4\pi^2}\right)\left(\frac{S_{D1}T_{eff}}{B_L}\right) = \left(\frac{386\ \text{in/s}^2}{4\pi^2}\right)\left(\frac{(0.56)(2.5\,\text{sec})}{(1.52)}\right) = 9.03\ \text{in}$$

4.2.2 Sizing the Bearings

Based on the effective properties and displacement demand, target values for the strength of the lead core and post-yield stiffness are developed, which are ultimately used to size the bearings. The following equations are used for the required strength of the lead core Q_D, yield displacement of the bearing d_y, post-yield stiffness k_2 and initial stiffness k_1:

$$Q_D = \frac{\pi}{2}\frac{\xi k_{eff} d^2}{(d - d_y)}$$

$$k_2 = k_{eff} - \frac{Q_D}{d}$$

$$k_1 = 10k_2$$

$$d_y = \frac{Q_D}{k_1 - k_2} = \frac{Q_D}{9k_2}$$

The sequence of calculations is iterative, because the yield displacement d_y is initially unknown. Alternative approaches that assume a value for yield displacement d_y, in lieu of assuming a value for the ratio of k_1/k_2 have been advocated (Ryan and Chopra, 2004). However, most sources, including bearing manufacturer product information (DIS, 2007), recommend assuming k_1/k_2=10 for design of the bearings, so this is the approach adopted here. To start the sequence of iterative calculations, d_y is assumed to be zero (Buckle et. al., 2006):

$$Q_D = \tfrac{1}{2}\pi\xi k_{eff} d = \tfrac{1}{2}\pi(0.20)(21.27\ \text{kip/in})(9.03\ \text{in}) = 60.36\ \text{kip}$$

Table 4-2 summarizes the iterative calculations to determine the stiffness and strength properties.

Table 4-2: Iterative calculations to determine stiffness and strength properties

	Q_D (kip)	k_2 (kip/in)	k_1 (kip/in)	d_y (in)
Iteration 1	60.36	14.59	145.9	0.46
Iteration 2	63.59	14.23	142.3	0.50
Iteration 3	63.87	14.20	142.0	0.50

Recall that the yield strength Q_D and post-yield stiffness k_2 (Figure 4-2) are determined by the size of the lead core and the stiffness of rubber, respectively. To size the lead core, the yield force F_y of lead is given as (Buckle et. al., 2006):

$$F_y = A_L \sigma_{yL} = \pi/4 \, D_L^2 \sigma_{yL}$$

where A_L and d_L are the area and diameter of the lead core, respectively, and σ_{yL} is the yield strength of the lead core, taken to be 1.3 ksi. Note also that the relation between F_y and Q_D is:

$$Q_D = F_y \left(1 - \frac{k_2}{k_1} \right) = 0.9 F_y$$

Thus, the required area and diameter of the lead core are calculated as:

$$A_L = \frac{F_y}{\sigma_{yL}} = \frac{Q_D}{0.9\sigma_{yL}} = \frac{63.9 \text{ kip}}{0.9(1.3 \text{ ksi})} = 54.6 \text{ in}^2$$

$$D_L = \sqrt{\tfrac{4}{\pi} A_L} = \sqrt{\tfrac{4}{\pi}(54.6 \text{ in}^2)} = 8.34 \text{ in}^2$$

The post-yield stiffness k_2 is related to the stiffness of rubber k_r according to:

$$k_2 = 1.1 k_r = 1.1 \frac{GA}{t_r}$$

where G is the effective shear modulus of the rubber, A is the cross-sectional area of rubber based on the bonded diameter of the bearing, and t_r is the total height of rubber including all rubber layers. The constraints on parameter selection vary by manufacturer; here the product information provided by DIS (DIS, 2007) is used to select the bearing parameters. For DIS bearings, the shear modulus can be selected from 55 to 100 psi, and the bearing diameter can be selected from pre-defined values. The total height of rubber can generally be selected without constraint, though ultimately limited by stability requirements.

Selection of the bearing diameter is the logical starting point, and can be guided by the axial load capacity and maximum displacement capacity. For the pier bearings, we select diameter D = 41.5 in, which is rated for a maximum axial load of 1900 kips and maximum displacement of 28 inches. Although the average design axial load is 1300 kips, we include an allowance for a) the supported weight is higher on one of the piers than the other, b) increased

load due to live load, and c) increased load due to overturning. To compute the area A_r of rubber used in the calculation of t_r, the bonded diameter D_b is assumed to be 1 inch less than the total diameter, i.e., $D_b = 40.5$ in. Thus, the total bonded area A of the bearing and the area of rubber A_r are computed next.

$$A = \frac{\pi}{4} D_b^2 = \frac{\pi}{4}(40.5)^2 \text{ in}^2 = 1288 \text{ in}^2$$

$$A_r = \frac{\pi}{4}\left(D_b^2 - D_L^2\right) = \frac{\pi}{4}\left((40.5)^2 - (8.34)^2\right) \text{ in}^2 = 1233.7 \text{ in}^2$$

The remaining parameters are chosen by trial and error:

$$G = 0.075 \text{ ksi}$$

$$t_r = 7.167 \text{ in}$$

$$k_2 = 1.1\frac{GA_r}{t_r} = 1.1\frac{(0.075 \text{ ksi})(1233.7 \text{ in}^2)}{7.167 \text{ in}} = 14.20 \text{ kip/in}$$

which leads to the required value of k_2. To complete the design, we select the number of rubber layers N, the thickness of the layers t, and thickness t_s of the steel shims.

$$N = 25$$

$$t = \frac{t_r}{N} = \frac{7.167 \text{ in}}{25} = 0.287 \text{ in}$$

$$t_s = 0.125 \text{ in}$$

The standard mounting plates are square plates with length 43.5 in. and thickness $t_p = 1.75$ in (DIS, 2007). The total height H of the bearing is calculated as:

$$H = t_r + (N-1)t_s + 2t_p = 7.167 \text{ in} + 24(0.125 \text{ in}) + 2(1.75 \text{ in}) = 13.67 \text{ in}$$

Note that the diameter of the lead core, number of rubber layers, and total height of the bearing are within the limits specified by DIS product information (DIS, 2007).

4.2.3 Design Checks

4.2.3.1 Lead Core Size

A series of other calculations are necessary to determine the adequacy of the bearing. First, the lead core should not be too small or too large to function properly. For this bearing,

$$\frac{D_L}{D_b} = \frac{8.34 \text{ in}}{40.5 \text{ in}} = 0.206$$

which satisfies the empirical requirement that lead core diameter should be in the range of 1/6 to 1/3 of the bonded diameter of the bearing (Buckle et. al., 2006). The Isolation Spec (AASHTO, 2010) also requires that the yield strength of the bearing be larger than the combined wind force on the bridge and braking force of the vehicles. This check was not completed here, since it is assumed that in a high seismic zone, these requirements will not control the design of the bearing.

4.2.3.2 Total Displacement Demand

Commentary Section 3.1 of the Isolation Spec recommends that the 2500 year earthquake be considered in design, and that the isolation devices be tested to the displacement demands in the 2500 year earthquake, also referred to as the Maximum Considered Earthquake (MCE). Aside from the testing requirements, some of the required design checks are with reference to d_t, which is defined by the Isolation Spec as the Total Design Displacement. However, the Isolation Spec is ambiguous as to whether d_t is intended to be defined with respect to the design (1000 year) earthquake or MCE (2500 year earthquake). We have chosen to interpret d_t as the displacement in the MCE.

Iteration is required to determine the effective isolation properties and the displacement demand d_t in the MCE. The 1 second spectral acceleration for the MCE, determined from the USGS ground motion calculator program (USGS, 2008), is S_{M1} = 0.878g. The equations used in the iterative procedure have been discussed previously, but are summarized here for convenience:

$$d_t = \left(\frac{g}{4\pi^2}\right)\left(\frac{S_{M1}T_{eff}}{B_L}\right)$$

$$f_{\max} = Q_D + k_2 d_t$$

$$k_{eff} = \frac{f_{\max}}{d_t}$$

$$T_{eff} = 2\pi\sqrt{\frac{W}{gk_{eff}}}$$

$$\xi = \frac{2}{\pi}\frac{Q_D(d_t - d_y)}{k_{eff}d_t^2}$$

$$B_L = \left(\frac{\xi}{0.05}\right)^{0.3}$$

The iteration commences with the assumption that T_{eff}= 2.5 sec and ξ= 0.20, which are the values for the design earthquake. The iterative calculations are summarized below in Table 4-3.

Table 4-3: Summary of iterations to calculate maximum displacement d_t

	T_{eff} (sec)	ξ	B_L	d_t (in)	$f_{\max}$ (kip)	k_{eff} (kip/in)
Iteration 1	2.5	0.2	1.516	14.2	264.9	18.71
Iteration 2	2.666	0.148	1.385	16.5	298.5	18.07
Iteration 3	2.713	0.132	1.338	17.4	311.0	17.87
Iteration 4	2.728	0.127	1.323	17.7	315.3	17.81
Iteration 5	2.732	0.125	1.317	17.8		

The calculations are considered to be converged at a displacement d_t= 17.8 in.

4.2.3.3 Minimum Restoring Force

To ensure that the isolation system provides a sufficient restoring force that prevents excessive accumulation of displacements, the Isolation Spec requires that when the restoring force depends on displacement, the minimum restoring force shall be

$$F(d_t) - F(0.5d_t) \geq \frac{W}{80}$$

which is equivalent to

$$k_2 \geq 0.025\frac{W}{d_t} = 0.025\left(\frac{1300 \text{ kip}}{17.8 \text{ in}}\right) = 1.83 \text{ kip/in}$$

Since k_2 = 14.20 kip/in, the requirement is satisfied. Furthermore, the Isolation Spec requires that regardless of weight, the period associated with the second slope stiffness k_2 be less than 6 seconds. For this system, the second slope period T_2 = 3.06 seconds, and the requirement is satisfied.

4.2.3.4 Bearing Stability

The stability of the bearing is checked according to equations in Section 12.3 of the Isolation Spec. These requirements are most pertinent for elastomeric bearings, whose stability must be checked both in the deformed and undeformed configuration. In the undeformed configuration, the vertical capacity must be at least 3 times the design load (unfactored dead load plus live load). The critical buckling load for an elastomeric bearing is calculated as:

$$P_{cr} = \sqrt{\frac{\pi^2 E_c IGA}{3t_r^2}}$$

where the compression modulus E_c and the bending inertia I are

$$E_c = 6GS^2 = 6(0.075 \text{ ksi})(33.8)^2 = 514.8 \text{ ksi}$$
$$I = \frac{\pi}{64}\left(d_b^4 - d_L^4\right) = \frac{\pi}{64}\left((40.5 \text{ in})^4 - (8.34 \text{ in})^4\right) = 131829 \text{ in}^4$$

and S is the bearing shape factor, computed as

$$S = \frac{D_b^2 - D_L^2}{4D_b t} = \frac{(40.5 \text{ in})^2 - (8.34 \text{ in})^2}{4(40.5 \text{ in})(0.287 \text{ in})} = 33.8$$

The formula for E_c neglects the contribution from the bulk modulus of rubber, which can be assumed to be infinite. The critical buckling load is easily defined in terms of pressure p_{cr} by dividing the critical load by the area:

$$p_{cr} = \sqrt{\frac{\pi^2 E_c IG}{3t_r^2 A}} = \sqrt{\frac{\pi^2 (514.8 \text{ ksi})(131829 \text{ in}^4)(0.075 \text{ ksi})}{3(7.167 \text{ in})^2 (1288.2 \text{ in}^2)}} = 15.91 \text{ ksi}$$

Bearings are usually sized with pressure in the range of 0.5 to 1.0 ksi. For the pier bearing, the design pressure is

$$p_{dead} = \frac{P}{A} = \frac{1300 \text{ kip}}{1288.2 \text{ in}^2} = 1.01 \text{ ksi}$$

Thus, the factor of safety against buckling in the undeformed configuration is

$$F.S. = \frac{p_{cr}}{p_{dead}} = \frac{15.91 \text{ ksi}}{1.01 \text{ ksi}} = 15.8$$

which is considerable and far exceeds the code required factor of safety of 3.

In the deformed configuration, the isolation system must be stable under 1.2 times the dead load plus any overturning axial forces due to the seismic load case. The deformation shall be taken as the greater of 1.1 times the MCE displacement or 1.5 times the design displacement (AASHTO, 2010), i.e.

$$d_{stab} = \max \begin{cases} 1.1 d_t = 1.1(17.8 \text{ in}) = 19.6 \text{ in} \\ 1.5 d_i = 1.5(9.03 \text{ in}) = 13.55 \text{ in} \end{cases}$$

Thus, the stability check is performed at the displacement of 19.6 in. An approximation for the critical pressure p_{cr}' of the bearing in the deformed configuration is computed from the following equations (Buckle et. al. 2006):

$$\delta = 2\cos^{-1}\left(\frac{d_{stab}}{D_b}\right) = 2\cos^{-1}\left(\frac{19.6 \text{ in}}{40.5 \text{ in}}\right) = 2.13$$

$$p_{cr}^{'} = p_{cr}\frac{A^{'}}{A} = p_{cr}(\delta - \sin\delta)/\pi = (15.91 \text{ ksi})(2.13 - \sin(2.13))/\pi = 6.51 \text{ ksi}$$

In these equations, A' is the overlapping area of the top and bottom plates of the bearing when it is deformed, which is computed geometrically based on the angle δ. If the overlap area is zero, the critical load of the bearing is estimated to be zero, which is the basis for recommendations that the maximum displacement be limited to 2/3 of the bearing diameter (DIS, 2007). However, this estimate of p_{cr}' is thought to be conservative (Mosqueda et. al., 2010). Neglecting the seismic overturning loads for now, the factor of safety against buckling in the deformed configuration is

$$F.S. = \frac{p_{cr}^{'}}{1.2\, p_{dead}} = \frac{6.51 \text{ ksi}}{1.2(1.1 \text{ ksi})} = 5.38$$

Since seismic overturning effects could not conceivably more than double the axial loads on the bearings, this check need not be repeated considering the seismic load effects.

4.2.3.5 Maximum Shear Strain Demands

The shear strain demands under different loads and load combinations are limited to safe values for the bearing. New equations are listed in Chapter 14 of the Isolation Spec. Maximum shear strain demands are defined for various situations: 1) γ_c = shear strain due to compression loads, 2) $\gamma_{s,s}$ non-seismic lateral deformation due to temperature, shrinking and shrink, 3) $\gamma_{s,eq}$ = shear strain due to seismic loading, and 4) γ_r = shear strain due to rotation.

$$\gamma_c = \frac{D_c p_{dead}}{GS} = \frac{(1.0)(1.01 \text{ ksi})}{(0.075 \text{ ksi})(33.8)} = 0.40$$

$$\gamma_{s,s} = \frac{\Delta s}{t_r}$$

$$\gamma_{s,eq} = \frac{d_t}{t_r} = \frac{17.6 \text{ in}}{7.167 \text{ in}} = 2.48$$

$$\gamma_r = \frac{D_r d_b^2 \theta}{t \cdot t_r} = \frac{(0.375)(40.5 \text{ in})^2 (0.005)}{(0.338 \text{ in})(7.167 \text{ in})} = 1.50$$

Most of the variables in the above equations have been defined previously. D_c = 1.0 and D_r = 0.375 are shape factors, Δs is the lateral deformation due to non-seismic effects, and θ is the rotation from applicable service load combinations. Assuming that non-seismic deformations will not control the design, Δs was not computed. Furthermore, in lieu of precise calculations, θ was estimated as 0.005, which is an upper bound value giving allowance for uncertainties (Sec. 14.4.2.1 of AASHTO, 2007). The LRFD Spec requires that $\gamma_c \leq 3$, which is satisfied. Service load combinations in the LRFD Spec are ignored. The seismic load combination in the Isolation Spec is

$$\gamma_c + \gamma_{s,eq} + 0.5\gamma_r \leq 5.5$$
$$0.40 + 2.48 + 0.5(1.5) = 3.63 \leq 5.5$$

which is also satisfied.

4.2.3.6 Property Modification Factors

The final steps in the design of lead-rubber bearings, prior to analytical confirmation, are to compute the property modification factors and vertical and torsional stiffness for modeling.

Property modification factors are used to estimate the likely variation in bearing strength and stiffness over the life of the bridge. The bridge design procedure accounts for this variation by considering upper bound properties for force controlled actions and lower bound properties for displacement controlled actions. Under normal circumstances, the final property modification factors are determined by characterization tests. However, for preliminary design, property modification can be estimated using the guidance and tables in Appendix A of the Isolation Spec.

First, initial lower and upper characteristic strengths Q_L and Q_U of the bearing are established, noting that the observed strength from testing is typically larger in the first cycle relative to subsequent cycles. The final bounds for Q_L and Q_U should be established from testing, but the following values are recommended in the absence of test data (Buckle et. al., 2006):

$$Q_L = Q_D = 63.87 \text{ kip}$$
$$Q_U = 1.25 Q_D = 79.83 \text{ kip}$$

The property modification factor $\lambda_{\min}$ to establish the minimum values of k_2 and Q_D is currently recommended to be taken as 1.0. The property modification factor $\lambda_{\max}$ to establish the maximum values of k_2 and Q_D is computed as:

$$\lambda_{\max} = (\lambda_{\max,t})(\lambda_{\max,a})(\lambda_{\max,v})(\lambda_{\max,tr})(\lambda_{\max,c})(\lambda_{\max,scrag})$$

where $\lambda_{\max,t}$ accounts for the effect of temperature variation, $\lambda_{\max,a}$ accounts for the effect of aging, $\lambda_{\max,v}$ accounts for the effect of velocity, $\lambda_{\max,tr}$ accounts for the effects of travel and wear, $\lambda_{\max,c}$ accounts for the effect of contamination, and $\lambda_{\max,scrag}$ accounts for the effect of scragging. These factors can have different values for Q_D and k_2. Values established by Appendix A of the Isolation Spec are

$$\lambda_{\max,t} = \begin{cases} 1.4 \text{ for } Q_D \\ 1.1 \text{ for } k_2 \end{cases}$$
$$\lambda_{\max,a} = \begin{cases} 1.1 \text{ for } Q_D \\ 1.1 \text{ for } k_2 \end{cases}$$

where $\lambda_{\max,t}$ accounts for the effect of temperature variation, $\lambda_{\max,a}$ accounts for the effect of aging, $\lambda_{\max,v}$ accounts for the effect of velocity, $\lambda_{\max,tr}$ accounts for the effects of travel and wear, $\lambda_{\max,c}$ accounts for the effect of contamination, and $\lambda_{\max,scrag}$ accounts for the effect of scragging. The values are a function of bearing type (low damping, high damping, lead rubber or neoprene

bearing) and the lowest expected temperatures in the bridge. The remaining modification factors are taken to be 1.0, as they are either established by test (such as $\lambda_{max,v}$) or are not relevant for a lead-rubber bearing (such as $\lambda_{max,scrag}$). The full values of $\lambda_{max,t}$ and $\lambda_{max,a}$ are assumed only for a critical bridge, and may be reduced or adjusted if the bridge is designed as a normal bridge. The adjustment factor is $f_a = 0.75$ for an essential bridge, and the adjustment procedure is demonstrated for $\lambda_{max,t}(Q_D)$ as follows:

$$\lambda_{adj} = 1 + f_a(\lambda_{max} - 1) = 1 + 0.75(1.4 - 1) = 1.3$$

Likewise, the adjusted values of the remaining modification factors are $\lambda_{max,t}(k_2) = \lambda_{max,a}(k_2) = \lambda_{max,a}(Q_D) = 1.075$.

The final global modification factors and associated maximum and minimum values of k_2 and Q_D are summarized below:

$$\lambda_{max}(Q_D) = (1.3)(1.075) = 1.398$$
$$\lambda_{max}(k2) = (1.075)(1.075) = 1.156$$
$$Q_{min} = 1.0 \cdot Q_L = 63.87 \text{ kip}$$
$$k_{2,min} = 1.0 \cdot k_2 = 14.20 \text{ kip/in}$$
$$Q_{max} = \lambda_{max}(Q_D) \cdot Q_U = (1.3)(79.83 \text{ kip}) = 111.6 \text{ kip}$$
$$k_{2,max} = \lambda_{max}(k_2) \cdot k_2 = (1.156)(14.20 \text{ kip/in}) = 16.42 \text{ kip/in}$$

4.2.3.7 Vertical and Torsional Stiffness

The vertical stiffness k_v and torsional stiffness k_T of the bearing can be computed

$$k_v = \frac{E_c A_r}{t_r} = \frac{(514.8 \text{ ksi})(1233.7 \text{ in}^2)}{(7.167 \text{ in})} = 92536 \text{ kip/in}$$
$$k_T = \frac{GJ}{t_r} = \frac{(0.075 \text{ ksi})(264e3 \text{ in}^4)}{(7.167 \text{ in})} = 2764 \text{ kip-in/rad}$$
$$J = \frac{\pi D_b^4}{4} = \frac{\pi(40.5 \text{ in})^4}{4} = 264e3 \text{ in}^4$$

E_c is the compression modulus, as defined above, and J is the polar moment of inertia for the bearings.

The calculations for the abutment bearings are summarized in Table 4-4. Since the gravity loads on the abutment bearings are much smaller, a smaller diameter bearing can be

selected initially to satisfy the design constraints. The controlling factor for the size is the displacement capacity. DIS product information (DIS, 2007) indicates that a 31.5 inch bearing is necessary to be stable at 1.1 times the MCE displacement, which is 19.6 inches. However, we elected to try and make a 29.5 inch bearing work, because the size of the lead core is a bit small for the 31.5 inch bearing. The stability of the bearing was improved by specifying a lower shear modulus and increasing the number of bearing layers to 30, which is the maximum number of layers allowed for this size bearing. The bearing is more stable than typical for this configuration due to the relatively small gravity loads. The factor of safety against buckling in the deformed configuration, required to exceed 1, is 2.42. This value will be reassessed after the dynamic analysis. However, the overturning effects on the abutment bearings are expected to be small.

4.2.4 Summary of Design Specifications

A summary of the design specifications for both the pier bearing and the abutment bearing is given in Table 4-4.

4.3 Design of Single Friction Pendulum Bearings

4.3.1 Design Parameters and Displacement Demand

Unlike the lead-rubber bearings, the design of friction pendulum bearings does not depend on the supported weight except for determining the size of the slider. Thus, only one bearing type is needed to for use at both the pier and abutment locations. In fact, supported weight is not even considered in the design until determining the final dimensions. For the lead-rubber bearings, we advocated an approach where the strength and post-yield stiffness of the bearing are selected to match a target period and damping ratio in the 1000 year design earthquake. This approach cannot be used as easily for a friction pendulum bearing; the

Table 4-4: Summary of Specifications, Lead-Rubber Bearings for Pier and Abutment

Target Design Parameters	*Abutment Bearing*	*Pier Bearing*		*Restoring Force Capacity*	*Abutment Bearing*	*Pier Bearing*
Estimated weight per bearing (kip)	740.0	1300.0		k_2 (kip/in)	8.08	14.2
Spectral Acceleration S_{D1} (g)	0.56	0.56		T_2 (sec) ≤ 6.0	3.06	3.06
Target Period T_{eff} (sec)	2.50	2.50		0.025 $W/d_t \leq k_2$	1.04	1.83
Target Damping Ratio ξ	0.20	0.20		*Stability and Buckling F.S.*		

Bearing Stiffness k_{eff} (kip/in)	12.11	21.27	Shape factor S	44.0	33.8
Seismic Response Coefficient C_{smd}	0.148	0.148	$E_c = 6GS^2$ (ksi)	649.6	514.8
Damping Factor B_L	1.52	1.52	I (in^4)	32310	131829
Displacement demand d (in)	9.03	9.03	Critical Pressure p_{cr} (ksi)	16.84	15.91
Target Force-Displacement			Design Load Pressure p_{dead} (ksi)	1.16	1.01
Q_D (kip)	36.4	63.9	Buckling F.S. (undeformed)	14.51	15.76
k_1 (kip/in)	40.8	142.0	Angle for overlap δ	1.63	2.13
k_2 (kip/in)	8.08	14.20	Critical pressure deformed p_{cr}' (ksi)	3.36	6.51
D_Y (in)	0.50	0.50	Buckling F.S. (deformed)	2.42	5.38
Bearing Dimension Calculations			***Shear Strain Checks***		
Yield force F_Y (kip)	20.4	71.0	γ_c (compression) ≤ 3.0	0.47	0.40
Area Lead Core A_L (in^2)	31.1	54.6	γ_{eq} (earthquake)	3.85	2.48
Diameter Lead Core D_L (in)	6.29	8.34	γ_r (rotation)	2.14	1.50
Bearing diameter D (in)	29.5	41.5	$\gamma_c + \gamma_{s,eq} + 0.5\gamma_r \le 5.5$	5.39	3.63
Bonded diameter D_b (in)	28.5	40.5	***Property Modification Factors***		
Bonded area A (in^2)	637.9	1288.2	Q_L (kip)	36.36	63.87
Area of Rubber A_r (in^2)	606.9	1233.7	Q_U (kip)	45.44	79.83
Target Shear Modulus G (ksi)	0.056	0.0750	$\lambda_{min}(Q_D)$	1.00	1.00
Height of rubber t_r (in)	4.62	7.167	$\lambda_{max}(Q_D)$	1.40	1.40
Number of layers N	30.0	25.0	$\lambda_{min}(k_2)$	1.00	1.00
Layer thickness rubber t (in)	0.154	0.287	$\lambda_{max}(k_2)$	1.16	1.16
Layer thickness steel shim t_s (in)	0.13	0.13	Q_{min} (kip)	36.36	63.87
Thickness end plate t_p (in)	1.25	1.75	Q_{max} (kip)	6.53	111.61
Total height bearing H (in)	10.75	13.67	$k_{2,min}$ (kip/in)	8.08	14.20
Design Checks			$k_{2,max}$ (kip/in)	9.34	16.42
Lead Core Size Check ($1/6 < D_L/D_b < 1/3$)	0.221	0.206	***Vertical and Torsional Bearing Stiffness***		
MCE Properties			$k_v = E_c A_r / t_r$ (kip/in)	89617	92536
Spectral Acceleration S_{M1} (g)	0.878	0.878	$J = \Pi d^4/32$ (in^4)	64770.8	264131.4
Target Period T_{eff} (sec)	2.732	2.732	$k_T = GJ/t_r$ (kip-in/rad)	784.4	2764.1
Target Damping Ratio ξ	0.125	0.125			
Displacement demand d (in)	17.80	17.80			

parameter selection is limited because the curvature of the dish, which controls the post-yield stiffness of the bearing, is manufactured in discrete sizes.

For the friction pendulum bearing, the radius of curvature of the dish and the target friction coefficient are selected, and the effective parameters such as period, damping ratio, and design displacement are determined by iteration. Available standard curvature radii include R = 39, 61, 88, 120, 156 and 244 in, which correspond to post-yield period T_2 = 2, 2.5, 3, 3.5, 4 and 5 sec, respectively (EPS, 2003). To be comparable to the lead-rubber design with effective period

T_{eff} = 2.5 sec, we select R = 88 in corresponding to T_2 = 3 sec, since the effective period will be somewhat less than T_2. Standard dynamic friction coefficients range from 3% to 12%; we select a value of μ = 6%. The friction coefficient is generally chosen by trial and error, increasing or decreasing to optimize the damping ratio and displacement demand.

The iterative calculations to determine effective properties are similar to those presented previously for the lead rubber bearing, except adjusted to be in weight normalized form as indicated below. Note that the yield displacement d_y is assumed to be zero for a single pendulum bearing, because there is no movement until the force overcomes the static friction coefficient and the bearing begins to slide.

$$d = \left(\frac{g}{4\pi^2}\right)\left(\frac{S_{D1}T_{eff}}{B_L}\right)$$

$$\frac{f_{\max}}{W} = \mu + \left(\frac{2\pi}{T_2}\right)^2\left(\frac{d}{g}\right)$$

$$T_{eff} = 2\pi\sqrt{\frac{d}{f_{\max}/W}}$$

$$\xi = \frac{2}{\pi}\frac{\mu}{\mu + \frac{d}{R}}$$

$$B_L = \left(\frac{\xi}{0.05}\right)^{0.3}$$

The iteration commences with the assumption that T_{eff} = 2 sec and ξ = 0.20, which are the values for the design earthquake. The iterative calculations are summarized below in Table 4-5.

Table 4-5: Summary of iterations to calculate design displacement *d* for single friction pendulum bearing

	T_{eff} (sec)	ξ	B_L	d (in)	F_{max}/W
Iteration 1	2.0	0.2	1.516	7.22	0.142
Iteration 2	2.280	0.269	1.656	7.54	0.146
Iteration 3	2.301	0.262	1.644	7.66	0.147
Iteration 4	2.308	0.260	1.639	7.71	0.148
Iteration 5	2.311	0.259	1.637	7.73	0.148

Thus, the effective period converges to T_{eff} = 2.31 sec, the effective damping converges to ξ = 26%, and the design displacement converges to d = 7.73 in. The same series of iterative calculations are repeated with a spectral acceleration S_{M1} = 0.878g to determine the effective

properties and total design displacement for the MCE earthquake (Table 4-6). The iterations commence with an assumed effective period T_{eff}= 2.5 sec and effective damping ratio ξ = 20%.

Table 4-6: of iterations to calculate MCE displacement d_t for a single friction pendulum bearing

	T_{eff} (sec)	ξ	B_L	d_t (in)	F_{max}/W
Iteration 1	2.5	0.2	1.516	14.16	0.221
Iteration 2	2.560	0.173	1.451	15.15	0.232
Iteration 3	2.583	0.165	1.430	15.51	0.236
Iteration 4	2.591	0.162	1.422	15.64	0.238
Iteration 5	2.594	0.161	1.419	15.69	0.238

In summary, the converged properties for the MCE are T_{eff}= 2.59 sec and ξ = 16.1%, with a total design displacement of d_t = 15.7 in. The friction coefficient was intentionally selected to increase the effective damping relative to the comparable lead-rubber bearing design. Such measures help to limit the displacement demand of the bearing, which is an economical measure to limit the overall size and hence cost of the bearing. The diameter of a single friction pendulum bearing is more than twice its displacement capacity.

4.3.2 Bearing Size

The bearing is sized to provide a displacement capacity of d_t = 15.7 in. The displacement capacity of the bearing is

$$d_{cap} = \frac{(R-h)}{R}\frac{(D_1 - D_2)}{2}$$

where h = 5 in is the height of the dish, D_1 and D_2 are the diameter of the bearing and the diameter of the slider, respectively. The slider diameter D_1 is selected to limit the pressure on the slider due to maximum probable combination of dead, live and seismic loads to 60 ksi. The maximum probable load is conservatively assumed to be 1600 kips for a bearing on bent 2. Thus the area and inner diameter of the inner slider are calculated as:

$$A_{slider} \geq \frac{P}{\sigma_{\max}} = \frac{1600 \text{ kip}}{60 \text{ ksi}} = 26.7 \text{ in}^2$$

$$D_2 \geq \sqrt{\frac{4}{\pi} A_{slider}} = \sqrt{\frac{4}{\pi}(26.7)} = 5.83 \text{ in}$$

The inner slider diameter is selected to be $D_2 = 6$ inches. From this, the required diameter D_1 of the bearing can be computed as follows

$$D_1 = D_2 + \frac{2 d_{cap} R}{R - h} = 6 \text{ in} + \frac{2(15.7 \text{ in})(88 \text{ in})}{(88 - 5) \text{ in}} = 39.3 \text{ in}$$

The total diameter of the bearing should be slightly larger to configure a displacement stop; D_1 = 42 in is selected.

Many of the design checks performed for the lead-rubber bearing are not relevant for friction devices, such as stability and shear strain checks. The minimum restoring force requirement is still applicable, and for a friction pendulum device can be expressed as

$$T_2 \le 6.0 \sec$$
$$R / d_t \le 40$$

Since the second slope period is 3.0 sec per the radius of gyration, and R/d_t = 88/15.7 = 5.6, the requirement is satisfied.

4.3.3 Property Modification Factors

Property modification factors are also evaluated for a friction pendulum bearing, with the assistance of Appendix A of the Isolation Spec (AASHTO, 2010) in lieu of characterization tests. These factors only apply to the friction coefficient because the geometry of the bearing that determines the post-yield stiffness does not change due to environmental factors. Where applicable, the factors for unlubricated PTFE sliders were used. In summary, the property modification factors and maximum/minimum values of the strength and stiffness parameters are calculated as follows.

$$\lambda_{\min} = 1.0$$
$$\lambda_{\max} = (\lambda_{\max,t})(\lambda_{\max,a})(\lambda_{\max,v})(\lambda_{\max,tr})(\lambda_{\max,c})(\lambda_{\max,scrag})$$

$$\lambda_{\max,t} = 1.2$$
$$\lambda_{\max,a} = 1.1$$

All other individual $\lambda_{\max}$ factors are unity. The adjusted values of $\lambda_{\max,t}$ and $\lambda_{\max,a}$ are:

$$\lambda_{\max,t} = 1 + f_a(\lambda_{\max,t} - 1) = 1 + 0.75(1.2 - 1) = 1.15$$
$$\lambda_{\max,a} = 1 + f_a(\lambda_{\max,a} - 1) = 1 + 0.75(1.1 - 1) = 1.075$$

$$\lambda_{\max} = (1.15)(1.075) = 1.236$$
$$\mu_L = 1.0\mu = 0.06$$
$$\mu_U = 1.2\mu = 0.072$$
$$\mu_{\min} = \lambda_{\min}\mu_L = 0.06$$
$$\mu_{\max} = \lambda_{\max}\mu_U = 0.089$$

Finally, the compression stiffness of the bearing should be determined for analytical modeling. The single pendulum bearings have no tensile resistance. Guidance is not provided to determine the exact vertical stiffness, but product information from EPS (EPS, 2003) indicates that the compression stiffness of single pendulum bearings is about 10 times that of an elastomeric bearing, which is easily 10,000 times the lateral stiffness of the bearing.

4.3.4 Summary of Design Specifications

The specifications for the friction pendulum bearing are summarized in Table 4-7.

Table 4-7: Summary of Specifications for Single Friction Pendulum Bearing

Bearing Parameters	*Standard Bearing*	*Target MCE Parameters*	*Standard Bearing*
Friction Coefficient μ	0.06	Spectral Acceleration S_{M1} (g)	
Radius of Curvature R (in)	88.0	Peak Force F_{max}/W	0.238
Post-yield Period T_2 (sec)	3.0	Target Period T_{eff} (sec)	2.59
Outer Diameter D_1 (in)	42.0	Target Damping Ratio ξ	0.16
Inner Diameter D_2 (in)	6.0	Displacement demand d_t (in)	15.69
Slider Height h (in)	5.0	Displacement capacity d_{cap} (in)	15.70
Target Design Parameters		*Property Modification Factors*	
Spectral Acceleration S_{D1} (g)	0.56	μ_L	0.06
Peak Force F_{max}/W	0.148	μ_U	0.072
Target Period T_{eff} (sec)	2.31	λ_{min}	1.0
Target Damping Ratio ξ	0.26	λ_{max}	1.236
Displacement demand d (in)	7.73	μ_{min}	0.06
Restoring Force Capacity		μ_{max}	0.089
T_2 (sec) ≤ 6.0	3.0		
$R/d_t \leq 40$	5.6		

4.4 Design of Triple Friction Pendulum Bearings

4.4.1 Unique Response Characteristics of Triple Friction Pendulum Bearings

As described previously, the triple pendulum bearing has multiple sliding surfaces with different friction coefficients and radii of curvature that can be activated in different intensity earthquakes. Conceptually, the inner slider should be designed with a small friction coefficient such that it is activated in frequent/small earthquakes. The outer sliders should be designed with larger coefficients and are activated in rare and very rare earthquakes.

The behavior of triple pendulum bearings has been described thoroughly by previous sources (Fenz and Constantinou, 2008; Morgan, 2007), and the reader is advised to refer to those sources for a more thorough understanding of the theoretical behavior. The theoretical behavior of the triple pendulum bearing is summarized here using the notation of Morgan (2007).

A cross-sectional view of the triple pendulum bearing defining the parameters of the different sliding surfaces is shown in Figure 4-7. The inner slider has radius of curvature R_1 and friction coefficient μ_1 for both sliding surfaces. The lower and upper outer sliding surfaces are designated as surfaces 2 and 3, with radii and friction coefficients R_2, μ_2 and R_3, μ_3, respectively. The outer slider radii R_2 and R_3 need not be equal, and the outer slider friction coefficients μ_2 and μ_3 need not be equal, though they commonly are assumed to be equal.

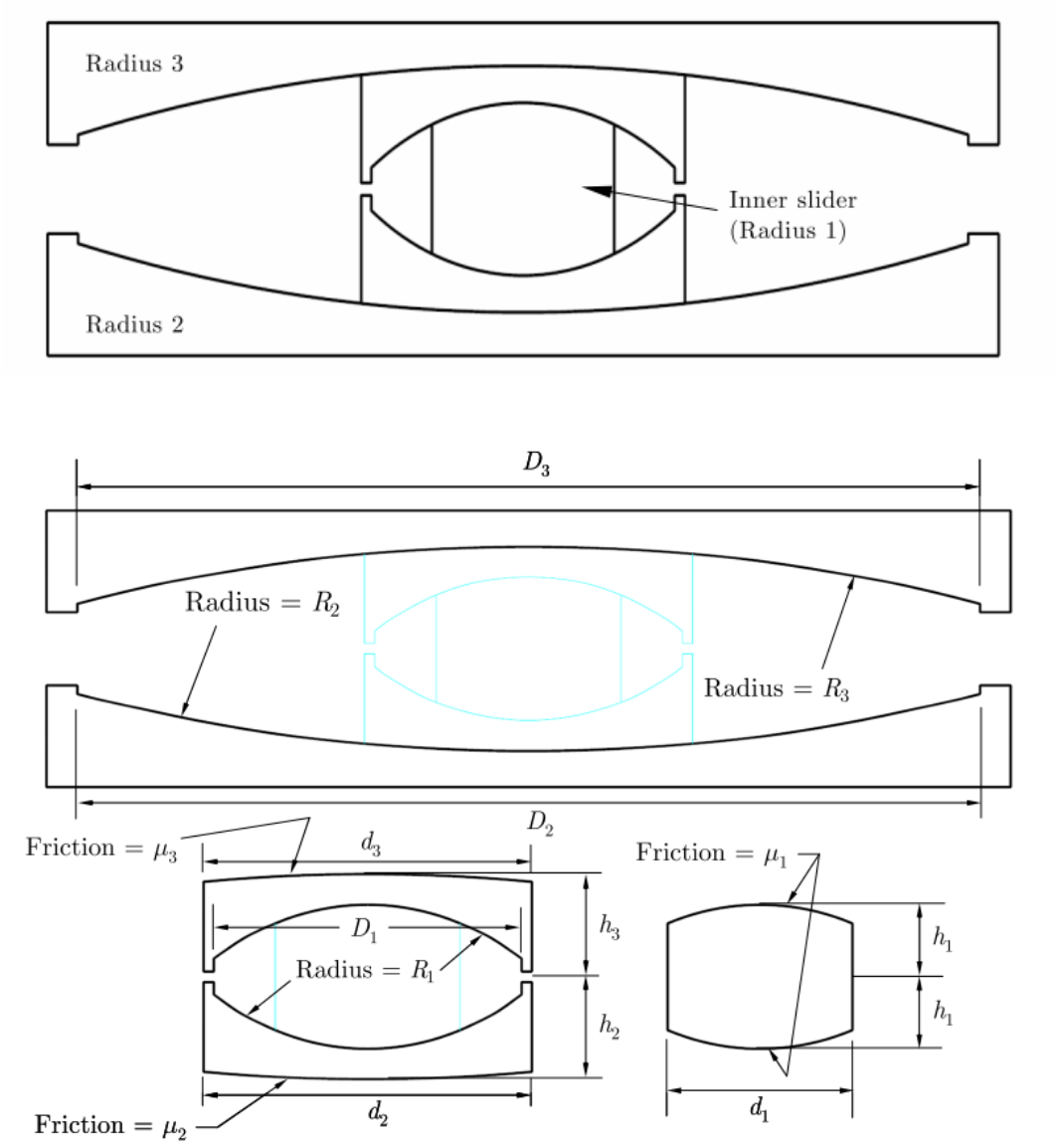

Figure 4-7: Geometry of a triple pendulum bearing indicating radii of curvature and friction coefficients for the different sliding surfaces. Source: Figure 3.6 and 3.7 of Morgan, 2007.

A backbone curve for the force-displacement relationship of the system is shown in Figure 4-8. The linear regions of the segment represent different stages of sliding. The transition forces on the backbone curve are determined by the relative friction coefficients while the stiffness (or slope) of the different regions are determined by effective pendulum lengths. No sliding occurs until the force exceeds the minimum friction coefficient μ_1. Recall that the post-yield stiffness k_2 of a single pendulum bearing is W/R; thus the relation between normalized force F/W and displacement u is $1/R$. For a triple pendulum bearing the relation between

normalized force and displacement in each sliding region is determined by the effective length L_{eff}, given as:

$$\frac{1}{L_{eff}^1} = \frac{1}{2L_1}$$
$$\frac{1}{L_{eff}^2} = \frac{1}{L_1 + L_2}$$
$$\frac{1}{L_{eff}^3} = \frac{1}{L_2 + L_3}$$
$$\frac{1}{L_{eff}^4} = \frac{1}{L_1 + L_3}$$
$$\frac{1}{L_{eff}^5} = \frac{1}{2L_1}$$

for sliding stages 1-5, respectively. The lengths L_1, L_2, L_3 are related to the radii of curvature R_1, R_2, R_3, according to:

$$L_1 = R_1 - h_1$$
$$L_2 = R_2 - h_2$$
$$L_3 = R_3 - h_3$$

where h_1, h_2 and h_3 are the half heights of the sliders as shown in Figure 4-7.

Cyclic force-displacement relations for the different stages of sliding are shown in Figure 4-9. In the first stage of sliding, the inner slider, which should have the smallest friction coefficient, is activated (Figure 4-9a). The parameters for stage 1 sliding are generally selected so that the bearing is activated in a small earthquake.

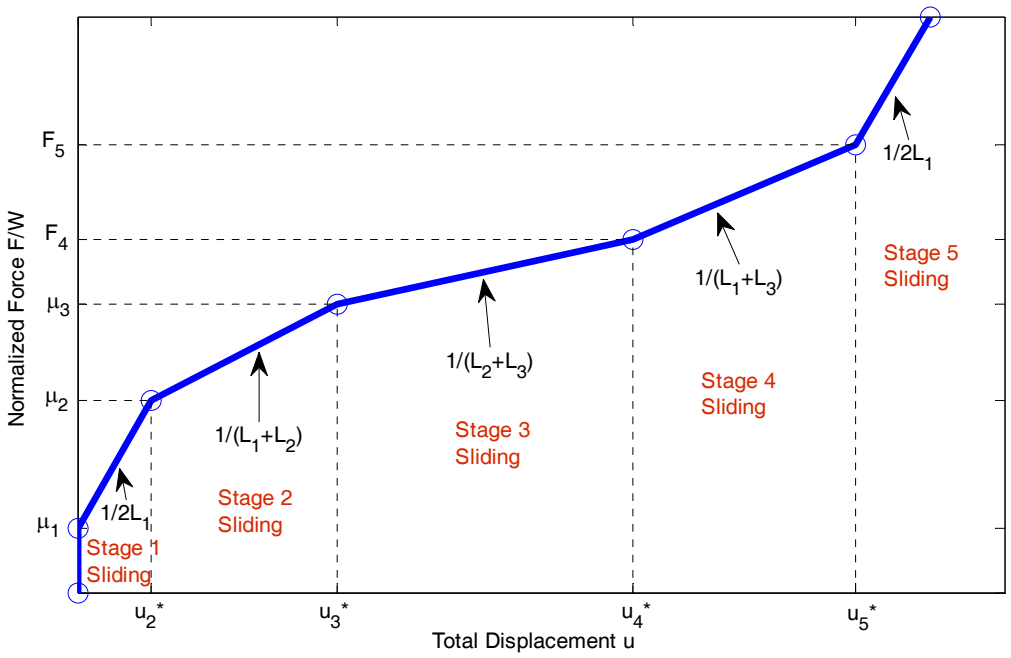

Figure 4-8: Force-displacement backbone curve for the triple pendulum bearing; arrows indicate slopes for each of the intermediate stages of sliding.

4.4.2 Multi-Objective Design Strategy

Previous researchers have described the concept of selecting the parameters of the triple pendulum bearings to optimize the performance for multiple seismic hazards constituting different intensity earthquakes. However, we were unable to find details for a recommended design strategy in the literature. For the Utah bridge, we elected to target distinct performance goals in 3 different events: a 72 year return period earthquake (frequent event), a 1000 year return period earthquake (the design event), and a 2500 year earthquake (the typical Maximum Considered Event or MCE). The performance goals extend to the effective vibration properties of the isolation system in the various earthquakes, but not to superstructure response, recognizing that if the isolation system responds as expected, the bridge superstructure and substructure response will be satisfactory. Initially, a target effective period and effective damping ratio was selected for each event. However, targeting a single period and damping ratio for each event turned out to be too restrictive, so instead target period and damping ratio *ranges* were defined.

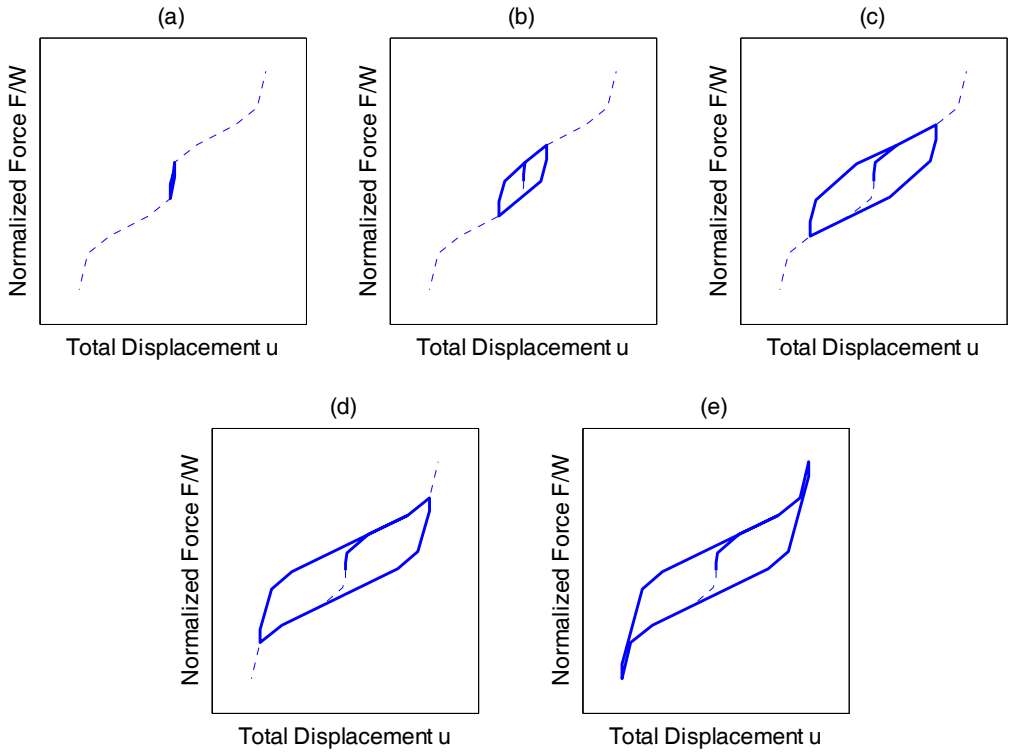

Figure 4-9: Cyclic force-displacement for different stages of sliding in a triple pendulum bearing: (a) stage 1 sliding, (b) stage 2 sliding, (c) stage 3 sliding, (d) stage 4 sliding, and (e) stage 5 sliding

The target ranges for each event are identified below, wherein the displacement demand is computed from the effective properties and the spectral intensity in the usual manner (Sec 4.2.1). In the following, the subscript F refers to the frequent event, D to the design event and M to the MCE.

Frequent Event (72 year)	Design Event (1000 year)	Maximum Event (2500 year)
Spectral Accel. S_{F1}=0.1g	Spectral Accel. S_{D1}=0.56g	Spectral Accel. S_{M1}=0.88g
Period T_F = 1-2 sec	Period T_D = 2-3 sec	Period T_M = 3-4 sec
Damping ratio ξ_F= 10-15%	Damping ratio ξ_D= 15-20%	Damping ratio ξ_M= 20-25%
Displacement d_F = 0.7-1.6 in	Displacement d_D = 7.2-11.8 in	Displacement d_M = 15.9-22.7 in

The target period and damping ratio range for the design event was selected to be comparable to the single target values that were used for the lead-rubber bearing and single pendulum bearing designs. The period ranges for the frequent and maximum events were reduced/increased by 1 second, respectively, relative to the design event, recognizing that the isolation system inevitably responds behaves stiffer in a smaller event and more flexible in a

larger event. The target damping ratio was decreased for the frequent event to prevent the isolation system from being overly damped and hence ineffective in a small earthquake. Likewise, the target damping ratio was increased for the maximum event to attempt to limit the displacements of the isolation system when extreme earthquake energy is transmitted to the bridge structure. A traditional bilinear isolation system performs the opposite of this; that is, the effective damping ratio consistently decreases as the intensity of the earthquake is increasing.

As shown earlier, for a bearing that cycles through displacement d at force f_{max}, the effective period T_{eff}, and damping ratio ξ_{eff} can be found as follows:

$$T_{eff} = 2\pi\sqrt{\frac{d}{f_{\max}/W}}$$

$$\xi_{eff} = \frac{1}{4\pi}\frac{W_D/W}{\frac{1}{2}\left(f_{\max}/W\right)d}$$

where W_D is the area of one cycle of the force-displacement loop at amplitude d. The equation for ξ has been generalized for arbitrary force-displacement compared to the equation given earlier.

For a triple pendulum bearing, the design parameters that can be selected to satisfy the objectives are the radius of each sliding surface (R_1, R_2, R_3), the height of each slider (h_1, h_2, h_3), the inner and outer diameter of each slider (D_{1i}, D_{2i}, D_{3i}, D_{1o}, D_{2o}, D_{3o}), and the friction coefficient of each sliding surface (μ_1, μ_2, μ_3). The radii with the slider heights together control the effective length of each pendulum. The radii and heights cannot be selected without constraints; as reported earlier the outer pendulum are manufactured in distinct sizes: R = 39, 61, 88, 120, 156, and 244 in (EPS, 2003). Effective lengths L_2 and L_3 are selected from these sizes assuming that the ratio of L_i/R_i for the outer pendulum is about 92%. Manufactured sizes for the smaller inner pendulum are unknown; however, the selection of effective length for the inner pendulum is thought to be less restrictive.

The geometry of the sliders also controls the displacement capacity of each sliding surface according to the following equations:

$$\overline{u}_1 = \frac{L_1}{R_1}\frac{(D_{1o} - D_{1i})}{2}$$
$$\overline{u}_2 = \frac{L_2}{R_2}\frac{(D_{2o} - D_{2i})}{2}$$
$$\overline{u}_3 = \frac{L_3}{R_3}\frac{(D_{3o} - D_{3i})}{2}$$

The displacement capacity of the inner slider $\overline{u}_1$ is relatively unimportant for design, assuming it is sufficiently long. The displacement capacities of the two outer sliders, $\overline{u}_2$ and $\overline{u}_3$, were assumed to be unconstrained for selection, as well as the three friction coefficients μ_1, μ_2, μ_3.

4.4.3 Parameter Selection for Frequent Event (72 year)

Parameters were selected for the frequent event such that the target displacement was reached at the end of stage 1 sliding. Stage 1 represents sliding of the inner pendulum only, which is generally characterized by a relatively small friction coefficient. In this way, sliding of the inner pendulum can be activated relatively easily in the small acceleration intensities that characterize a frequent event. Since the displacements in the frequent event are small, it is desirable not to engage one of the outer sliders generally associated with a larger level of energy dissipation. At the end of stage 1 sliding:

$$d_F = u_2^* = 2L_1(\mu_2 - \mu_1)$$
$$\frac{F_F}{W} = \tilde{F}_2 = \mu_2$$
$$\frac{W_{DF}}{W} = 4\frac{Q_F}{W}d_F \quad \text{where} \quad \frac{Q_F}{W} = \tilde{F}_1 = \mu_1$$

Thus, the response in the frequent event is controlled by three parameters, L_1, μ_1 and μ_2. Since equations for d_F, T_F and ξ_F are functions of these three parameters, it is possible to solve for the L_1, μ_1 and μ_2 for precise target values using iterative solution methods for nonlinear equations. For this bridge, we selected parameters that led to effective properties in the target range through trial and error. We observed that the best way to control the parameters was to limit the friction coefficient μ_1 of the inner slider to small values, to select the effective length L_1 of the inner slider to meet the target displacement range, and to select the friction coefficient μ_2 of the first outer slider to meet the target period and damping ranges. The parameters selected for this bridge were:

$$L_1 = 14 \text{ in}$$
$$\mu_1 = 0.01$$
$$\mu_2 = 0.05$$

which led to

$$T_F = 1.51 \text{ sec}$$
$$\xi_F = 12.7\%$$
$$d_F = 1.12 \text{ in}$$

which falls within the range of parameters for the frequent event. The friction coefficient μ_1 = 0.01 likely does not satisfy the AASHTO requirement for minimum force capacity to resist wind and braking loads (AASHTO, 2010). Wind restraint devices could be added, but strengthening the system is counteractive to the objective to provide a system with low damping initially that is effective in a frequent earthquake. To our knowledge, no bridge has been designed in the United States with triple pendulum bearings to date. Using a multi-objective design strategy with triple pendulum bearings is something that should be addressed in future versions of the AASHTO Guide Specifications for Seismic Isolation Design.

4.4.4 Parameter Selection for Design Event (1000 year)

Parameters were selected for the design event such that the target displacement was reached at the end of stage 2 sliding. (Stage 2 sliding activates the outer slider with the lesser friction coefficient). In principle, the design displacement could be reached somewhere in the middle of stage 3 sliding; however, given that maximum displacements are generally on the order of twice the design displacements, it is desirable for most of the incremental maximum displacement to take place in stage 3 to avoid overactivating the stiffening range for the MCE. At the end of stage 2 sliding:

$$d_D = u_3^* = u_2^* + (L_1 + L_2)(\mu_3 - \mu_2)$$

$$\frac{F_D}{W} = \tilde{F}_3 = \mu_3$$

$$\frac{W_{DD}}{W} = 4\frac{Q_D}{W}d_D - 2\frac{A_{T1}}{W} \quad \text{where}$$

$$\frac{Q_D}{W} = \frac{2\mu_1 L_1 + \mu_2(L_2 - L_1)}{(L_1 + L_2)}$$

$$\frac{A_{T1}}{W} = \frac{1}{2}\left[\frac{1}{2L_1} - \frac{1}{(L_1 + L_2)}\right](2u_2^*)^2$$

Note that Q_D is the force or value of the line for stage 2 sliding, which passes through $\tilde{F}_2$ and $\tilde{F}_3$, extended back to the y-intercept, and A_{T1} is the area of each of the triangles that are cut out of the top left and bottom right of the force-displacement loop, as shown in Figure 4-9(b). Since L_1, μ_1 and μ_2 have already been selected, only the effective length L_2 of the first outer pendulum and the friction coefficient μ_3 of the second outer pendulum slider surface can be selected independently for the design event. In this case, target values of displacement, period, and damping ratio cannot all be simultaneously satisfied since only two parameters are available for three constraints. However, it becomes feasible to select parameters that put the system within the target range identified previously. The parameters selected to control the design event were:

$$L_2 = 110 \text{ in}$$
$$\mu_3 = 0.13$$

which led to

$$T_D = 2.95 \text{ sec}$$
$$\xi_D = 18.5\%$$
$$d_D = 11.04 \text{ in}$$

Note that this displacement does not exactly fall on the spectrum characterized by S_{D1} = 0.56g, but it is close enough for a preliminary design purpose.

4.4.5 Parameter Selection for Maximum Event (2500 year)

Parameters were selected for the maximum event such that the target displacement was reached one quarter of the way through stage 4 sliding (i.e. one fourth of the distance from u_3* to

u_4*). By positioning the maximum event near the beginning of stage 4, the large displacement stiffening region is activated and the effective damping is increased, which slows the bearing and limit displacement as desired. However, the displacement capacity of the bearing is still far from being reached. The displacement, force and associated values one fourth of the way through stage 4 sliding are as follows:

$$d_M = \frac{3}{4}u_4^* + \frac{1}{4}u_5^* \quad \text{where}$$

$$u_4^* = u_3^* + \left(\frac{\overline{u}_2}{L_2} + \mu_2 - \mu_3\right)(L_2 + L_3)$$

$$u_5^* = u_4^* + \left(\frac{\overline{u}_3}{L_3} + \mu_3 - \frac{\overline{u}_2}{L_2} - \mu_2\right)(L_1 + L_3)$$

$$\frac{F_M}{W} = \frac{3}{4}\tilde{F}_4 + \frac{1}{4}\tilde{F}_5 \quad \text{where}$$

$$\tilde{F}_4 = \frac{\overline{u}_2}{L_2} + \mu_2$$

$$\tilde{F}_5 = \frac{\overline{u}_3}{L_3} + \mu_3$$

$$\frac{W_{DM}}{W} = 4\frac{Q_M}{W}d_M - 2\frac{A_{T2}}{W} \quad \text{where}$$

$$\frac{Q_M}{W} = \frac{2\mu_1 L_1 + \mu_2(L_2 - L_1) + \mu_3(L_3 - L_1)}{(L_2 + L_3)}$$

$$\frac{A_{T2}}{W} = \frac{1}{2}\left[\frac{1}{(L_1 + L_2)} - \frac{1}{(L_2 + L_3)}\right](2u_3^*)^2$$

Similar to earlier notation, QM is the force or value of the line for stage 3 sliding, which passes through $\tilde{F}_3$ and $\tilde{F}_4$, extended back to the y-intercept, and A_{T2} is the area of each of the large triangles that are cut out of the top left and bottom right of the force-displacement loop, as shown in Figure 4-9(c). The smaller triangles adjacent to stage 4 loading and unloading slopes have been neglected, assuming that their areas are both small and essentially cancel each other out (Figure 4-9(c)).

The parameters that remain to be selected are the effective length L_3 of the second outer pendulum and the displacement capacities $\overline{u}_2$ and $\overline{u}_3$ of the outer sliding surfaces. Although L_3 can in principle be selected independently of L_2, we chose to make L_3 identical to L_2 as selecting L_3 independently did not lead to an appreciable advantage in terms of matching target design

parameters. Likewise, although $\bar{u}_2$ and $\bar{u}_3$ could be varied independently, only their sum was influential in matching target parameters, and keeping them identical leads to a bearing with nice geometry that is easy to build. As such, these three parameters were selected by trial and error as:

$$L_3 = 110 \text{ in}$$
$$\bar{u}_2 = 11.5 \text{ in}$$
$$\bar{u}_3 = 11.5 \text{ in}$$

which led to

$$T_M = 3.33 \text{ sec}$$
$$\xi_M = 20.8\%$$
$$d_M = 18.9 \text{ in}$$

Again this displacement is not exactly on the spectrum characterized by $S_{M1} = 0.88g$, but is considered to be sufficiently close.

4.4.6 Finalizing the Geometry of the Bearing

The final steps in the design of the triple pendulum bearing involve selecting the heights and diameters of each of the sliders. As discussed previously, the pendulum lengths L_2 and L_3 were selected with regard to pre-determined manufacturer sizes for radii. For this design, lengths $L_2 = L_3 = 110$ in correspond to radii $R_2 = R_3 = 120$ in. Accordingly, the heights governing the outer sliders are $h_2 = h_3 = 10$ in. By inspection of the typical geometry of a triple pendulum bearing (Figure 4-7), the inner slider is generally about half the height of the outer slider. Accordingly, we selected the inner slider height to be $h_1 = 5$ in, which leads to an inner pendulum radius $R_1 = 19$ in.

The inner slider inner diameter d_1 is selected to limit the pressure on the slider due to maximum probable combination of dead, live and seismic loads to 60 ksi. The maximum probable load is conservatively assumed to be 1600 kips for a bearing on bent 2. Thus the area and inner diameter of the inner slider are calculated as:

$$A_{slider} \geq \frac{P}{\sigma_{\max}} = \frac{1600 kip}{60 ksi} = 26.7 \text{ in}^2$$

$$D_{1i} \geq \sqrt{\frac{4}{\pi} A_{slider}} = \sqrt{\frac{4}{\pi}(26.7)} = 5.83 \text{ in}$$

The inner slider diameter was selected to be 6 inches.

As mentioned previously, the inner slider capacity is considered to be relatively unimportant for design, as long as it is sufficient to achieve the desired backbone curve. The inner slider capacity must therefore exceed the assumed stage 1 displacement of 1.12 in. We assumed an inner slider displacement capacity of 2.5 in. Thus, the required outer diameter D_{1o} of the inner slider is:

$$D_{1o} = D_{1i} + \frac{2\bar{u}_1 R_1}{L_1} = 6 \text{ in} + \frac{2(2.5 \text{ in})(19 \text{ in})}{14 \text{ in}} = 12.8 \text{ in}$$

The outer diameter D_{1o} is selected to be 13 in. The outer diameter D_{1o} of the inner slider is also the inner diameter of the outer sliders; hence $D_{2i} = D_{3i} = 13$ in. Finally, the outer diameters $D_{2o} = D_{3o}$ of the outer sliders are selected:

$$D_{2o} = D_{2i} + \frac{2\bar{u}_2 R_2}{L_2} = 13 \text{ in} + \frac{2(11.5 \text{ in})(120 \text{ in})}{110 \text{ in}} = 38.1 \text{ in}$$

D_{2o} and D_{3o} are selected to be 38 in.

5. Inspection and Maintenance of Bridges with Seismic Isolation Bearings

Little guidance is publicly available regarding proper maintenance practices for seismically isolated bridges. The most recent Isolation Spec is silent with regard to inspection and maintenance, stating only that special requirements for maintenance and inspection must be submitted to the engineer prior to the start of prototype testing. This implies that development of proper maintenance practices are at the discretion of the owner on a case-by-case basis.

For advice on inspection and maintenance, we consulted with Professor Ian Buckle of the University of Nevada, Reno, who is a renowned expert on seismic isolation, especially with regard to its application in bridges. The discussion that follows is based primarily on this consultation.

A typical biennial bridge inspection should include inspection of the isolation bearings. First, the inspector should check carefully that the isolation gap or clearance at the abutments is properly maintained. Litter or debris may collect in the isolation gap and should be cleared out. A contractor may unknowingly fill the gap between the abutment ends and the backwall or wing walls. Analogous examples can be cited for buildings where portions of the moat have been filled in. The inspector should also check that the free relative movement above and below the isolators has not been obstructed; for example, elements of the superstructure not directly above the isolators should not be connected directly to the bent cap. Finally, the inspector should check for other modifications to the bridge that might affect the ability of the isolators to deform. An example was given where a structural modification above the bridge deck had resulted in mortar flowing down and hardening around the isolators, which would inhibit their ability to respond as indicated. If modifications are required, such as running electrical wires or pipes across the isolation gap, they should be detailed for flexibility in the transverse direction.

The inspection of the isolation bearings is similar to inspection practices for standard non-seismic bearings. An elastomeric isolation bearing is surrounded by a layer of cover rubber that protects the internal part of the bearing from exposure to the elements. DIS advertises that the bearings do not contain any moving parts that can be degraded by road salts or other

environmental conditions. The bearing has been designed such that damage to the cover layer occurs first. Substantial damage or wear is apparent when touching the cover rubber causes a powder residue to be dispersed over the fingers. However, damage to the cover rubber alone does not necessarily imply that the working part of the bearing is damaged. If the occurrence of powder residue is accompanied by significant visible signs of damage such as discoloration, splitting or cracking, bearing replacement is advisable. Another source of damage to bearings is bulging of the rubber layers that most likely signifies separation, or delamination, of the rubber layers from the steel shims. If bulging is substantial enough to be observed through the cover rubber layer, the isolation bearing should also be replaced.

Elastomeric bearings can develop a "residual displacement" when subjected to any amount of lateral forces or movement. Such residual displacement can be produced by thermal expansion, creep, small seismic events, etc. Most experts advise that residual displacement is not a concern, and small residual displacements can be ignored. Significant residual displacement should only be present after a large seismic event. Recentering the bearings after initial creep and temperature expansion is advisable. If significant creep or thermal expansion is observed within the first six months, the bearings should be recentered, and the original contractor may be the best person to contact. Long bridges may also be subjected to shortening under prestress, and periodic adjustments are advisable.

For friction pendulum bearings, the inspector may look for corrosion that occurs in the exposed metal parts. A highly corroded friction bearing should be replaced; less severe corrosion should be treated for preventive maintenance. EPS advertises that their isolation bearings maintain their design stiffness and damping over extreme temperature variation (-54°F to 102°F). Single pendulum bearings are manufactured with exposed parts, while triple pendulum bearings are also developed with a cover layer to better protect the internal working parts of the bearing. EPS also advertises that their bearings provide resistance to environmental deterioration and aging, while the sliding surface is defined by higher strength and wear durability than a typical PTFE material. Friction pendulum bearings are less likely to be used in small highway bridges due to lack of a vendor that competes for this market share.

6. Summary / Conclusion

In accordance with the purpose stated in the introductory portions of this report, the design criteria and seismic performance of a typical highway bridge designed with conventional lateral resistance and alternatively with a seismic isolation system, have been compared for high performance criteria. The overall findings of the design and analysis are hereby summarized, and the properties of each type of element are compared.

The as-built Legacy Bridge was evaluated with reference to the latest LRFD design specifications and seismic design specifications (AASHTO 2009a, 2009b). Because the Seismic Spec (AASHTO 2009a) does not contain acceptance criteria for the performance objectives of Essential or Critical bridges evaluated by the displacement-based approach, common relations between response modification factor and ductility were employed to derive an upper bound ductility capacity of 2. The bridge satisfies this performance criteria with a maximum ductility demand = 1.5, as determined from response spectrum analysis. However, at this displacement demand, the bridge bent has reached the maximum force capacity as determined from pushover analysis, implying that plastic hinges have formed in all the columns. Therefore, we question whether the operational performance objective will be met, and may depend greatly on the amount of overstrength that has not been directly accounted for in the analysis. Also, the abutment foundation had only a marginal factor of safety in the transverse direction, and would be considered inadequate under the spectral demands corresponding to the high performance objectives.

After incorporating configuration and modeling changes to incorporate a seismic isolation system, the bridge was re-evaluated using comparable linear response spectrum analysis to determine the seismic demands. As already discussed, isolating a structure changes the seismic response by shifting the period away from the high acceleration region of the response spectrum, reducing the lateral force demands, and changing the fundamental mode shapes so that nearly all of the displacement demand is concentrated in the isolators. The period of the bridge was lengthened from 0.40 to 2.61 seconds, reducing the spectral acceleration of the bridge by about 86%.

The bridge columns and foundations were redesigned with the objective of keeping the substructure response elastic under the design earthquake. As shown in Section 3.4.1, the reduction in overall demands greatly reduces the forces on the bents, and the column section sizes can be significantly reduced, even while preserving the elastic response objective. For the Isolated Bridge configuration, the columns are reduced from 6 feet to 4.5 feet in diameter, using 60% less concrete and 70% less longitudinal steel than for the conventional Legacy Bridge.

The reduction in column force demand also passes to the foundations, such that a substantially reduced pier pile group is possible (Section **Error! Reference source not found.**). The foundations are also significantly smaller; the piers require only 12 piles 25 feet long instead of the original 32 piles 50 feet long, and each pier pile cap has only 44% of the original plan area and only half the thickness (22% of the original volume of concrete), requiring only 24 #8 bars for longitudinal reinforcement instead of the original 47 #10 bars (32% of the original area of the bottom layer longitudinal steel). Additional reductions in transverse steel are expected, but not quantified.

A summary and comparison of the demands in the columns and foundations is found in Section 3.6. The reduction in column and foundation size should lead to a significant cost decrease in materials and labor, making up for the added cost related to the isolation system and any special detailing that may be required to accommodate these changes. The Isolated Bridge is expected to be more cost effective, and surpass performance expectations ensuring that the design objective is met.

Based on the analyses performed above, it appears that the isolated bridge designed for this case study performs much better than the conventionally designed bridge, and would likely be less expensive to construct, given the magnitude of the reductions in column and foundation size. Bridge isolation is therefore considered an efficient and cost-effective approach to achieve high seismic performance objectives for small multi-span highway bridges.

7. References

American Association of State Highway and Transportation Officials (AASHTO), (2006). *LRFD Bridge Design Specifications*, *4th Edition*.

American Association of State Highway and Transportation Officials (AASHTO), (2009a). *AASHTO Guide Specification for LRFD Seismic Bridge Design, 1st Edition.*

American Association of State Highway and Transportation Officials (AASHTO), (2009b). *AASHTO LRFD Bridge Design Specifications, with 2009 Interim Revisions, 4th Edition*.

American Association of State Highway and Transportation Officials (AASHTO), (2009c). *Seismic Design Parameters CD, Version 2.10,* http://earthquake.usgs.gov/hazards/designmaps/aashtocd.php [11 November 2010].

American Association of State Highway and Transportation Officials (AASHTO), (2010). *AASHTO Guide Specifications for Seismic Isolation Design, 3rd Edition.*

Applied Technology Council (ATC) and Multidisciplinary Center for Earthquake Engineering Research (MCEER), (2003). *Recommended LRFD Guidelines for the Seismic Design of Highway Bridges, Part I. Specifications and Part II. Commentary and Appendices*. MCEER-03-SP03.

Buckle, I., Constantinou, M., Dicleli, M., and Ghasemi, H. (2006). *Seismic Isolation of Highway Bridges*, *Special Report MCEER-06-SP07*, MCEER, University of Buffalo, The State University of New York.

Chopra, A. K. (2003). *Dynamics of Structures, Theory and Applications to Earthquake Engineering*, Prentice Hall, 3rd Edition.

Dynamic Isolation Systems (DIS), (2007). "Seismic Isolation for Buildings and Bridges, the Best Earthquake Protection Technology in the World", *Seismic Isolation Brochure*, http://www.dis-inc.com/brochures.html [12 July 2010].

Earthquake Protection Systems, Inc. (EPS), (2003). "Technical Characteristics of Friction Pendulum Bearings", [12 July 2010].

Earthquake Protection Systems, Inc. (EPS), (2010). http://www.earthquakeprotection.com [12 July 2010].

Fenz, D. M. and Constantinou, M. C. (2008). "Spherical sliding isolation bearings with adaptive behavior: Theory", *Earthquake Engineering and Structural Dynamics*, 37:163-183.

Morgan, T. A. (2007). "The Use of Innovative Base Isolation Systems to Achieve Complex Seismic Performance Objectives", *PhD Dissertation*, University of California, Berkeley.

Mosqueda, G., Masroor, A., and Sanchez, J. (2010). Preliminary Results from Bearing Stability Studies, Unpublished.

Ryan, K. L., and Chopra, A. K. (2004). "Estimation of Seismic Demands on Isolators Based on Nonlinear Analysis", *Journal of Structural Engineering*, ASCE, 130(3):392-402.

United States Geological Survey (USGS), (2008). *AASHTO Seismic Demand Parameters CD*, Publication USGSSEIS-1-CD, Available from American Association of State Highway Transportation Officials (AASHTO)
or http://earthquake.usgs.gov/hazards/designmaps/aashtocd.php.

Appendix A: Supporting Analysis for the Legacy Bridge

A1. Mander Confined Concrete Model

(Units: Kip-ft)

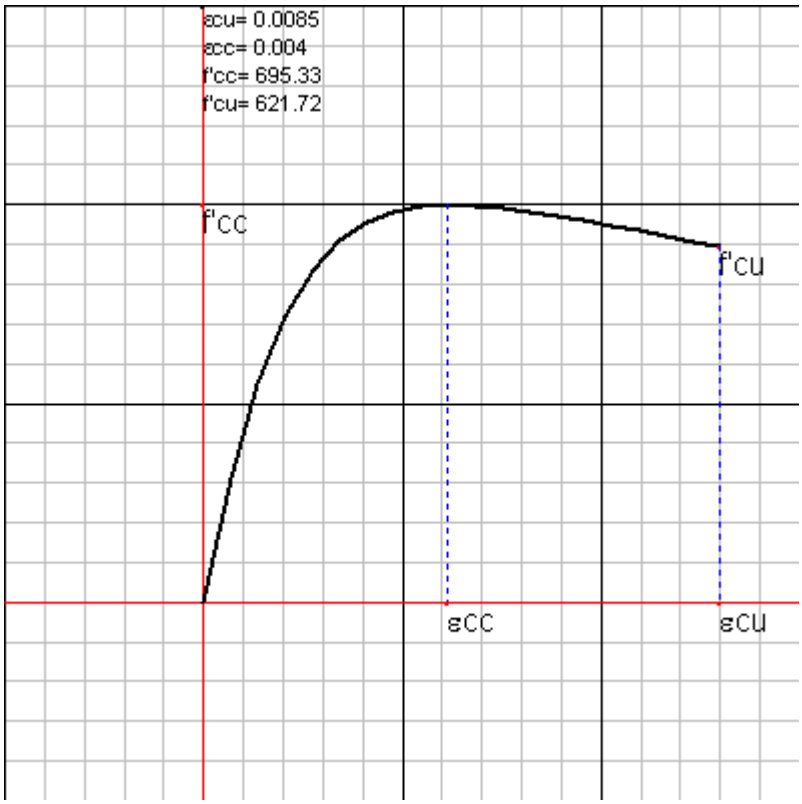

Point	Strain	Stress
1.	0.	0.
2.	4.451E-04	214.8681
3.	8.902E-04	381.3913
4.	1.335E-03	499.6618
5.	1.780E-03	579.6106
6.	2.225E-03	631.6122
7.	2.671E-03	663.9801
8.	3.116E-03	682.7751
9.	3.561E-03	692.2476
10.	4.006E-03	695.3343
11.	4.451E-03	694.0582
12.	4.896E-03	689.816
13.	5.341E-03	683.5771
14.	5.786E-03	676.0179

15.	6.231E-03	667.6129
16.	6.676E-03	658.6966
17.	7.122E-03	649.5052
18.	7.567E-03	640.2053
19.	8.012E-03	630.9147
20.	8.457E-03	621.7157

CONCRETE PROPERTIES

w = Unit weight of concrete = 0.144

f'_{co} = Compressive strength of unconfined concrete = 576.

E_c = Tangent modulus of elasticity of concrete = 33 $w^{1.5}$ $(f'_{co})^{1/2}$ ...(in psi) = 519120

ε_{co} = Concrete strain at f'_{co} = 2.000E-03

CONFINEMENT STEEL PROPERTIES

Confinement Type = Spiral

f_{syh} = Yield stress of the confinement steel = 9792.

d_b = Dia of confinement steel = 0.0833

ε_{su} = Strain at maximum tensile stress = 0.06

$\varepsilon_{cu(limit)}$ = Maximum Limit for ultimate concrete strain capacity = 0.05

CROSS SECTION DETAILS

A_s = Area of main column bars = 0.2381

A_{sp} = Area of confinement steel = 5.486E-03

s = C/C distance between spiral = 1.

d_s = Diameter of the spiral = 5.4167

A_c = Area of concrete core = $\pi/4\ d_s^2$ = 23.0438

CALCULATIONS

ρ_{cc} = Main column steel ratio = A_s / A_c = 0.0103

A_{cc} = Concrete core area excluding long. bars = $A_c(1 - \rho_{cc})$ = 22.8057

s' = Clear distance between hoops/spiral = $s - d_b$ = 0.9167

A_e = Concrete area confined effectively = $\pi/4\ d_s^2\ (1 - s'/(2d_s))$ = 21.0939

k_e = Confinement effectiveness coefficient = A_e / A_{cc} = 0.9249

ρ_s = Volumetric ratio of transverse confinement steel to the concrete core

$\rho_s = 4\ A_{sp} / (d_s\ s)$ = 0.0103

f_l = Lateral pressure on concrete provided by the confinement steel = $1/2\ \rho_s\ f_{yh}$ = 19.8351

f'_l = Effective lateral pressure on concrete provided by the confinement steel = $k_e\ f_l$ = 18.3463

f'_{cc} = Compressive strength of confined concrete

$f'_{cc} = f'_{co}\ (2.254\ (1 + 7.94\ f'_l / f'_{co})^{1/2} - 2f'_l / f'_{co} - 1.254)$

f'_{cc} = 694.2335

ε'_{cc} = Concrete strain at f'_{cc}

$\varepsilon'_{cc} = [5\ (f'_{cc} / f'_{co} - 1) + 1]\ \varepsilon'_{co}$

ε'_{cc} = 4.053E-03

E_{sec} = Secent modulus of elasticity of concrete = $f'_{cc}/\varepsilon'_{cc}$ = 171303

ε_{cu}

$\varepsilon_{cu} < \varepsilon_{cu(limit)}$ ..... OK

f_c and ε_c

ε_c = Compressive concrete strain

ε_c = Ranges from 0 to ε_{cu}

f_c = Compressive concrete stress

$f_c = (f'_{cc} \, x \, r)/(r - 1 + x^r)$

where

$x = \varepsilon_c / \varepsilon'_{cc}$

$r = E_c / (E_c - E_{sec}) = 1.4925$

A2. Mander Unconfined Concrete Model

(Units: Kip-ft)

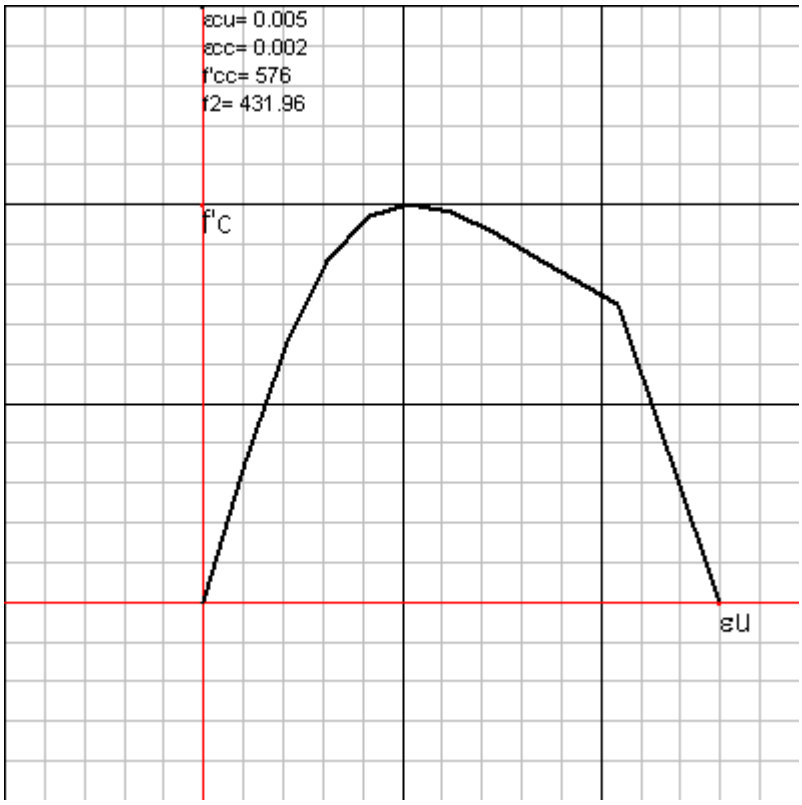

Point	Strain	Stress
1.	0.	0.
2.	4.000E-04	203.2572
3.	8.000E-04	376.6931
4.	1.200E-03	496.4604
5.	1.600E-03	558.8864
6.	2.000E-03	576.
7.	2.400E-03	564.0991
8.	2.800E-03	536.6188
9.	3.200E-03	502.4262
10.	3.600E-03	466.6489
11.	4.000E-03	431.9639
12.	5.000E-03	0.

CONCRETE PROPERTIES

w = Unit weight of concrete = 0.144

f'_{co} = Compressive strnegth of unconfined concrete = 576.

ε'_{co} = Concrete strain at f'_{co} = 2.000E-03

ε'_{sp} = Concrete spalling strain

$\varepsilon_{cu} = \varepsilon'_{sp}$ = Ultimate concrete capacity of concrete = 5.000E-03

$\varepsilon'_{cc} = \varepsilon'_{c0}$

$f'_{cc} = f'_{cc}$

MODULUS OF ELASTICITY

E_c = Tangent modulus of elasticity of concrete = $33\, w^{1.5}\, (f'_{co})^{1/2}$ ... in psi = 519120

E_{sec} = Secent modulus of elasticity of concrete = $f'_{cc}/\varepsilon'_{cc}$ = 288000

CALCULATIONS

The equations for the unconfined concrete are divided into two segments

Segment1

For $\varepsilon_c <= 2\varepsilon_{co}$

$f_c = (f'_{cc}\, x\, r)/(r - 1 + x^r)$

where

$x = \varepsilon_c / \varepsilon'_{cc}$

$r = E_c / (E_c - E_{sec})$ = 2.2461

Segment2

For $2\varepsilon'_{c0} < \varepsilon_c <= \varepsilon'_{sp}$

It is a line that takes the concrete stress from end of segment one to the stress of zero at ε'_{sp}

A3. Park Steel Model

(Units: Kip-ft)

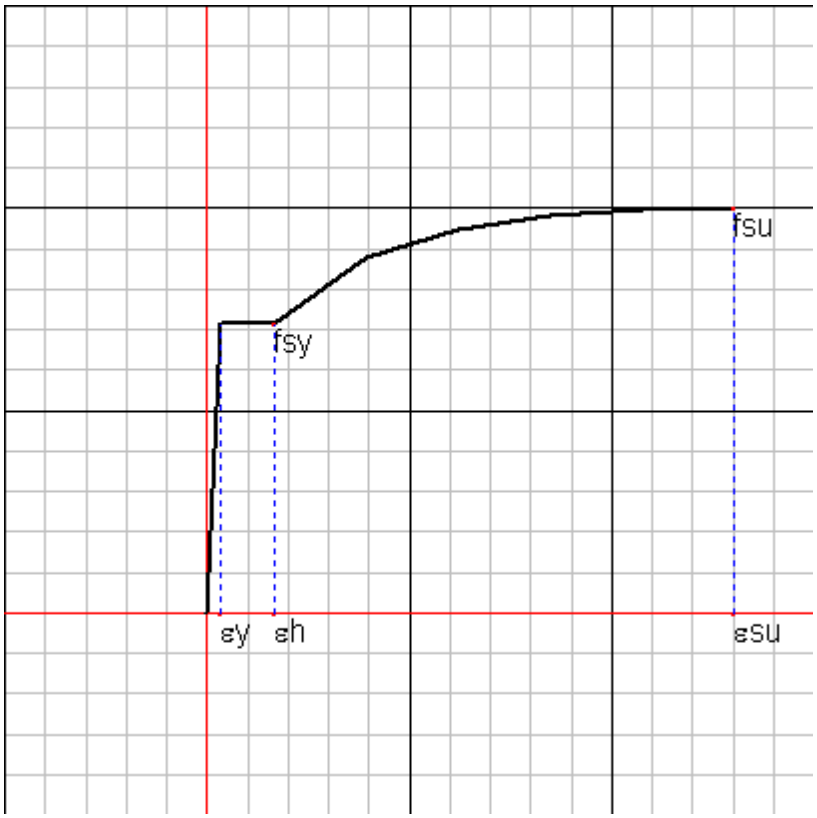

Point	Strain	Stress
1.	0.	0.
2.	2.300E-03	9792.
3.	0.0115	9792.
4.	0.0272	11988
5.	0.0429	12959
6.	0.0586	13422
7.	0.0743	13626
8.	0.09	13680

STEEL PROPERTIES

ε_{sy} = Yield strain of steel = 2.300E-03

f_{sy} = Yield stress of steel = 9792.

ε_{sh} = Strain in steel at onset of strain hardening = 0.0115

ε_{su} = Ultimate strain capacity of steel = 0.09
f_{su} = Ultimate stress capacity of steel = 13680

CALCULATIONS

For $\varepsilon_s <= \varepsilon_{sy}$

$f_s = E_s \varepsilon_s$

For $\varepsilon_{sy} < \varepsilon_s <= \varepsilon_{sh}$

$f_s = f_{sy}$

For $\varepsilon_{sh} < \varepsilon_s <= \varepsilon_{su}$

$f_s = f_{sy} [(m(\varepsilon_s - \varepsilon_{sh}) + 2) / (60 (\varepsilon_s - \varepsilon_{sh}) + 2) + ((\varepsilon_s - \varepsilon_{sh}) (60 - m)) / (2 (30 r + 1)^2)]$

Where

$r = \varepsilon_{su} - \varepsilon_{sh}$

$m = [(f_{su}/f_{sy}) (30 r + 1)^2 - 60 r - 1] / (15 r^2)$

A4. SAP Moment-Curvature *(M-□)* Results

Units: k-ft
Axial Load = 0.
Moment Angle = 0.

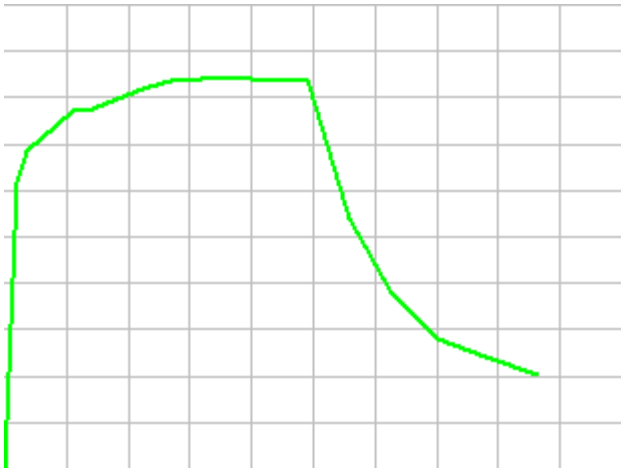

Results For Exact-Integration
$\phi_{y(Initial)}$ = 5.400E-04
M_y = 3516.7999
ϕ_{max} = 0.0345
M_{max} = 1603.7557
$\phi_{concrete}$ = 7.670E-03
$M_{concrete}$ = 6425.7988
ϕ_{steel} = 0.0206
M_{steel} = 5800.3168

Concrete Strain	Neutral Axis	Steel Strain	Concrete Compression	Steel Compression	Steel Tension	Net Force	Curvature	Moment
0.	0.	0.	0.	0.	0.	0.	0	0.
-4.612E-04	1.6027	1.390E-03	-537.198	-64.5311	600.8234	-0.9057	0.0003301	2473.1432
-1.093E-03	1.6753	3.536E-03	-1107	-143.3251	1249.9186	-0.5347	0.0008252	4934.1786
-1.711E-03	1.8479	6.620E-03	-1298	-190.3427	1487.7771	-0.1259	0.001485	5494.4502
-2.410E-03	1.9571	0.0106	-1377	-234.6568	1610.1989	-1.5336	0.00231	5698.7847
-3.251E-03	2.0152	0.0153	-1416	-292.0407	1707.4353	-0.2431	0.003301	5891.7017
-4.318E-03	2.0308	0.0207	-1443	-363.5617	1806.6259	-0.2066	0.004456	6158.4646

-6.099E-03	1.944	0.0263	-1416	-447.8247	1862.9386	-0.6957	0.005776	6215.3457
-7.960E-03	1.9037	0.0328	-1442	-484.3685	1926.5752	0.5155	0.007261	6380.5139
-9.966E-03	1.8816	0.04	-1484	-510.244	1994.3728	0.0133	0.008912	6563.5047
-0.0123	1.8511	0.0478	-1513	-538.3343	2051.3369	-0.138	0.0107	6690.8424
-0.0152	1.8002	0.056	-1516	-566.338	2082.7586	0.072	0.0127	6714.8396
-0.0184	1.7626	0.0649	-1511	-597.4233	2109.8356	1.2361	0.0149	6744.5635
-0.0223	1.6993	0.074	-1487	-617.4336	2103.5681	-1.303	0.0172	6705.1462
-0.0262	1.6662	0.084	-1474	-641.2426	2115.6145	0.0639	0.0196	6707.2745
-0.025	1.8769	0.0999	-1093	-552.6377	1646.502	0.4433	0.0223	4304.9051
-0.0245	2.022	0.1162	-897.4287	-509.6413	1407.2401	0.1701	0.0251	3029.3591
-0.0253	2.0997	0.1321	-756.5677	-437.4829	1193.6292	-0.4215	0.0281	2258.3703
-0.0271	2.1311	0.1479	-688.0795	-439.0294	1127.935	0.8261	0.0312	1914.189
-0.0289	2.1615	0.1646	-625.9938	-440.4264	1066.9088	0.4886	0.0345	1603.7557

A5. Excel Moment-Curvature Macro - VBA Code

```
Private Sub cmdGoalSeek_Click()
  Dim Start As Double, Step As Double, Finish As Double, Current As Double, Moment As Double, Count
As Integer
  Dim wRngStrain As Range, wRngMoment As Range, wRngOut As Range
  Start = Range("D10")
  Step = Range("D11")
  Finish = Range("D12")
  Set wRngStrain = Range("G11")
  Set wRngMoment = Range("L45")
  Set wRngOut = Worksheets("MK").Range("A2")

  Current = Start
  Count = 1

  Do While Current <= Finish
     wRngStrain = Current
        'Range("Diff").GoalSeek Goal:=0, ChangingCell:=Range("NA") 'Using Goal Seek
     Call SolverOptions(150, 5000, 10 ^ -4, 0, 0, 1, 1, 1, 0.001, 0, 10 ^ -4, 0)
        'SolverOptions(MaxTime, Iterations, Precision, AssumeLinear, StepThru, Estimates, Derivatives,
Search, IntTolerance, Scaling, Convergence, AssumeNonNeg)
     SolverOptions MaxTime:=5000
     SolverOK SetCell:=Range("Diff"), MaxMinVal:=3, ByChange:=Range("NA"), ValueOf:=0
     SolverSolve UserFinish:=True

     Moment = wRngMoment
     wRngOut(Count, 1) = Count                          'iteration
     wRngOut(Count, 2) = Current                        'top strain
     wRngOut(Count, 3) = Range("G2") - Range("NA")          'NA (from top)
     wRngOut(Count, 4) = Moment                         'Total Moment
     wRngOut(Count, 5) = Current / (Range("G2") - Range("NA"))   'Curvature
     wRngOut(Count, 6) = Range("Diff")                  'Solution error
     Count = Count + 1         'increment counter
     Current = Round(Current + Step, 6)   'increment strain; rounding to eliminate floating point error

  Loop
End Sub


Private Sub cmdReplay_Click()
  Dim wRngStrain As Range, wRngNA As Range, wRngOut As Range, wil As Integer, wseStart As Single,
wbH As Boolean
  Set wRngStrain = Range("G11")
  Set wRngNA = Range("NA")
  Set wRngOut = Worksheets("MK").Range("A2")
```

```
    For wiI = 1 To wRngOut.CurrentRegion.Rows.Count - 1
        'Worksheets("Column").EnableCalculation = False
        wRngStrain = wRngOut.Cells(wiI, 2)
        wRngNA = Range("G2") - wRngOut.Cells(wiI, 3)
        'Worksheets("Column").EnableCalculation = True

        wseStart = Timer
        Do While Timer < (wseStart + 0.25)
          DoEvents
        Loop

    Next
End Sub
```

A6. Foundation Pushover Curves

Pier Foundations - 5% steps				
Step	% Design	V_x (k)	Δ (in)	Slope
0	0%	0	0	-
2	10%	80.9	0.008	-
3	15%	121.3	0.012	12.10
4	20%	161.7	0.017	12.09
5	25%	202.2	0.021	12.10
6	30%	242.6	0.025	11.86
7	35%	283.0	0.030	11.27
8	40%	323.4	0.034	10.86
9	45%	363.9	0.039	10.75
10	50%	404.3	0.044	10.65
11	55%	444.7	0.049	9.78
12	60%	485.2	0.055	9.14
13	65%	525.6	0.060	9.08
14	70%	566.0	0.066	8.71
15	75%	606.5	0.072	8.50
16	80%	646.9	0.078	8.32
17	85%	687.3	0.084	8.14
18	90%	727.7	0.092	7.32
19	95%	768.2	0.098	7.08
20	100%	808.6	0.105	7.54
21	105%	849.0	0.112	7.43
22	110%	889.5	0.119	7.32
23	115%	929.9	0.126	7.23
24	120%	970.3	0.134	6.78
25	125%	1010.8	0.141	6.58
26	130%	1051.2	0.148	6.73
27	135%	1091.6	0.156	6.64
28	140%	1132.0	0.164	6.55
29	145%	1172.5	0.171	6.47
30	150%	1212.9	#N/A	#N/A

Abutment Foundations - 5% steps

Step	% Load	V_x (k)	Avg ΔX (in)	Avg ΔY (in)	Avg Δ (in)	X Slope	Y Slope
0	0%	0	0	0	0	-	-
2	10%	110.0	0.011	0.031	0.021	-	-
3	15%	165.0	0.017	0.047	0.032	8.69	3.03
4	20%	220.0	0.023	0.064	0.044	8.58	2.99
5	25%	275.0	0.029	0.081	0.055	8.42	2.93
6	30%	330.0	0.035	0.099	0.067	8.42	2.85
7	35%	385.0	0.041	0.116	0.079	8.36	2.88
8	40%	440.0	0.047	0.135	0.091	8.32	2.83
9	45%	495.0	0.053	0.152	0.103	8.32	2.80
10	50%	550.0	0.059	0.175	0.117	8.28	2.54
11	55%	605.0	0.065	0.215	0.140	8.34	1.71
12	60%	660.0	0.071	0.236	0.153	8.31	1.85
13	65%	715.0	0.077	0.265	0.171	8.29	2.09
14	70%	770.0	0.083	0.300	0.191	8.33	1.57
15	75%	825.0	0.089	0.337	0.213	8.33	1.39
16	80%	880.0	0.095	0.366	0.230	8.35	1.54
17	85%	935.0	0.101	0.405	0.253	8.34	1.51
18	90%	990.0	0.107	0.439	0.273	8.32	1.37
19	95%	1045.0	0.113	0.470	0.291	8.33	1.56
20	100%	1100.0	0.119	0.506	0.313	8.12	1.51

THIS PAGE INTENTIONALLY LEFT BLANK

Appendix B. Isolator Vendor Product Information

B1. DIS – Seismic Isolation for Buildings and Bridges

THIS PAGE INTENTIONALLY LEFT BLANK

B2. DIS – Project List Bridges

THIS PAGE INTENTIONALLY LEFT BLANK

B3. EPS – Friction Pendulum Seismic Isolation

THIS PAGE INTENTIONALLY LEFT BLANK

B4. EPS – Technical Characteristics

THIS PAGE INTENTIONALLY LEFT BLANK